



2013 | Faculteit Wetenschappen



DOCTORAATSPROEFSCHRIFT



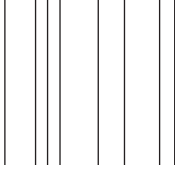
Synthesis and characterization of imidazolium-substituted ionic (co)polythiophenes for applications in organic photovoltaics

Proefschrift voorgelegd tot het behalen van de graad van doctor
in de wetenschappen, chemie, te verdedigen door



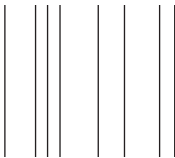
Toon Ghoois

Promotor: prof. dr. Wouter Maes

Copromotoren: prof. dr. Dirk Vanderzande en dr. Laurence Lutsen



D/2013/2451/53



Chairman	Prof. dr. Karin Coninx, UHasselt
Promoter	Prof. dr. Wouter Maes, UHasselt
Copromoter	Prof. dr. Dirk Vanderzande, UHasselt Dr. Laurence Lutsen, IMEC/IMOMECE
Members of the jury	Prof. dr. Laurence Vignau, Laboratoire IMS Institut Polytechnique de Bordeaux Prof. dr. Bruno Van Mele, Vrije Universiteit Brussel Prof. dr. Thomas Junkers, UHasselt Prof. dr. Peter Adriaenssens, UHasselt

Dankwoord

Velen zetten het dankwoord op het einde maar ik zou er graag mee willen beginnen aangezien vele personen rechtstreeks of onrechtstreeks bijgedragen hebben tot de realisatie van dit werk. Zij verdienen hiervoor een welverdiend woordje van dank.

In eerste instantie zou ik mijn promotor, prof. dr. Wouter Maes, willen bedanken. Zonder hem zou het finaliseren van dit doctoraat ‘fameus in het honderd’ gelopen zijn. Hij heeft met zijn kritische pen dit werk tot een mooi niveau opgekrikt. Wouter weet zeer goed hoe hij zijn studenten moet motiveren en mobiliseren. Bovendien is zijn aanwezigheid en bereikbaarheid een positief gegeven voor de vele bachelor en doctoraatsstudenten. Ook mijn copromotor, prof. dr. Dirk Vanderzande, verdient een woordje van dank. Zo heeft hij mij vier jaar geleden de kans gegeven om dit doctoraats-avontuur te starten. I also want to thank, dr. Laurence Lutsen, for the opportunities she gave me in the European Project “Orion”. Thanks to this project, I had the opportunity to visit some beautiful places and to meet some interesting and brilliant scientists. Verder wil ik ook prof. dr. Thomas Junkers en prof. dr. Peter Adriaensens bedanken voor respectievelijk de hulp bij het bespreken van de GPC en NMR resultaten. Prof. dr. Henk Bolink, spijtig dat je er niet kan bij zijn tijdens mijn verdediging. Ik wil u graag bedanken voor de zeer fijne en productieve week die ik gehad heb in Valencia. Alejandra and Olga, you two had a great deal in this very productive week. Olga, thanks for the nice collaboration and take care of your “little” boy, I wish you all the best and success in your further career. Graag wil ik ook

de leden van de jury bedanken voor de bereidheid om dit werk te evalueren. De UHasselt (voor mij toch nog steeds een beetje het LUC) zou ik graag willen bedanken voor de financiële steun tijdens deze doctoraatsjaren.

Naast de proffen, welke een grote invloed hebben op de richting en de inhoud van het doctoraatswerk zijn er de collega doctoraatsstudenten die de werksfeer in het labo en op 'den bureau' maken of kraken. Zij hebben er alvast voor gezorgd dat ik mij in een mum van tijd heb kunnen thuis voelen. Ik werd gepromoveerd van 'de jongste van de groep' (bij Janssen Pharmaceutica) tot nagenoeg de oudste. Deze eer was weggelegd voor Raoul Mens, de beste "koekoek" die ze bij DIPs ooit gehad hebben. Bedankt voor de haast filosofische en motiverende gesprekken tijdens de "PhD-meetings".

In het labo zorgde mijn naaste burens voor een onvergetelijke sfeer ondanks mijn zangtalent. Ans, je hebt mij het langst moeten dulden als buur, ik hoop dat uw beeld van organische synthese niet vernauwd is tot kolommen, kolommen en kolommen. Sarah, ik denk niet dat ik al een meer toegewijde doctoraatsstudent ontmoet heb dan jij. Ik hoop dat je nog een zeer succesvolle carrière tegemoet mag gaan. Rafael, je was een waardige vervanger vol nieuwe, verregaande en zeer grappige ideeën. Rafke, ik zal uw hersenspinsels niet snel vergeten en als we later groot zijn gaan we, zoals echte mannen, samen op jacht naar gekloonde mammoeten. Tom, uw aanwezigheid in het labo gaf om één of andere reden altijd een aanleiding tot zever, ... gezever. Ik ben u daar zeer dankbaar voor. Inge, in het labo hebben we niet echt samengewerkt maar als 'bouncing' buurvrouw zorgde je wel voor een fijne sfeer en was je altijd bereid voor een babbeltje. Gelukkig nam jij de organisatie van,

vanalles en nog wat, over toen Hanne, ‘ons moeder’ en de ‘hygiënisch verantwoordelijke’ van de groep niet aanwezig was. Het zou me echter te ver leiden om iedereen apart te bedanken, daarom wil ik al de andere collega’s, een gezamenlijke dankuwel geven. Ik heb altijd gezegd dat ik de UHasselt niet zou missen, maar ik moet toegeven dat dit toch niet helemaal het geval is. Ik denk namelijk nog dikwijls terug aan de fijne, ongedwongen sfeer die er hing. Bedankt Pieter, Wouter, Joke, Lidia, Julija, Suleyman, Wibren, (David)², Brecht, Gunter, Erik, Veerle, Iris, Stephan, Neomy, Veronique, Linny, onze duitse collega’s Matthias en Benjamin en natuurlijk mag ik ‘Crazy’ Katy niet vergeten.

Ik vermoed dat er nu één iemand zit te ‘protten’ dat zijn naam nog niet vernoemd is. Jurgen, bedankt voor de hulp bij het schrijven van één van de artikels en tevens hoofdstuk. Je bent niet alleen een aangename collega en klim-kameraad, maar ik wil van dit moment ook gebruik maken om u te promoveren tot “vriend” ;-).

Tijdens mijn doctoraatsjaren heb ik ook de kans gekregen om enkele bachelor studenten te begeleiden (entertainen) tijdens hun bachelor stage. Thomas en Mathias, ik hoop dat jullie er iets van opgestoken hebben, jullie waren alvast een grote hulp voor mij.

Naast collega’s en studenten zijn er ook vaste werkkrachten, die de boel draaiende houden, bedankt Huguette, NMR-Koen en Jan-de-massa-man. Het didactische team, Rita, Gène en Hilde, jullie zorgden er telkens voor dat de studenten tijdens de labo’s niets te kort kwamen. Bedankt Ivo, al was het maar voor de leuke babbeltjes in het labo, want echt samenwerken hebben we niet gedaan. Bovendien zal de link met mijn huidige werkgever ook geen negatieve invloed gehad hebben.

Naast mijn collega's wil ik ook graag mijn familie en vrienden bedanken. In eerste instantie mijn ouders om mij alle (financiële, materiële en emotionele) steun te geven die ik nodig had om tot hier te geraken. Thomas, je bent de beste broer die ik ooit gehad heb ;-), je hebt ook voor een toffe schoonzus gezorgd, Melanie, welkom in onze familie. Jos, Ann, Hilde en Jo, bedankt voor de morele steun tijdens deze periode, maar ook voor de praktische ideeën en hulp bij het klussen. Graag zou ik ook alle klim-kameraden willen bedanken die samen wat tegen de muur zijn komen hangen. Wannes, Q (Steven), Bart, Wim, Jurgen en nog veel meer anderen, dit was een zeer aangename verpozing tijdens de 'zware' studie en werkjaren.

Maar de laatste woorden van dank gaan geheel naar mijn vriendin, Karolien. Ook zij krijgt een enorme dankuwel, niet enkel om er voor mij te zijn op moeilijke momenten, maar ze heeft ervoor gezorgd dat er überhaupt sprake is van dit doctoraat. Zonder haar aanmoediging zou ik nooit aan dergelijk avontuur begonnen zijn. Verder wil ik haar ook nog bedanken voor de ruim 12 jaar die we ondertussen samen beleefd hebben en hopelijk komen er nog vele jaren bij.

Bedankt allemaal!

Table of Contents

Dankwoord

Chapter 1: Introduction

1 - 32

1.1 General introduction

1.2 Conjugated polymers

1.3 Polythiophenes

1.3.1 Introduction

1.3.2 Nickel-catalyzed coupling polymerization

1.3.3 The GRIM polymerization method

1.3.4 Synthesis of all-conjugated block copolythiophenes

1.3.5 Polythiophene-based conjugated polyelectrolytes (CPEs)

1.4 Photovoltaics

1.4.1 Organic photovoltaics

1.4.1.1 Working principles of an organic solar cell

1.4.1.2 Organic solar cell performance features

1.5 Thesis overview

1.6 References

Chapter 2: Imidazolium-substituted ionic (co)polythiophenes: synthesis, material characterization and solution behavior

33 - 90

2.1 Introduction

2.2 Results and discussion

2.2.1 Polymer synthesis and characterization.

2.2.2 Solution behavior

2.2.2.1 UV-Vis absorption studies

2.2.2.2 DLS experiments

2.2.3 Solid-state properties

2.2.3.1 Optical properties in film

2.2.3.2 Thermal stability

2.2.3.3 Thermal transitions

2.3 Experimental section

2.3.1 General experimental methods

2.3.2 Monomer synthesis

2.3.3 Precursor polymer synthesis

2.3.3.1 P3HT-P3BHT series

2.3.3.2 P3POET-P3BHOET series

2.3.3.3 P3MEEET/P3BHOET series

2.3.3.4 General procedure for polymer functionalization with *N*-methylimidazole

2.3.3.5 General procedure for counter ion exchange

2.4 Conclusions

2.5 References

2.6 Supporting information

Chapter 3: Solution-processed bi-layer polythiophene-fullerene

organic solar cells

91 - 122

3.1 Introduction

3.2 Experimental section

3.2.1 Synthesis and characterization

3.2.2 Monomer synthesis

3.2.3 Polymer synthesis: poly(3-(6-bromohexyl)thiophene) or P3BHT

3.2.4 Polymer functionalization with *N*-methylimidazole: poly[3-(6-(1-methylimidazolium-3-yl)hexyl)thiophene] bromide or P3(mim)HT-Br

3.2.5 Counter ion exchange: poly[3-(6-(1-methylimidazolium-3-yl)hexyl)thiophene] bis(trifluorosulfonyl)imide or P3(mim)HT-TFSI

3.2.6 Device fabrication

3.3 Results and discussion

3.3.1 Polymer synthesis and characterization

3.3.2 Device construction and analysis

3.4 Conclusions

3.5 References

3.6 Supporting information

**Chapter 4: Imidazolium-substituted polythiophenes as efficient
electron transport layer improving photovoltaic
performance**

123 - 154

4.1 Introduction

4.2 Experimental section

4.3 Results and discussion

4.4 Conclusions

4.5 References

4.6 Supplementary material

Chapter 5: Amphiphilic N-methylimidazole-functionalized diblock copolythiophenes for organic photovoltaics	155 - 184
5.1 Introduction	
5.2 Results and discussion	
5.2.1 Block copolymer synthesis	
5.2.2 Solution behavior	
5.2.3 Characterization of the micellar structures	
5.2.4 Thermal analysis	
5.3 Conclusions	
5.4 Experimental Section	
5.4.1 General experimental methods	
5.4.2 Polymer synthesis	
5.4.3 Ionic block copolymer synthesis	
5.5 References	
5.6 Supporting information	
Chapter 6: General conclusions	185 - 189
List of publications	190

Chapter 1

Introduction

1.1 General introduction

Due to the continuous industrialization and growth of the human population the energy consumption in 2050 is expected to be 28–35 TW. With the current energy sources it is impossible to cope with this increasing demand. Most of our present energy is derived from fossil fuels (coal, oil, gas) but this supply is finite. Moreover, the combustion of fossil fuels produces CO₂, which is supposed to be the main responsible for the acceleration of global warming. This limited supply of fossil fuel sources and the negative effects of CO₂ request an intensification of research and development efforts toward renewable energy sources (e.g. nuclear, wind, hydropower, biomass and solar energy). Harvesting energy from non-CO₂-emissive sources is required to prevent irreversible climate changes.

Extensive efforts have been made in exploiting various renewable sources to respond to the growing energy demand. It is well-known that the sun provides as much energy in one hour as is required for all human needs in a whole year. For that reason, harvesting energy directly from sunlight and converting it into electrical energy using photovoltaic (PV) technologies is increasingly recognized as an important part of the solution to the growing energy challenge and a fundamental factor of the future global renewable energy production.

To date, silicon-based solar cells are almost solely used in photovoltaic panels. The silicon technology has, however, some disadvantages. The silicon purification processes are expensive and the silicon availability is limited due to its widespread use in the field of microelectronics. Consequently, the production cost of silicon-based solar panels is quite

high. Cost is one of the major motivations for the development of alternative photovoltaic technologies. Organic photovoltaics (OPV) exhibit some valuable advantages such as device flexibility, aesthetics, and cheaper fabrication from abundant materials.

The development of this new type of photovoltaic cells was initiated by the discovery of semiconducting polymers in 1977 by A. McDiarmid, H. Shirakawa and A. Heeger, who were honored with the Nobel Prize in Chemistry in 2000. In 1986, the Eastman Kodak corporation introduced the first efficient bilayer organic solar cell (OSC), giving 1% efficiency. Today, the most successful OPV technology is based on solution-processed bulk heterojunction (BHJ) OSCs with an active layer composed of a mixture of an electron-donating semiconducting polymer and an electron-accepting fullerene derivative. In the past decade, many improvements have been made in the field, including new photoactive materials, deposition techniques, device architectures and electrode materials. These changes resulted in certified power conversion efficiencies (PCEs) of over 10%, which is an important milestone. However, the efficiency of OPV devices is still significantly lower than for their inorganic counterparts, although they show a higher efficiency at low light level, extending their effectiveness across the day and during cloudy periods.

Numerous factors limit the performance of BHJ organic solar cells. Several physical processes occur successively - absorption of photons, creation of excitons, exciton diffusion, exciton dissociation and finally the transport of charge carriers to the electrodes - and problems may occur at any of these steps. The blend morphology of the active layer

thin films plays a very important role and affects both the processes of exciton formation and dissociation and the charge transport to the electrodes. The majority of OSC research carried out has focused on the donor/acceptor bulk heterojunction approach using a conjugated semiconducting polymer as the donor and a fullerene derivative as the acceptor, which should form an intimately mixed blend to give highest performance. The most successful and widely studied system consists of a physical mixture of poly(3-hexylthiophene) (P3HT) and [6,6]-phenyl-C₆₁-butyric acid methyl ester (PCBM). In most cases, it is quite difficult to control the morphology of the active layer and its evolution in time, as there is a tendency toward demixing of the two components, destroying in this way the efficiency of the device. A lot of research has been done to overcome this thermally activated phase separation problem. In our group, the use of functionalized (co)polythiophenes was employed to improve the morphological stability of the active layer.

OPV of course wants to be a “green” technology. Until now, however, the different organic components still need environmentally harmful solvents (such as chloroform and chlorobenzene) for their processing. Via functionalization of the side chains of the polymers it is possible to render them soluble in more environmentally friendly solvents such as ethyl acetate or alcohols. The ultimate goal is to make high-efficiency fully water-processable stable OSCs.

1.2 Conjugated polymers

Traditionally, polymers (or the plastics derived from them) were considered good insulators and were hence applied as such, e.g. in

coatings for electrical wires. This common belief was only reconsidered when one discovered the (semi)conducting properties of conjugated polymers. Conjugated polymers are organic molecules with alternating single and double bonds, allowing the π -electrons to be delocalized along the backbone (π -conjugated materials). Conjugated polymers are in this way able to merge the interesting electrical and optical properties of semiconductors with the appealing mechanical characteristics and processability of polymers. The most simple example of a conjugated polymer is polyacetylene (**Figure 1.1**), which was first synthesized in the 1950s by Natta *et al.*¹ The black, insoluble and air-sensitive powder was, however, not considered that interesting. Later, in the 1970s, conductive polyacetylene was accidentally discovered by a student in the group of Prof. Hideki Shirakawa. Together with Alan J. Heeger and Alan D. MacDiarmid, Shirakawa showed that doping of polyacetylenes with iodine vapor resulted in a 10^8 -fold increase in conductivity, approaching metal conductivity values.²

In 1990, a second breakthrough was achieved by the discovery of electroluminescence in poly(*p*-phenylene vinylene) (PPV) (**Figure 1.1**).³ Conjugated polymers were then successfully used for the first time as the emissive layer in polymer-based light-emitting diodes (PLEDs).

The importance of conjugated polymers was highlighted in 2000, when the three pioneers in this domain - Shirakawa, Heeger and MacDiarmid - were honored with the Nobel prize in Chemistry "*for the discovery and development of conductive polymers*". From that point on, the field started to expand almost exponentially, resulting in a wide variety of

conjugated polymers suitable for multiple applications. Some notable examples of conjugated polymers are displayed in **Figure 1.1**.

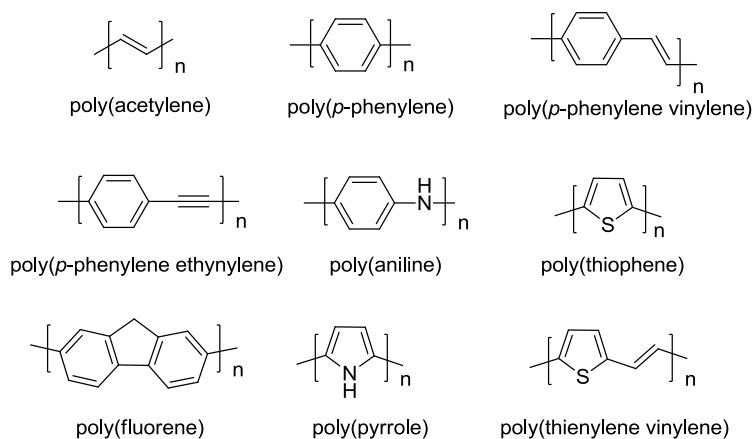


Figure 1.1: Structures of some important conjugated polymer classes.

1.3 Polythiophenes

1.3.1 Introduction

The development of thiophene-based conjugated polymers started with the synthesis of “bare” (unfunctionalized) polythiophene. Two research groups reported in 1980, almost at the same time, the synthesis of this polymer.^{4,5} Yamamoto *et al.* described the nickel-catalyzed polycondensation of 2,5-dibromothiophene.⁴ This monomer was reacted with magnesium in THF, affording 2-magnesiobromo-5-bromothiophene, which produced 2,5-polythiophene in the presence of Ni(bipy)Cl₂ (bipy = 2,2'-bipyridyl). On the other hand, Lin *et al.*⁵ described another example of a metal-catalyzed synthesis route to produce 2,5-polythiophene by using acetylacetonates of Ni, Pd, Co or Fe as catalysts. Although this was a nice step forward, 2,5-polythiophene is

an insoluble polymer, which cannot be processed for the use into (opto)electronic devices. In the search for a soluble derivative of 2,5-polythiophene, 3-alkylthiophenes were developed. Elsenbaumer *et al.*⁶ were the first to produce a soluble poly(3-alkylthiophene) (P3AT) in 1985, using a similar method to that used to prepare 2,5-polythiophene. The polymerization of the asymmetric 3-hexylthiophene (toward poly(3-hexylthiophene) or P3HT) generally results in a mixture of three possible coupling patterns along the polythiophene backbone, i.e. 2,5'-(head-to-tail, HT), 2,2'-(head-to-head, HH) and 5,5'-(tail-to-tail, TT) coupled (**Figure 1.2**). A lot of efforts were put into control of the regiochemistry during the synthesis of P3HT, which simultaneously also resulted in a large improvement of the structural, electronic and optical properties of this polymer.

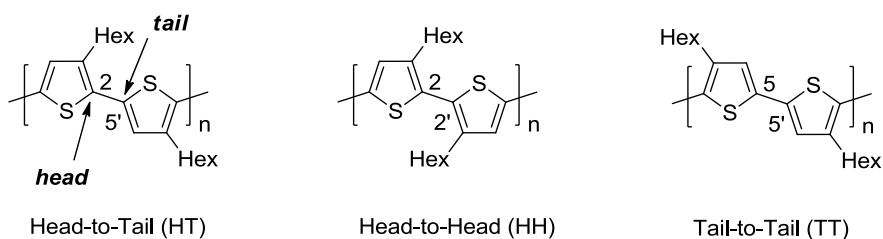


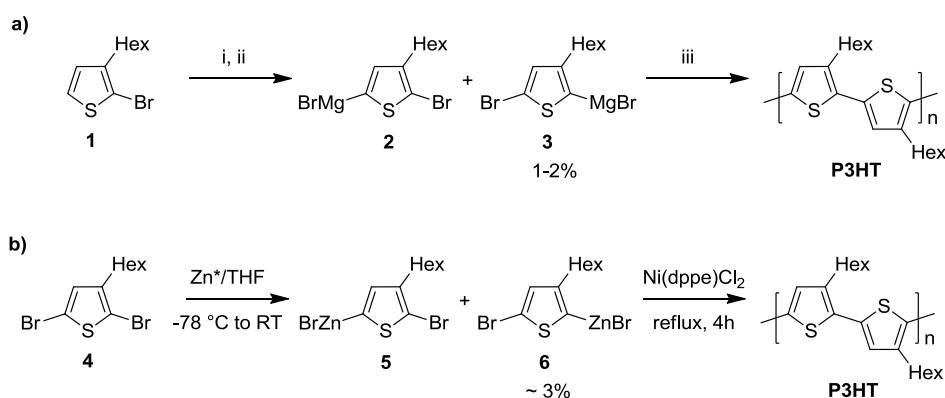
Figure 1.2: Coupling regiochemistry of P3HT isomers.

1.3.2 Nickel-catalyzed coupling polymerization

Polymerization to regioregular P3HT (rr-P3HT) based on nickel-catalyzed Kumada cross-coupling was first developed by McCullough *et al.* (**Scheme 1.1a**).⁷ This procedure was later on modified by replacing magnesium bromide etherate with $ZnCl_2$, providing a better solubility of

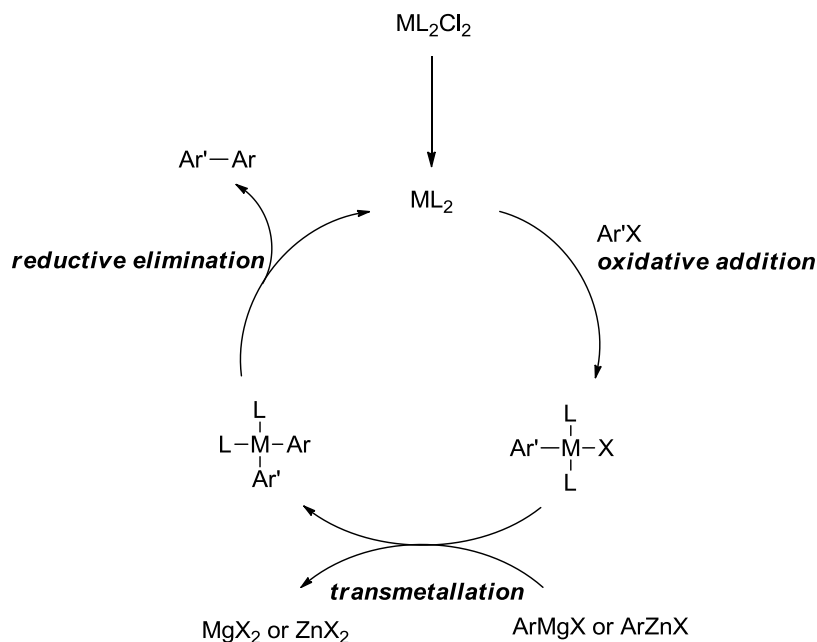
Chapter 1

the organometallic intermediate in THF at $-78\text{ }^{\circ}\text{C}$.⁸ Shortly thereafter, Chen and Rieke⁹ reported the use of the highly reactive *Rieke zinc* (Zn^*) in the controlled synthesis of rr-P3HT (**Scheme 1.1b**).



Scheme 1.1: a) Synthesis of rr-P3HT by McCullough's method: i. LDA, THF, $-40\text{ }^{\circ}\text{C}$, 40 min; ii. $\text{MgBr}_2\cdot\text{Et}_2\text{O}$, -60 to $-40\text{ }^{\circ}\text{C}$ over 40 min, -40 to $5\text{ }^{\circ}\text{C}$ over 20 min; iii. $\text{Ni}(\text{dppp})\text{Cl}_2$, -5 to $25\text{ }^{\circ}\text{C}$, 18 h. b) Synthesis of rr-P3HT by the Rieke method.

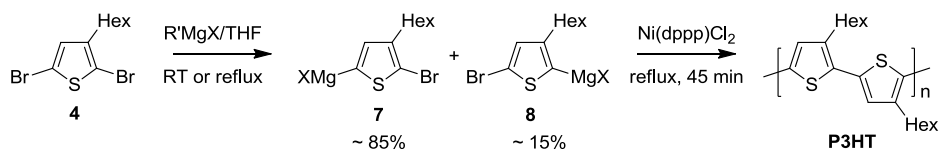
The polymerization methods reported above operate via a metal-catalyzed cross-coupling system (**Scheme 1.2**), which has been extensively investigated.¹⁰ The catalytic cycle consists of three steps: (1) oxidative addition of a transition metal catalyst to an organic aryl halide with, (2) transmetalation (disproportionation) of the catalyst complex by a reactive organometallic reagent (i.e. organomagnesium, organozinc, organoboron, organoaluminium, organotin) to generate a diorganometallic complex and (3) reductive elimination of the coupled product with regeneration of the catalyst.



Scheme 1.2: Catalytic cycle of transition metal-mediated cross-coupling reactions.

1.3.3 The GRIM polymerization method

In 2001, a new synthetic method toward rr-P3HT was reported by McCullough and coworkers (**Scheme 1.3**).¹¹ This new polymerization method is performed under milder conditions, as it is not necessary to use cryogenic temperatures and highly active metals.



Scheme 1.3: Synthesis of rr-P3HT by the Grignard metathesis (GRIM) method.

The 2,5-dibromo-3-hexylthiophene monomer (**4**) is treated with one equivalent of an alkyl/vinyl Grignard reagent, which results in a magnesium-halide exchange, the Grignard metathesis (GRIM) reaction. The metathesis step proceeds with a moderate degree of regioselectivity, affording an ~85:15 ratio of the two regio-isomers **7:8**, and this ratio seems to be independent on the reaction time, temperature and Grignard reagent applied. The polymerization occurs, however, with a good selectivity for one of the isomers (**7**) and still affords P3HT with a regioregularity of ~98%. The authors explain this high regioregularity by a combination of kinetic and thermodynamic effects resulting from steric and electronic factors in the catalytic cycle.¹¹

The generally accepted mechanism for cross-coupling reactions involves oxidative addition, transmetallation and reductive elimination (**Scheme 1.2**). As such, polymerizations applying these reactions are considered polycondensation reactions, generally proceeding via a step-growth mechanism and affording polymers with a limited control on molecular weight and high polydispersities. Yokozawa and coworkers proposed in 2004 that the polymerizations described by McCullough and via the GRIM method proceed in a chain-growth fashion to obtain rr-P3HT with a controlled molecular weight and low polydispersity. However, one always observed a shoulder in the gel permeation chromatography (GPC) profiles, corresponding to a fraction with a molecular weight double of the main peak.¹² A little later, Yokozawa et al. reported that this shoulder is the result of the formation of a small portion of polymer with higher molecular weight upon quenching the polymerization reaction with water, which promotes disproportionation of the active

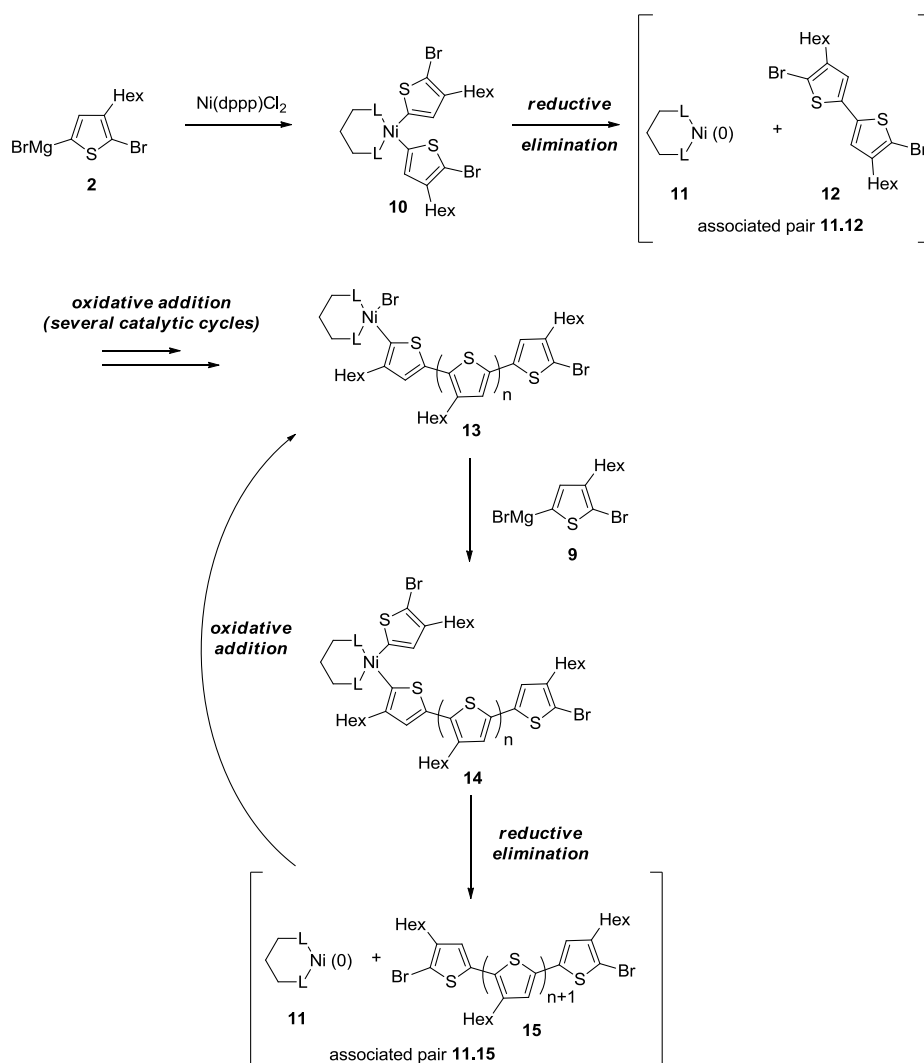
P3HT-Ni(II)Br chain, followed by reductive elimination of P3HT-P3HT.¹³ In 2011, this was also observed by Thelakkat *et al.* upon quenching of the polymerization reaction in MeOH.¹⁴ This side reaction can be avoided by quenching the polymerization with a 5M HCl solution, promoting protonation instead of disproportionation and resulting in a lower polydispersity.

It was also found that the McCullough and the GRIM polymerization method not only proceed via a chain-growth mechanism, but they also display “living” characteristics. McCullough and coworkers provided an explanation for this living chain-growth nature.¹⁵ They assume that there is complexation of nickel(0) to the oligothiophene growing chain. In this way an associated pair is formed which is supposed to limit the polymerization to one end of the polymer chain. The mechanism is shown in **Scheme 1.4** (slightly modified according to the used GRIM polymerization method).

The first step in the mechanism is the reaction of two equivalents of 2-bromo-5-bromomagnesio-3-hexylthiophene (**2**), generated *in situ* from 2,5-dibromo-3-hexylthiophene, with Ni(dppp)Cl₂, yielding the bis-organonickel complex **10**. In a second step, reductive elimination of the latter results in the immediate formation of the complex [**11.12**] [nickel(0) species **11** and the tail-to-tail coupled dimer **12**]. Dimer **12** undergoes fast oxidative addition to the nickel center, thus generating a new organonickel compound **13** (keeping in mind the formation of the complex [**11.12**], eliminating the potential separation of **11** from **12**). Subsequently, the polymer chain grows by insertion of one monomer unit at a time, and the Ni(dppp) moiety stays always bound to the

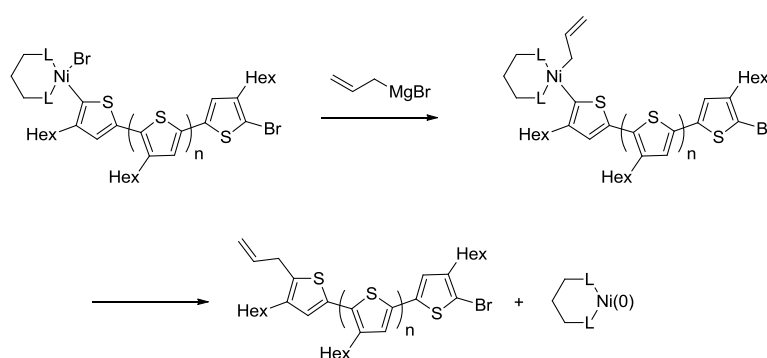
Chapter 1

polymer chain as an end-group. When considering this mechanism, only one defect (tail-to-tail coupling) can be found in the polymer chain, situated at the very beginning of the chain and incorporated during the first step.



Scheme 1.4: McCullough's mechanism for the nickel-catalyzed cross-coupling polymerization.¹⁵

Due to its living nature, the GRIM polymerization allows the synthesis of end-functionalized P3HT. A versatile method for *in situ* end-group functionalization of regioregular P3HT synthesized via GRIM has been reported by McCullough and coworkers.¹⁵ As an example, it is possible to synthesize P3HT with an allyl end group by addition of allyl magnesiumbromide to the nickel-terminated P3HT synthesized via GRIM (**Scheme 1.5**).

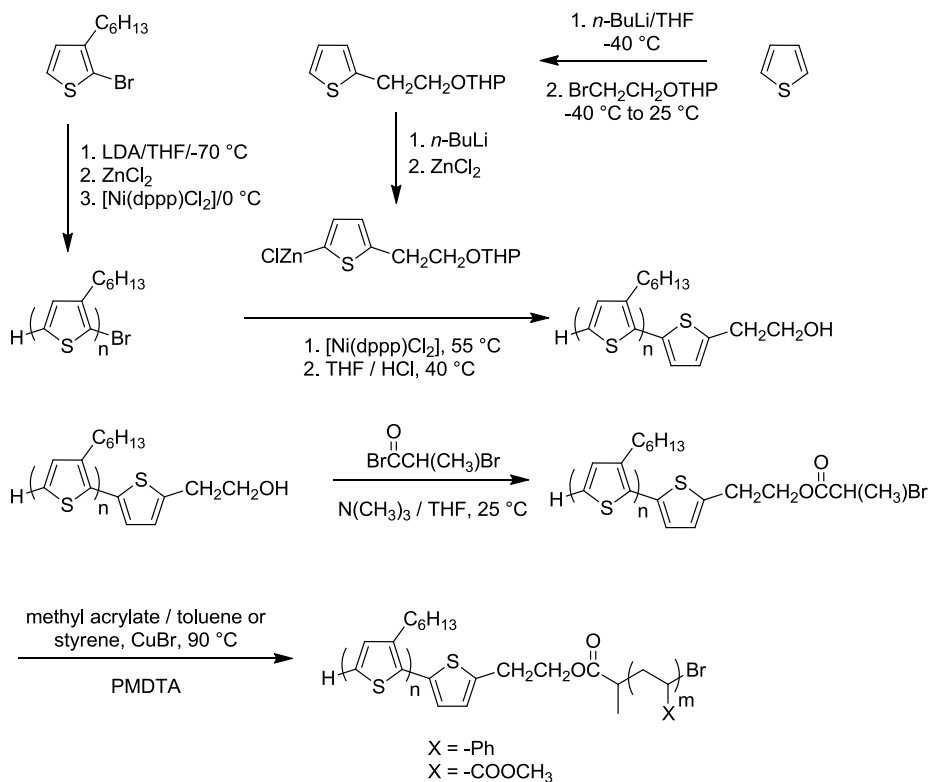


Scheme 1.5: *In situ* end-capping of regioregular P3HT with allyl magnesiumbromide.

1.3.4 Synthesis of all-conjugated block copolythiophenes

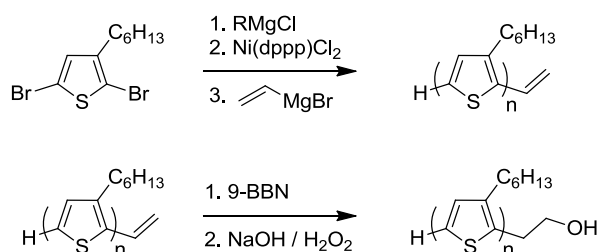
The easy *in situ* end group functionalization of P3HT triggered the development of various block copolymers containing polythiophene parts. McCullough and coworkers reported the synthesis of diblock and triblock copolymers containing a conjugated P3HT block together with a classical, non-conjugated polystyrene or poly(methyl acrylate) block.¹⁶ The polymers were prepared using a combination of the McCullough polymerization method and atom transfer radical polymerization (ATRP). The methodology applied required a lot of steps and cryogenic temperatures (**Scheme 1.6**).

Chapter 1



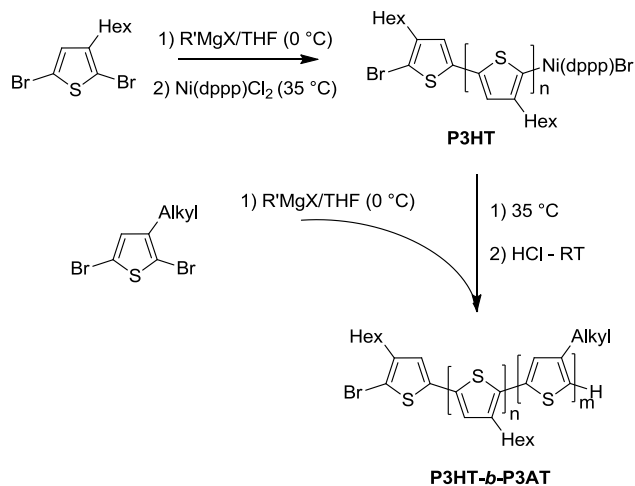
Scheme 1.6: Synthesis of P3HT-PS and P3HT-PMA diblock copolymers by the McCullough method and ATRP.

Later on, a more simple method was reported, in which vinyl- or allyl-terminated P3HT was first obtained by *in situ* end-capping using the corresponding Grignard reagent, followed by a hydroboration/oxidation reaction to generate the hydroxy-terminated P3HT (**Scheme 1.7**).¹⁷



Scheme 1.7: Synthesis of hydroxyethyl-terminated P3HT.

The living nature of the GRIM polymerization method can also be beneficially applied to produce all-conjugated block copolythiophenes.^{18,19} The conjugated polythiophene generated in the first step is a living polymer, with the nickel moiety connected to the polymer as an end group. Sequential addition of the organomagnesium derivate of another thiophene monomer allows the growth of a second conjugated block to obtain the final all-conjugated diblock copolythiophene with different 3-alkyl side chains (**Scheme 1.8**).



Scheme 1.8: Synthesis of all-conjugated diblock copolythiophenes by the GRIM polymerization method.

When considering the living character of the GRIM polymerization method, it should also be possible to make conjugated triblock copolythiophenes (or even more).

Not only diblock copolythiophenes can be made by this method. Some other conjugated blocks can be formed as well. Two of them are shown in **Figure 1.3**.^{20,21} The diblock copolymer containing the poly(2,5-dihexyloxy-*p*-phenylene) block was first synthesized by Yokozawa *et al.*^{20a} They found that the order of polymerization was of crucial importance to get narrow polydispersities. McCullough and coworkers²¹ discovered the living character of the polyfluorene synthesis via the GRIM polymerization method. A little later they also reported the synthesis of poly(9,9-dioctyl-2,7-fluorene)-*b*-poly(3-hexylthiophene) copolymers.^{21b}

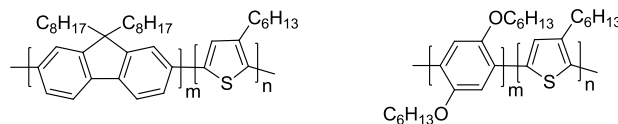


Figure 1.3: Schematic representation of poly(9,9-dioctyl-2,7-fluorene)-*b*-poly(3-hexylthiophene) and poly(2,5-dihexyloxy-*p*-phenylene)-*b*-poly(3-hexylthiophene).

All-conjugated block copolythiophenes have been synthesized for different reasons. When block copolymers composed of two different alkylthiophenes were prepared, it was found that phase separation occurred when the alkyl substituents differ in length by more than two carbon atoms.^{19a,b} This has an influence on the crystallinity and the morphological stability of the polythiophene thin films. The chiroptical behavior of block copoly(3-alkylthiophene)s, of which one block is chiral, was also studied.^{19b} It was shown that if the two blocks aggregate at a different non-solvent content, the block aggregating first determines the stacking behavior of the second as well. Park²² and Hayward²³ described the synthesis of conjugated poly(3-hexylthiophene)-*block*-poly(ethylene glycol thiophene) copolymers. Both research groups reported the formation of superstructures of these amphiphilic diblock copolymers in solution. Hayward and coworkers reported that the polymers efficiently assemble into well-defined fibers in the presence of the highly selective solvent methanol. Upon addition of potassium iodide, complexation of the K^+ ions to the triethylene glycol side chains occurs, and this complexation drives the formation of helical ribbons, which further associate into superhelical structures.²³

1.3.5 Polythiophene-based conjugated polyelectrolytes (CPEs)

A particular series of functionalized polythiophenes are the ones decorated with ionic functional groups. Leclerc and coworkers already in 1997 presented the synthesis of water-soluble sodium poly[2-(3-thienyloxy)ethane sulfonate] and sodium poly[2-(4-methyl-3-thienyloxy)ethane sulfonate] (**Figure 1.4a**), with an electric conductivity of the latter up to 5 S/cm.²⁴ In 2003, the same group presented the synthesis of poly(3-alkoxy-4-methylthiophenes) with a cationic 1,2-dimethylimidazolium group (**Figure 1.4b**).²⁵ They found that these polymers are capable of detecting iodide anions in solution via an optical method, due to the conformational modification of the conjugated backbone upon anion binding. A couple years later, Firestone presented the synthesis of a P3HT-like polyelectrolyte, poly[3-(10-(methylimidazolyl)decyl)-thiophene] nitrate salt (**Figure 1.4c**).²⁶

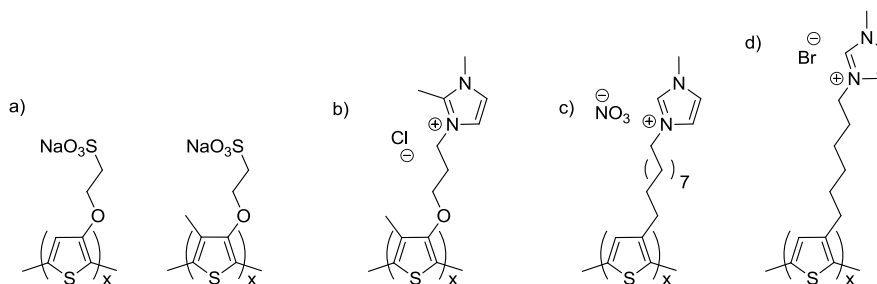


Figure 1.4: Structures of a) sodium poly[2-(3-thienyloxy)-ethanesulfonate] and sodium poly[2-(4-methyl-3-thienyloxy)ethanesulfonate], b) cationic poly(3-alkoxy-4-methylthiophenes), c) poly[3-(10-(methylimidazolyl)decyl)thiophene] nitrate salt and d) poly[3-(6-(methylimidazolyl)hexyl)thiophene].

All the above mentioned polythiophene polyelectrolytes were prepared by stoichiometric oxidative polymerizations of the corresponding

monomers with FeCl_3 , affording regiorandom polythiophenes. It is known that the functional properties of a polythiophene strongly depend on the degree of regioregularity. McCullough and coworkers²⁷ reported the synthesis of regioregular poly(thiophene-3-alkanoic acid)s which become water-soluble CPEs after addition of a base. The regioregular polymers in this report were synthesized by the Stille/CuO polymerization. More recently, in 2010, Vohlidal *et al.*²⁸ described the synthesis of a cationic polyelectrolyte with a regioregular poly(3-alkylthiophene) backbone and ionic liquid-like side chains (**Figure 1.4d**). The GRIM polymerization route was used to synthesize these CPEs. In a first step, a (non-ionic) precursor polymer was synthesized, and the imidazolium moiety was incorporated in a second post-polymerization step. They concluded that the polymers have an important contribution of ionic conductivity to the polymer overall conductivity, in particular at temperatures above 80–85 °C where the ionic conductivity becomes predominant. Boury *et al.*²⁹ showed that such polymers can form homogenous polymer/silica hybrid materials without destroying the π -conjugated structure of the polymer due to the strong ionic interaction between the cationic imidazolium groups and the protonated silanol moieties generated in the sol-gel reaction of tetraethoxysilane.

1.4 Photovoltaics

The photovoltaic effect - a method of generating electrical power by converting solar radiation into direct current electricity using semiconductors - was first observed in 1839 by A. E. Becquerel. He

found that the conductivity rose when a device consisting of a platinum electrode and a silver-chloride electrolyte was illuminated.³⁰ The photovoltaic technology has grown ever since and has advanced considerably toward improved efficiencies, stabilities and the production of lighter and cheaper devices.

The so-called **first generation** solar cells are constructed from mono- or polycrystalline silicon (Si), reaching around 25% power conversion efficiency (PCE)³¹ and they cover the majority of the consumer market.³² Later on, thinner film PV technologies were developed, such as copper-indium-gallium-selenide (CIGS) and cadmium-telluride (CdTe) cells. These **second generation** solar cell technologies have been developed to reduce the production costs. The cheaper production is the result of the smaller material quantities needed for the thin films and the less expensive fabrication processes. Laboratory efficiencies of up to 20% (and 18% for a 16 cm² module) (CIGS) have been obtained.³¹ Although the reached efficiencies are rather satisfying, the shortage of the required materials and their toxicity remain important obstacles. This is why a **third generation** of (thin film) solar cell technologies is currently explored, aiming at high efficiency at low cost. This new generation encompasses both organic and inorganic light absorbers (including polymer blend, small molecule,³³ dye-sensitized,³⁴ and hybrid organic/inorganic solar cells).³⁵

1.4.1 Organic photovoltaics

As denoted before, the initial development of organic photovoltaics started already in the 1970s by the discovery of the conductivity of

polyacetylene after doping the polymer with halides. In 1986, Tang reported the first organic photovoltaic cell, based on small molecules.³⁶ He used the so-called bi-layer architecture, in which a copper phthalocyanine (CuPc) layer as the electron donor material and a perylene layer as the electron acceptor material were sandwiched between two electrodes, affording a reasonable PCE of ~1%. In 1992, Sariciftci and coworkers used the same bi-layer approach for the first polymer solar cell with a donor layer of poly[2-methoxy-5-(2'-ethylhexyloxy)-*p*-phenylene vinylene] (MEH-PPV) and an acceptor layer of buckminsterfullerene (C₆₀) (**Figure 1.5**).³⁷

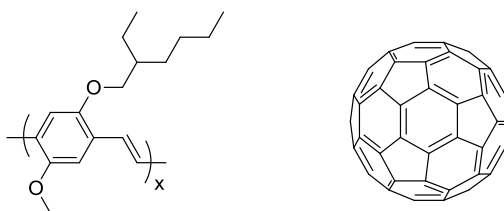


Figure 1.5: Schematic representation of poly[2-methoxy-5-(2'-ethylhexyloxy)-*p*-phenylene vinylene] (MEH-PPV) and buckminsterfullerene (C₆₀).

Although the power conversion efficiency was very low (0.04%), it was proven that photoinduced electron transfer between the donor and the acceptor material occurred and charge separation was taking place. The low efficiencies were mainly the result of the poor charge separation, as this can only occur near the interface between the donor and the acceptor layer because of the short diffusion length of the created excitons. Increasing the interface area between the two materials can lead to an improved charge separation. Heeger and Holmes introduced, in 1995,

the bulk heterojunction (BHJ) concept for organic solar cells, which was a major breakthrough in the development of organic photovoltaics.

Organic materials (both conjugated polymers and small molecules) have some advantages compared to inorganic semiconductors. One of them is their lower production cost, as processing of these materials can in most cases be performed from solution and this is less energy consuming than the high temperatures needed for vacuum deposition of (most) inorganic materials. For BHJ organic solar cells, the active layer is prepared by processing a mixture of a donor and an acceptor material from solution. When the substrate is rigid, such as glass, a series of solution processing techniques are available. Spin coating is mostly used for small substrates. If larger samples are prepared, this technique has, however, a higher chance to give inhomogeneous layers. Another disadvantage of the spin coating technique is the amount of material that is wasted; only 2–5% of the material is dispensed onto the substrate and 95–98% of the material is used to coat the interior of the coating bowl. Larger substrates can be coated in a very efficient way via doctor blading. An emerging processing technique in the field of thin film PVs is roll to roll (R2R) printing. This method enables to produce thin films on rigid but also on flexible substrates and at higher speeds. In all these cases, after the coating an intimate intermixed active layer is formed upon evaporation of the solvent. This intermixed morphology facilitates charge transfer and charge separation.

1.4.1.1 Working principles of an organic solar cell

The general mechanism for energy generation in organic photovoltaics involves four steps, which are illustrated in **Figure 1.6** in a schematic way. In a first step, a photon is absorbed by the donor material (often a conjugated polymer) and this absorption promotes an electron from the highest occupied molecular orbital (HOMO) to the lowest unoccupied molecular orbital (LUMO), creating an exciton which is bound via Coulombic interactions. These excitons, which are represented as electron-hole pairs, diffuse in a second step toward a donor-acceptor (D-A) interface. At this interface, the exciton will dissociate into free charges (step 3) due to the driving force provided by the energy offset between the LUMO levels of the donor and the acceptor (in many cases a fullerene derivative). This energy offset should be at least 0.3 eV for effective charge separation. In a final step, the free electrons are transported by the acceptor and extracted at the cathode, while on the opposite side the positive holes are transported through the donor material followed by charge extraction at the anode.

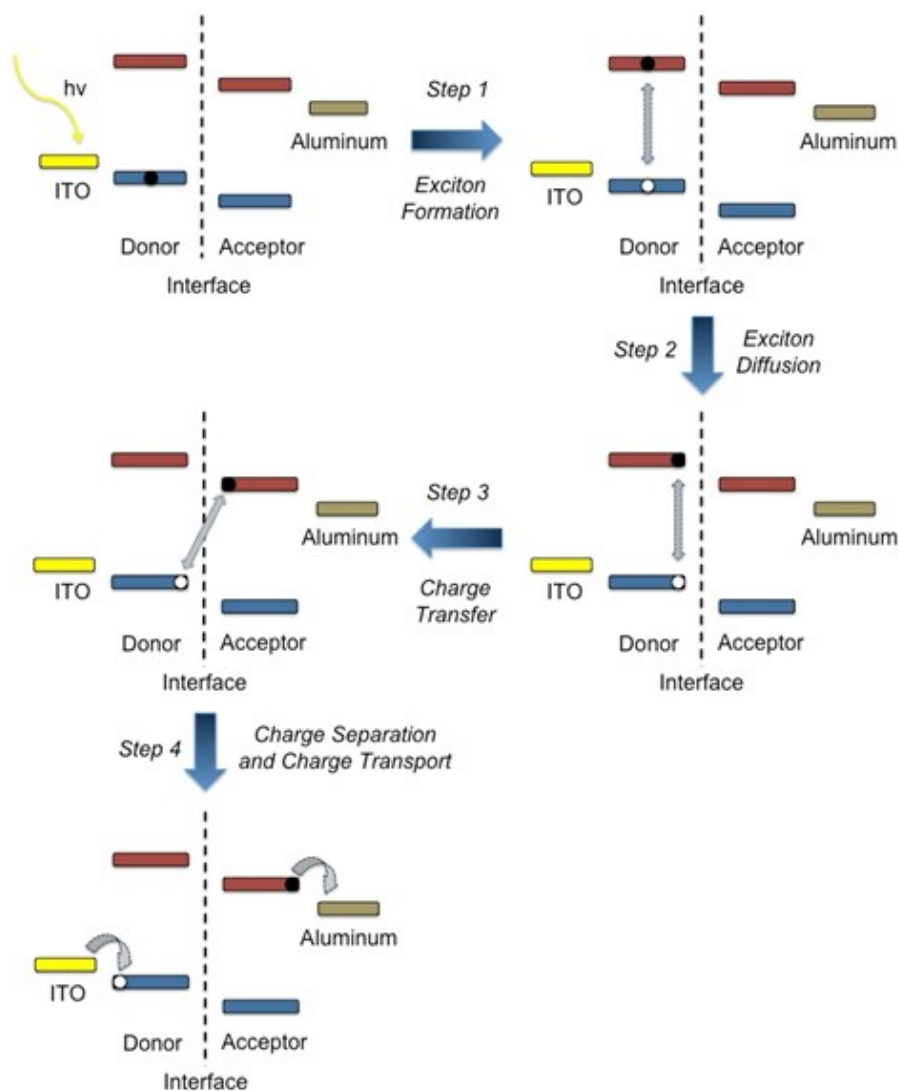


Figure 1.6: Schematic presentation of energy conversion in an organic solar cell (HOMO and LUMO levels are depicted in blue and red, respectively).

The performance of an organic solar cell depends on each of these four steps, and losses can occur at every step. When the exciton is formed, a couple of recombination pathways are available. Due to the limited lifetime and small exciton diffusion length, the exciton will decay before

24

dissociation can occur when it is created too far from the D-A interface. This is why bulk heterojunction devices are outperforming bi-layer solar cells. However, even after successful dissociation, geminate recombination of the bound electron pair is still possible, as well as bimolecular recombination of free charge carriers during transport to the electrodes. It is very important to have percolated pathways in the donor and acceptor materials, which can reduce the recombination losses before collection at the electrodes occurs.

1.4.1.2 Organic solar cell performance features

An organic solar cell is in general manufactured on a transparent substrate (mostly glass), which is coated with a high work function anode material such as indium tin oxide (ITO). A hole conducting material, most often poly(3,4-ethylenedioxythiophene):poly(styrene-sulfonate) (PEDOT:PSS) is deposited on top of the ITO layer to improve the contact properties. The PEDOT:PSS layer also provides a good wettability for the active layer and it smoothens the surface of the electrode. Afterwards, the active layer, consisting of donor and acceptor organic materials, can be deposited from solution. Numerous solution-processing techniques can be used, e.g. spin coating, spray coating, blade coating, meniscus coating, gravure printing or ink jet printing. These techniques offer OPV industry a cheap and rapid way of processing. On top of the active layer, a low work function cathode, e.g. consisting of calcium and aluminium, is deposited by thermal evaporation. An additional electron transport layer (ETL) can be placed

in between the active layer and the cathode to promote the extraction of the electrons.

Under illumination, a solar cell is evaluated by a series of parameters, i.e. the short-circuit current density (J_{sc}), the open-circuit voltage (V_{oc}), the fill factor (FF) and the power conversion efficiency (PCE) (**Figure 1.7**).

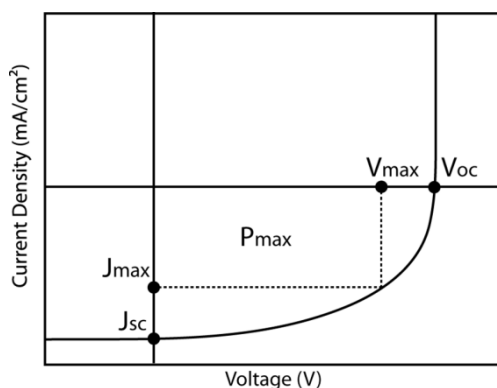


Figure 1.7: Current density-voltage curve of a solar cell under illumination.

The short-circuit current is the current flowing in the illuminated device at 0 V bias, and is the maximum current that a device is able to produce. The amount of current is determined by the number of excitons created during solar illumination and this is correlated to the overlap between the absorption spectrum of the solar cell and the solar spectrum. In other words, the current will be higher when more photons can be harvested, i.e. when the absorption window of the photoactive material is broader. The current is in this way dependent on the absorptivity and bandgap of the organic material, but also on the intensity of the sunlight, the thickness of the active layer and the excitation/charge collection

efficiency. The V_{oc} on the other hand is the maximum voltage measured when no current is flowing through the cell. The V_{oc} is connected to the energy difference between the HOMO level of the donor material and the LUMO level of the acceptor material.

The theoretical maximal power output (P_{theor}) delivered by a solar cell can be determined by the product of the maximum current, J_{sc} , and the maximum voltage, V_{oc} . The maximal power output (P_{max}) that is experimentally produced by a solar cell is given by the product of J_{max} and V_{max} , i.e. the current and the voltage at maximum power point. The FF is a useful quantity comparing the actual maximal power output to its theoretical maximum. In this way it shows how well an organic solar cell performs. The FF can be calculated by following formula:

$$FF = \frac{P_{max}}{J_{sc}V_{oc}} = \frac{J_{max}V_{max}}{J_{sc}V_{oc}}$$

Finally, the power conversion efficiency (PCE or η) shows the performance of the solar cell and is annotated as the ratio of the power that comes out of the device (P_{out} or P_{max}) to the total power input of photon irradiation. The efficiency of a solar cell can be calculated according to the following formula:

$$PCE (\eta) = \frac{P_{max}}{P_{in}} = \frac{J_{max}V_{max}}{P_{in}} = FF \frac{J_{sc}V_{oc}}{P_{in}}$$

One must be aware of using standard test conditions when reporting or comparing the efficiencies of solar cells. In general, the standard test conditions are specified by a temperature of 25 °C and an irradiation of 1000 W/m² with an air mass 1.5 (AM 1.5) spectrum. The AM 1.5 spectrum corresponds to the solar irradiation with the sun at 45° above the horizon.

1.5 Thesis overview

The general goal of the research work presented here was to use the Grignard methathesis (GRIM) polymerization route to synthesize regioregular functionalized (block) (co)polythiophenes, which could be modified after the polymerization protocol to enhance their solubility in more environmentally friendly solvents and to explore the possible applications of the novel materials in organic photovoltaics.

In **Chapter 2**, a series of random (co)polythiophene derivatives is synthesized and post-polymerization functionalization reactions are applied to obtain ionic (co)polythiophenes. Due to these polar functional groups, the solubility changes drastically and for some polymers ordered structures or “nanoaggregates” are observed in solution.

Chapter 3 describes the synthesis and application of polar polythiophenes with pendant ionic liquid-like side chains as a promising class of active layer materials for bi-layer organic solar cells. Due to the orthogonal solubility of the ionic P3AT derivatives and PCBM, it is possible to process bi-layer configurations from solution. Using these polymers in combination with PC₇₁BM as the acceptor, power

conversion efficiencies of 1.6% are achieved for these solution-processed simple bi-layer solar cells.

In **Chapter 4**, the application of an imidazolium-substituted ionic polythiophene as an electron transport layer (ETL) for polymer solar cells is reported. The ETL boosts the inherent I - V properties of the devices, resulting in a decrease in possible loss mechanisms and a gain in overall photovoltaic output (resulting in ~1% increase in PCE up to an average value of 6.2% for PCDTBT:PC₇₁BM-based devices).

In **Chapter 5**, the quasi-living GRIM polymerization method is used to synthesize ionic all-conjugated diblock copolymers. As in Chapter 2, first precursor block copolymers are synthesized in different building block ratios, followed by functionalization with *N*-methylimidazole toward the ionic derivatives.

Finally, in **Chapter 6**, general conclusions are drawn.

1.6 References

- 1 Natta, G.; Mazzanti, G.; Corradini, P. *Atti Accad. Naz. Lincei Cl. Sci. Fis. Mat. Nat. Rend.*, **1958**, 25, 3–12.
- 2 Chiang, C. K.; Druy, M. A.; Gau, S. C.; Heeger, A. J.; Louis, E. J.; MacDiarmid, A. G.; Park, Y. W.; Shirakawa, H. *J. Am. Chem. Soc.*, **1978**, 100(3), 1013–1015.
- 3 Burroughes, J. H.; Bradley, D. D. C.; Brown, A. R.; Marks, R. N.; Mackay, K.; Friend, R. H.; Burns, P. L.; Holmes, A. B. *Nature*, **1990**, 347, 539–541.
- 4 Yamamoto, T.; Sanechika, K.; Yamamoto, A. *J. Polym. Sci., Polym. Lett. Ed.*, **1980**, 18, 9–12.
- 5 Lin, J. W. P.; Dudek, L. P. *J. Polym. Sci., Polym. Chem. Ed.*, **1980**, 18, 2869–2873.
- 6 Jen, K. Y.; Oboodi, R.; Elsenbaumer, R. L. *Polym. Mater. Sci. Eng.*, **1985**, 53, 79–83.
- 7 McCullough, R. D.; Lowe, R. D. *J. Chem. Soc., Chem. Commun.*, **1992**, 1, 70–72.
- 8 Sheina, E. E.; Liu, J.; Iovu, M. C.; Laird, D. W.; McCullough, R. D. *Macromolecules*, **2004**, 37(10), 3526–3528.
- 9 (a) Chen, T. A.; Rieke, R. D. *J. Am. Chem. Soc.*, **1992**, 114(25), 10087–10088; (b) Chen, T. A.; O'Brien, R. A.; Rieke, R. D. *Macromolecules*, **1993**, 26(13), 3462–3463.
- 10 (a) Tamao, K.; Sumitani, K.; Kumada, M. *J. Am. Chem. Soc.*, **1972**, 94(12), 4374–4376; (b) Tamao, K.; Miyaura, N. *Cross-Coupling Reactions*, **2002**, 219, 1–9.
- 11 Loewe, R. S.; Ewbank, P. C.; Liu, J.; Zhai, L.; McCullough, R. D. *Macromolecules*, **2001**, 34, 4324–4333.
- 12 Yokoyama, A.; Miyakoshi, R.; Yokozawa, T. *Macromolecules*, **2004**, 37(4), 1169–1171.
- 13 Miyakoshi, R.; Yokoyama, A.; Yokozawa, T. *Macromol. Rapid Commun.*, **2004**, 25(19), 1663–1666.
- 14 Lohwasser, R. H.; Thelakkat, M. *Macromolecules*, **2011**, 44(9), 3388–3397.

-
- 15 (a) Jeffries-EL, M.; Sauv , G.; McCullough, R. D. *Adv. Mater.*, **2004**, 16(12), 1017–1019; (b) Jeffries-El, M.; Sauv , G.; McCullough, R. D. *Macromolecules*, **2005**, 38(25), 10346–10352.
- 16 Liu, J.; Sheina, E.; Kowalewski, T.; McCullough, R. D. *Angew. Chem. Int. Ed.*, **2002**, 41(2), 329–332.
- 17 Iovu, M. C.; Jeffries-El, M.; Sheina, E. E.; Cooper, J. R.; McCullough, R. D. *Polymer*, **2005**, 46(19), 8582–8586.
- 18 Iovu, M. C.; Sheina, E. E.; Gil, R. R.; McCullough, R. D. *Macromolecules*, **2005**, 38(21), 8649–8656.
- 19 (a) Wu, P.-T.; Ren, G.; Li, C.; Mezzenga, R.; Jenekhe, S. A. *Macromolecules*, **2009**, 42(7), 2317–2320; (b) Ge, J.; He, M.; Qiu, F.; Yang, Y. *Macromolecules*, **2010**, 43(15), 6422–6428; (c) Verswyvel, M.; Monnaie, F.; Koeckelberghs, G. *Macromolecules*, **2011**, 44(24), 9489–9498.
- 20 (a) Miyakoshi, R.; Yokoyama, A.; Yokozawa, T. *Chem. Lett.*, **2008**, 37(10), 1022–1023; (b) Wu, S.; Bu, L.; Huang, L.; Yu, X.; Han, Y.; Geng, Y.; Wang, F. *Polymer*, **2009**, 50(26), 6245–6251.
- 21 (a) Stefan, M. C.; Javier, A. E.; Osaka, I.; McCullough, R. D. *Macromolecules*, **2009**, 42(1), 30–32; (b) Javier, A. E.; Varshney, S. R.; McCullough, R. D. *Macromolecules*, **2010**, 43(7), 3233–3237.
- 22 (a) Kim, J.; Song, I. Y.; Park, T. *Chem. Commun.*, **2011**, 47(16), 4697–4699; (b) Song, I. Y.; Kim, J.; Im, M. J.; Moon, B. J.; Park, T. *Macromolecules*, **2012**, 45(12), 5058–5068.
- 23 Lee, E.; Hammer, B.; Kim, J. K.; Page, Z.; Emrick, T.; Hayward, R. C. *J. Am. Chem. Soc.*, **2011**, 133(27), 10390–10393.
- 24 Chayer, M.; Fa d, K.; Leclerc, M. *Chem. Mater.*, **1997**, 9(12), 2902–2905.
- 25 Ho, H. A.; Leclerc, M. *J. Am. Chem. Soc.*, **2003**, 125(15), 4412–4413.
- 26 Burns, C. T.; Lee, S.; Seifert, S.; Firestone, M. A. *Polym. Adv. Tech.*, **2008**, 19(10), 1369–1382.
- 27 Ewbank, P. C.; Loewe, R. S.; Zhai, L.; Reddinger, J.; Sauv , G.; McCullough, R. D. *Tetrahedron*, **2004**, 60(49), 11269–11275.

Chapter 1

- 28 Bondarev, D.; Zedník, J.; Šloufová, I.; Sharf, A.; Procházka, M.; Pflieger, J.; Vohlídal, J. *J. Polym. Sc. Part A: Polym. Chem.*, **2010**, 48(14), 3073–3081.
- 29 Clément, S.; Tizit, A.; Desbief, S.; Mehdi, A.; De Winter, J.; Gerbaux, P.; Lazzaroni, R.; Boury, B. *J. Mater. Chem.*, **2011**, 21(8), 2733.
- 30 Becquerel, A. E. *Comptes Rendus*, **1839**, 9, 561.
- 31 Green, M. A.; Emery, K.; Hishikawa, Y.; Warta, W.; Dunlop, E. D. *Prog. Photovolt: Res. Appl.*, **2012**, 20, 12–20.
- 32 Jäger-Waldau, A. *PV Status Report*, **2012**, 1–48.
- 33 Sun, Y.; Welch, G. C.; Leong, W. L.; Takacs, C. J.; Bazan, G. C.; Heeger, A. J. *Nat. Mater.*, **2012**, 11(1), 44–48.
- 34 Yella, A.; Lee, H.-W.; Tsao, H. N.; Yi, C.; Chandiran, A. K.; Nazeeruddin, M. K.; Diau, E. W.-G.; Grätzel, M. *Science*, **2011**, 334(6056), 629–634.
- 35 Lee, M. M.; Teuscher, J.; Miyasaka, T.; Murakami, T. N.; Snaith, H. J. *Science*, **2012**, 338, 643–647.
- 36 Tang, C. W. *Appl. Phys. Lett.*, **1986**, 48(2), 183–185.
- 37 Sariciftci, N. S.; Braun, D.; Zhang, C.; Srdanov, V. I.; Heeger, A. J.; Stucky, G.; Wudl, F. *Appl. Phys. Lett.*, **1993**, 62(6), 585–587.

Chapter 2

Imidazolium-substituted ionic (co)polythiophenes: compositional influence on solution behavior and thermal properties

Ghoos, T.; Brassinne, J.; Fustin, C.-A.; Gohy, J.-F.; Defour, M.; Van den Brande, N.;
Van Mele, B.; Lutsen, L.; Vanderzande, D. J.; Maes, W. manuscript submitted to
Polymer

2.1 Introduction

The field of organic photovoltaics (OPV) has grown spectacularly in the past few years, inspired by the appealing prospects of this emerging renewable technology, such as simple preparation, aesthetics, low weight and mechanical flexibility, semi-transparency and better performance under diffuse light conditions.¹ In contrast to traditional silicon-based solar cells, solution-processability of the active layer materials allows low-cost large-area thin film fabrication by e.g. roll-to-roll (R2R) printing. For polymer solar cells, bulk heterojunction (BHJ) architectures – based on a blend comprising a conjugated electron donor polymer and a (mostly fullerene-based) electron acceptor material – have afforded single junction power conversion efficiencies approaching 10%.² Major remaining issues to allow OPV to grow to a mature and market-competitive PV technology are solar cell module efficiency and reliability. Moreover, there is a clear need for next generation PV technologies to allow printability from ‘green’ or less environmentally imposing solvents.³ Solubility of the active layer materials in more benign solvents, e.g. alcohols and ultimately water, can be achieved by the addition of polar moieties, either neutral or charged, to the (side chains of the) organic semiconductor structures. The traditional approach was to introduce oligo(ethylene glycol) patterns in the polymer and/or fullerene side chains, but this is generally accompanied by a strong reduction in glass transition temperature (T_g), limiting the stability of the required intimately mixed donor–acceptor BHJ blend morphology. By the introduction of ionic entities on the backbone of conjugated polymers, which is most straightforward in the side chains,

conjugated polyelectrolytes (CPEs) are obtained,⁴ a class of organic semiconducting materials combining the unique optical and electrical properties of conjugated polymers with the ionic features of the charged side chain end groups. Due to the appended ionic moieties, CPEs generally show a good solubility in polar solvents and sometimes also in water. On the other hand, the increased polarity also gives rise to a higher dielectric constant, which has been considered as a possible pathway to a new efficiency regime for OPV.⁵ Recently, a number of CPEs have shown impressive results as charge injection and/or transport layers in organic solar cell stacks.⁶ The optoelectronic properties of CPEs are particularly dependent on their molecular conformation and structural organization, both in solution and in the solid state.⁷ Water-soluble polyfluorene CPEs were for instance shown to form rod-like aggregates in water, a process driven by the highly hydrophobic fluorene backbone and the hydrophilic side chains carrying charged quaternary amines.^{7a}

In the OPV field, poly(3-hexylthiophene) or P3HT is by far the most widely used conjugated polymer donor material.⁸ More advanced polythiophene derivatives, e.g. end-group or side-chain functionalized and statistical or block copolymer structures, have been synthesized toward morphology control and stability.⁹ Conjugated polyelectrolytes based on ionic polythiophenes, realized via the introduction of pendant ionic functionalities on the alkyl side chains, have scarcely been reported and some of these have shown high potential as interlayer materials.^{6b,e,10} In this paper, we report on the synthesis and physicochemical characterization of a large family of polythiophene-based CPEs, both

homopolymers and random copolymers, varying in the side chain composition, building block ratio and counter ions, toward a better fundamental understanding of the structure-property relations of these derivatives in OPV applications, essential to achieve further progress in the field. Before evaluation of all novel materials in organic solar cells, either as components of the photoactive layer or as interlayer materials (in continuation of recent promising results obtained with model compounds of the same family),^{3e,6e} proper material analysis is essential. To get a feeling of the solution behavior of the (co)polymers in environmentally more acceptable solvents, their solution properties are screened by UV–Vis and dynamic light scattering (DLS) studies. On the other hand, film properties are analyzed by UV–Vis experiments combined with thermal analysis.

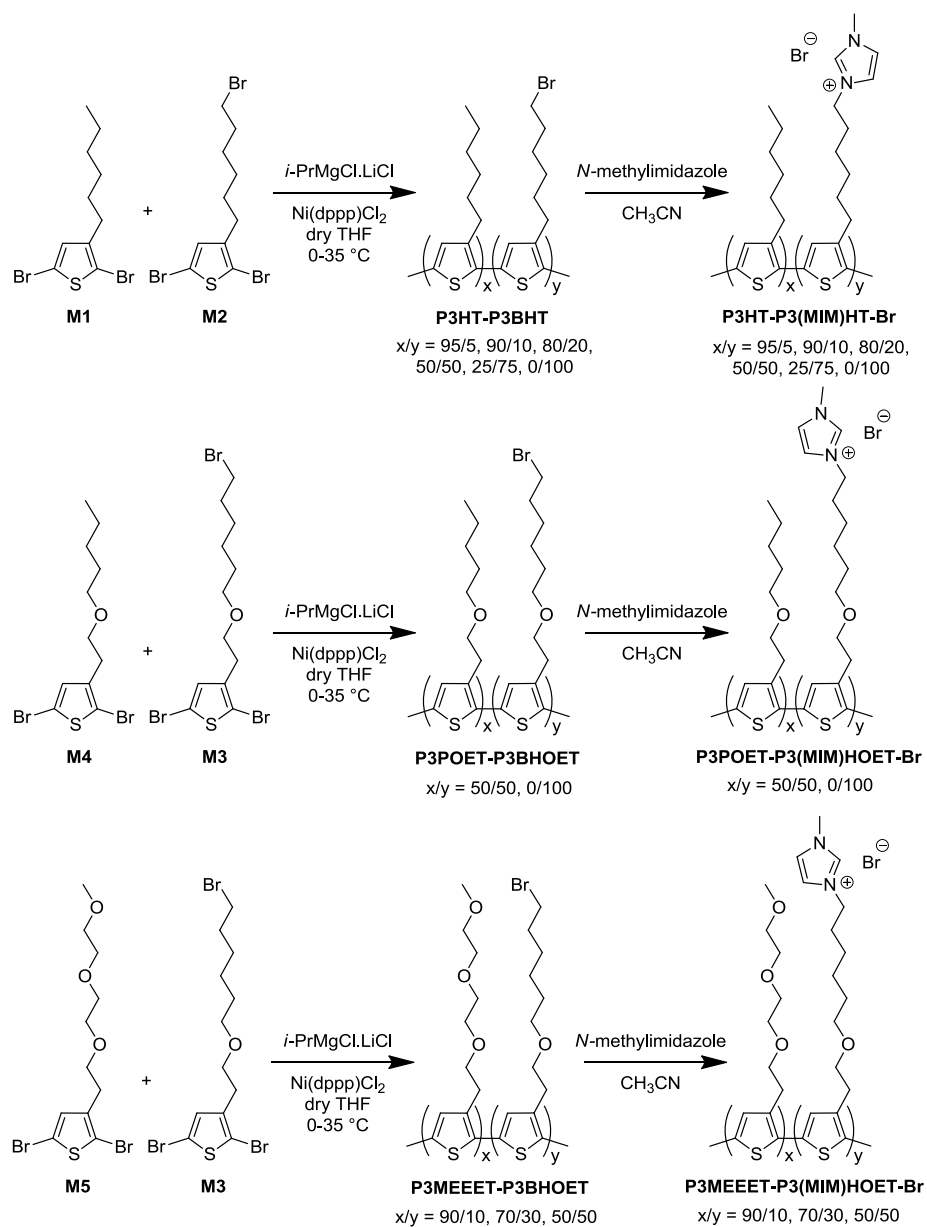
2.2 Results and discussion

2.2.1 Polymer synthesis and characterization

To synthesize highly regioregular ionic copolythiophenes we have chosen a stepwise procedure, first preparing the non-ionic precursor copolymers by an adapted GRIM polymerization procedure^{8,11} followed by a subsequent substitution reaction on the bromoalkyl side chains with *N*-methylimidazole, affording polar 6-(1-methylimidazolium-3-yl)alkyl side chains with bromine counter ions (**Scheme 2.1**).^{10b} In this approach, the regioregularity is already determined in the precursor polymers and the functionalization of the latter with ionic moieties does not affect this anymore. The homopolymers were also prepared for comparison. Besides the common 2,5-dibromo-3-hexylthiophene (**M1**), four other

dibromothiophene monomers **M2–M5** were applied as well to increase the structural diversity (**Scheme 2.1**). These building blocks were chosen based on the expected variation in solubility and/or thermal properties, taking into account synthetic ease and availability.

First of all, a series of poly[(3-hexylthiophene-2,5-diyl)-*co*-(3-(6-bromohexyl)thiophene-2,5-diyl)] (**P3HT-P3BHT**) copolymers was prepared (**Scheme 2.1**). Different monomer feed ratios were applied, affording the precursor polymers in 95/5, 90/10, 80/20, 50/50, 25/75 and 0/100 molar ratios. The copolymers were purified by soxhlet extractions with methanol, *n*-hexane and chloroform, respectively, and finally precipitated in methanol. The isolated polymer yields were around 60%, which is fairly high considering the inherent 15–25% monomer loss due to non-selective transmetalation, with molecular weight averages $M_n = 1.5\text{--}3.3 \times 10^4$ (**Table 2.1**). Although the GRIM polymerization method is rather sensitive to traces of moisture and impurities in the monomer composition, polythiophenes with rather narrow polydispersity indices (PDI) were obtained in a reproducible fashion (**Table 2.1**).



Scheme 2.1: Synthesis of the ionic (co)polythiophene materials.

Imidazolium-substituted ionic (co)polythiophenes

Table 2.1: Characterization data for the precursor (co)polymers.

Polymer	M_n (kDa)	M_w (kDa)	PDI	Yield (%)	Ratio ^a
P3HT/P3BHT 95/5	23	29	1.3	68	/ ^b
P3HT/P3BHT 90/10	28	40	1.5	63	85/15
P3HT/P3BHT 80/20	33	56	1.7	68	77/23
P3HT/P3BHT 50/50	29	32	1.1	57	52/48
P3HT/P3BHT 25/75	15	25	1.7	53	22/78
P3BHT	30	40	1.3	64	/
P3POET/P3BHOET 50/50	11	19	1.7	48	53/47
P3BHOET	18	31	1.7	57	/
P3MEEET/P3BHOET 90/10	20	24	1.2	68	/ ^c
P3MEEET/P3BHOET 70/30	33	45	1.4	23	/ ^c
P3MEEET/P3BHOET 50/50	34	64	1.8	55	/ ^c

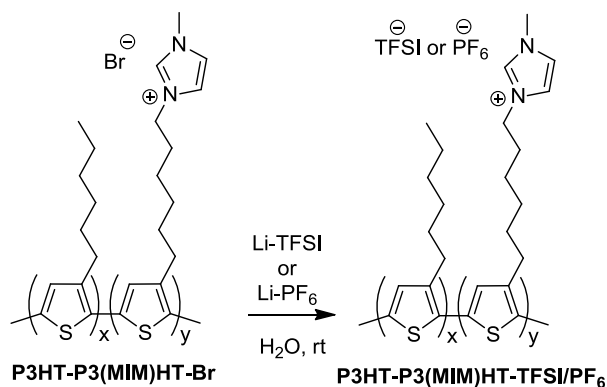
^a As determined by ¹H NMR. ^b Hard to identify to the low content of the second monomer. ^c Impossible to resolve due to overlapping signals.

In the next phase, the **P3HT-P3BHT** precursor polymers were converted to ionic polymers by treatment with *N*-methylimidazole. Functionalization was rather slow when traditional heating was used.^{10b} The reaction needed 48 h to ensure complete conversion to the ionic poly[(3-hexylthiophene-2,5-diyl)-*co*-(3-(6-(*N*-methylimidazolium)-hexyl)thiophene-2,5-diyl)] (**P3HT-P3(MIM)HT-Br**) derivatives (**Scheme 2.1**). When microwave irradiation was applied, the reaction time could be significantly reduced to 4 h (in acetonitrile as a solvent at 100 °C). The resulting ionic polymers were precipitated in the non-solvent diethyl ether, washed several times and used further without any other purification.

From ^1H NMR analysis of both the precursor and ionic copolymers (see SI and **Table 2.1**), one can easily notice that the ratio of the two monomers in the polymers is in good agreement with the feed ratio. The efficiency of the functionalization reaction can also be verified by ^1H NMR, by following the shift of the protons on the side-chain carbon atoms next to the end groups, going from ~ 3.4 ppm for the **P3HT-P3BHT** copolymers to ~ 4.2 ppm for the **P3HT-P3(MIM)HT** copolymers.

It is known that imidazolium-type ionic liquids with bromine counter ions are hygroscopic and only fairly soluble in most common (low to medium polarity) organic solvents.¹² For that reason we have exchanged the bromine counter ions for some of the ionic polymers to bis(trifluoromethanesulfonyl)imide (TFSI) and/or hexafluorophosphate (PF_6^-) counter ions, which are known to be more hydrophobic (**Scheme 2.2**).¹³ The anion exchange procedures are rather easy. The copolymers were dissolved in water and a Li-TFSI or Li- PF_6 solution was added drop wise. The resulting precipitates were filtered on a cellulose membrane, washed and dried *in vacuo*. The relevance of the counter ions for OPV applications has already been demonstrated previously.^{3e} Upon exchanging the bromine counter ions of the **P3(MIM)HT-Br** homopolymer for TFSI, the material became more soluble in solvents suitable for bi-layer processing, resulting in neat films as prepared by meniscus coating from 2,2,3,3-tetrafluoro-1-propanol (TFP). The counter ions are also of particular relevance when one desires to take additional advantage of ionic movement to assist in the charge separation process.¹⁴

Imidazolium-substituted ionic (co)polythiophenes



Scheme 2.2: General counter ion exchange procedure.

To broaden the structural variations, some other ionic (co)polythiophene derivatives were also synthesized in an analogous way to allow fine tuning of the polymer polarity and the solution behavior. At first, one of the side-chain carbon atoms was replaced by an oxygen atom, affording two poly[(3-(pentyloxyethyl)thiophene-2,5-diyl)-*co*-(3-(6-bromohexyloxy)ethyl)thiophene-2,5-diyl] or **P3POET-P3BHOET** (co)polymers (50/50 and 0/100; **Scheme 2.1**). This small change can already afford a quite different solubility, crystallinity and stacking ability. To render the (co)polythiophenes even more soluble in polar solvents, a triethylene glycol-type side chain was incorporated, resulting in poly[(3-(((methoxyethoxy)ethoxy)ethyl)thiophene-2,5-diyl)-*co*-(3-(6-bromohexyloxy)ethyl)thiophene-2,5-diyl] or **P3MEEET-P3BHOET** copolymers (90/10, 70/30 and 50/50; **Scheme 2.1**). For the purification of the latter precursor copolymers, standard soxhlet purification with methanol was not possible as too much of the polymer dissolved under these conditions. Recycling size exclusion chromatography in chloroform was used to get rid of small amounts of lower molecular

weight species. For both precursor copolymer series, a more restricted number of (proof-of-principle) feed ratios was applied. Standard characterization data are gathered in **Table 2.1**. The precursor polymers were again smoothly converted to the imidazolium-functionalized ionic copolythiophenes (**Scheme 2.1**) and for some derivatives bromine-TFSI counter ion exchange was performed as well (see exp. part).

2.2.2 Solution behaviour

The different sets of ionic (co)polythiophenes were then subjected to preliminary solubility tests, starting with the extended series of **P3HT-P3(MIM)HT-Br** (co)polymers. The materials with a high amount (> 50%) of ionic moieties were soluble in polar solvents such as water, methanol (and other alcohols), *N,N*-dimethylformamide (DMF) and dimethyl sulfoxide (DMSO). The derivatives with a lower amount (50–25%) of functionalized side chains were less soluble in these solvents, but could generally be dissolved in a mixture of a polar and an apolar solvent. The copolymers with a low amount of ionic groups (< 25%) were not soluble anymore in the range of polar solvents as outlined above, but they became soluble in pristine P3HT solvents such as chloroform and tetrahydrofuran (THF). Within this series, one derivative showed a quite particular behavior and was therefore explored in somewhat more detail. The **P3HT-P3(MIM)HT-Br 50/50** random copolymer was not directly soluble in water nor THF, but it could be dissolved in a range of THF/water mixtures (**Figure 2.1**). One can easily see that the solution darkens upon increasing the water content, which

can be regarded as an indication of aggregation or organization of the polymer chains in solution.¹⁵

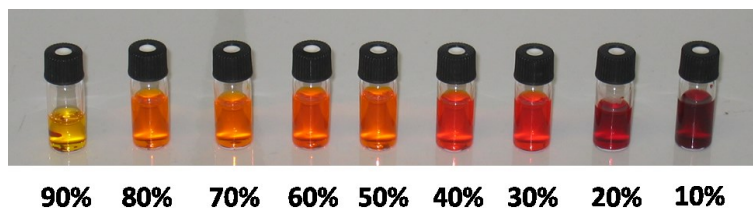


Figure 2.1: Solutions of **P3HT-P3(MIM)HT-Br 50/50** in THF/water mixtures (from 90 to 10% THF in water).

By converting the **P3(MIM)HT-Br** homopolymer to the **P3(MIM)HT-TFSI** analogue, the polymer was not soluble anymore in water, but it gained solubility in acetone and acetonitrile. When the same polymer was converted to **P3(MIM)HT-PF₆**, similar effects were observed. The polymer could not be dissolved in MeOH anymore but it was found soluble in some more apolar alcohols such as TFP.

For the **P3POET-P3(MIM)HOET-Br** materials, the solution behavior was very similar. The solubility of the more polar **P3MEEET-P3(MIM)HOET-Br** copolymers was, however, strikingly different, as these polymers were already soluble in polar solvents at the precursor stage, i.e. without the ionic groups in place.

2.2.2.1 UV-Vis absorption studies

The results of these initial solubility tests were then substantiated by UV-Vis absorption studies. McCullough and coworkers previously

observed that P3HT can self-assemble into a supramolecular or lamellar structure,^{15a} in which the planarized chains stack onto each other due to intermolecular π -interactions of the aromatic polymer backbone. This organization gives rise to a bathochromic shift and a vibronic structure at higher wavelengths. The absorption spectrum of aggregated P3HT was later on reported to consist of three chromophores:^{15b} one band related to the polymer in its disordered random coil-like conformation (~450 nm), a second transition from the individual planar stacked polymer chains (~550 nm, with vibronic finestructure), and a third transition due to a transition dipole moment delocalized over multiple aggregated polymer chains (~604 nm for P3HT).

In the UV–Vis absorption spectra of the different ionic (co)polymers, the same red shift and finestructure as for regular P3HT were observed, depending on the solvent used. Some absorption spectra for the **P3HT-P3(MIM)HT-Br** (co)polythiophene series are shown in **Figure 2.2**. One can see that MeOH is a good solvent for the ionic homopolymer and the **25/75** copolymer by the fact that only the random coil-like band was observed. A definite band broadening was observed when the **50/50** copolymer was dissolved in MeOH. A comparable spectrum was obtained when the same polymer was dissolved in a 20/80 (vol/vol) THF/water mixture. These solvents apparently already promote individual stacking of the polymer chains. When a 10/90 THF/water solvent mixture was used, the color of the solution changed to ‘Bordeaux’ red and a vibronic finestructure appeared in the absorption spectrum, most probably due to the formation of larger aggregates of different polymer chains. The **80/20** copolymer could not be dissolved in

pure MeOH. In DMSO, however, the absorption spectrum again showed the vibronic finestructure (and even more pronounced). In this solvent, the polymer is definitely aggregated into supramolecular structures. The 10% ionic copolymer (**90/10**) could only be dissolved in THF and chloroform and the spectra point toward a random coil-like conformation in these solutions.

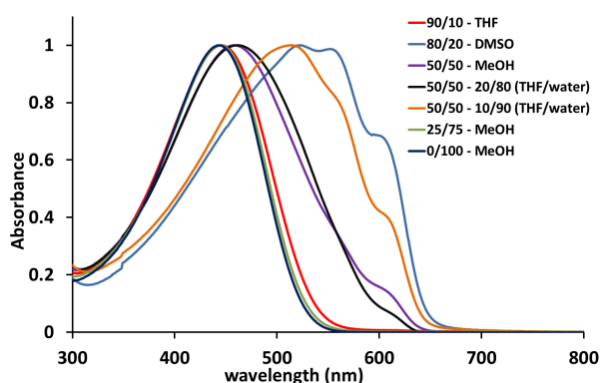


Figure 2.2: Absorption spectra (normalized) for the **P3HT-P3(MIM)HT-Br** series in different solvents.

The self-assembly behavior of the ionic **P3HT-P3(MIM)HT-Br 50/50** copolythiophene was then investigated in different THF/water mixtures to enable comparison with the color changes as observed before (see **Figure 2.1**). The solution behavior was found to depend on the way the solutions were prepared. **Figure 2.3a** shows the evolution starting from dissolution of the copolymer in a good solvent mixture (30/70 THF/water) to which water was gradually added to trigger the formation of aggregates. For comparison, the copolymer was also dissolved in a 10/90 THF/water mixture to which THF was gradually added (**Figure 2.3b**). Although one would expect the same absorption profiles for the

two different experiments, this was clearly not the case. In the first experiment the polymer was molecularly dissolved in the initial 30/70 THF/water mixture and when the solvent quality was gradually decreased, the absorption band slightly broadened but did not show any vibronic bands at higher wavelengths. In the second experiment the polymer was initially ‘dissolved’ in a 10/90 THF/water solvent mixture and vibronic finestructure was already present from the start. When THF was added the absorption band underwent a hypsochromic shift toward the absorption profile of molecularly dissolved polythiophene (with $\lambda_{\max} = 450$ nm), without any noticeable vibronic bands. When the **50/50** random copolymer is dissolved in a bad solvent, the stacked or ordered structure as present in the solid state is apparently maintained. On the other hand, the same structure cannot be reached when the polymer is first molecularly dissolved in a good solvent.

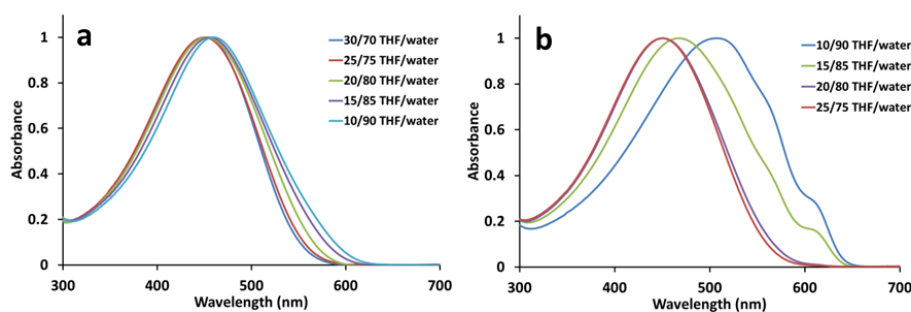


Figure 2.3: Aggregation behavior of P3HT-P3(MIM)HT-Br 50/50 in THF/water mixtures a) starting from 30/70 THF/water, and b) starting from 10/90 THF/water.

2.2.2.2 DLS experiments

To achieve further insights on the behavior of the ionic polymers in different solvents and trying to identify the nature of the objects present in solution - such as molecularly dissolved chains (unimers), aggregates or ordered structures - DLS experiments were performed.

To investigate the effect of water on the formation of aggregates, the **P3HT-P3(MIM)HT-Br 50/50** copolymer was first dissolved, at 1 g/L, in a 80/20 THF/water mixture, and water was added to reach an equivolume THF/water mixture. At this point, the quality of the solvent mixture favors complete dissolution of the copolymer, as shown by the UV-Vis studies. This was also confirmed by the DLS measurements since this sample emitted only a very weak scattered intensity characteristic of isolated chains. Water was then further added to gradually reach a 10/90 THF/water mixture. The evolution of the scattered intensity was monitored and is shown in **Figure 2.4**. At a 30/70 composition, only a small increase of the scattered intensity was observed, and a 20/80 composition had to be reached to induce a clear increase of the signal, indicating the aggregation of the polymer chains. This is again in good agreement with the UV-Vis studies since a clear color change was observed for the 20/80 solvent composition (see **Figure 2.1**). Despite this increase, the scattered intensity remained rather low, even for a 10/90 mixture, and it was difficult to obtain a reliable size measurement. A broad and ill-resolved bimodal size distribution was obtained by a Contin analysis, showing a first population with an apparent hydrodynamic radius (R_h) around 7 nm and a second one around 250 nm. This indicates that water-rich solvent mixtures can

indeed induce the formation of aggregates, but that these aggregates are probably highly swollen by solvent. More specifically, the hydrophobic part of the aggregates would be swollen by THF, which is a good solvent for the non-charged part of the copolymer. The low intensity of the measured scattered intensity is in line with the formation of such swollen aggregates. To further prove this point, the 10/90 THF/water solution was dialyzed against pure water to remove THF and de-swell the aggregates. DLS measurements revealed a size distribution with three well-defined populations around 10, 75 and 380 nm (**Figure 2.5**).

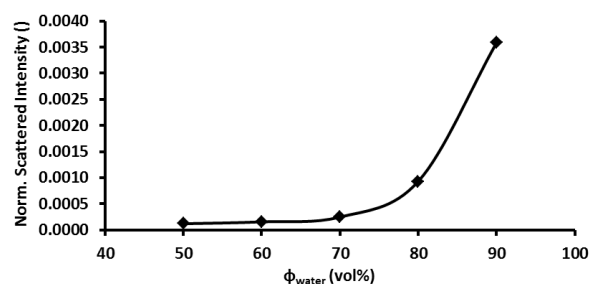


Figure 2.4: Evolution of the normalized scattered intensity for the **P3HT-P3(MIM)HT-Br 50/50** copolymer solutions with an increasing water content.

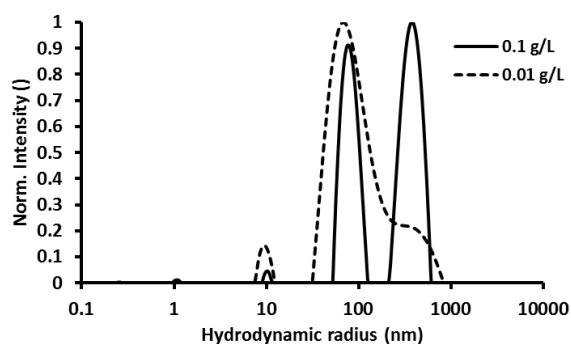


Figure 2.5: Size distribution histogram after dialysis of the **P3HT-P3(MIM)HT-Br 50/50** copolymer prepared by sequential addition of water.

The absence of unimer chains arises from the poor solubility of the 50% ionic polythiophene in pure water, which thus exclusively forms self-assembled structures. The peak at 10 nm could be assigned to isolated particles, while the one around 75 nm could be attributed to clusters of particles. Finally, the last population around 380 nm could be related to the so-called ‘polyelectrolyte’ effect since half of the repeating units of the copolymer bears a charged imidazolium group. To clarify this situation, the sample was further diluted to reach a concentration of about 0.01 g/L. At such a low concentration, the first two populations remained almost unchanged, whereas the intensity of the population around 380 nm decreased strongly (**Figure 2.5**), providing thus an additional hint that this population might be due to a polyelectrolyte effect.

2.2.3 Solid-state properties

2.2.3.1 Optical properties in film

When UV–Vis spectra were taken for films of the **P3HT-P3BHT** precursor (co)polymers, prepared by drop-casting from a chloroform solution, a difference depending on the percentage of functionalized side chains was observed. For the lower percentages (*i.e.* 5–20 mol%) of bromine-functionalized hexyl side chains, the typical finestructure was observed at higher wavelengths (**Figure 2.6**), resembling the π - π stacking properties of pristine P3HT. However, when the amount of bromine end groups was increased to 50%, a distinct shift was observed. The maxima at 558 and 605 nm almost completely disappeared. For the 100% **P3BHT** polymer the effect was even more pronounced and the

finestructure was completely absent (**Figure 2.6a**). This difference is also visible by the naked eye, as the **P3BHT** film is red compared to dark purple for the 5–20% copolymer films. This behavior can probably be related to the fact that the higher amount of bromine groups disturbs the stacking ability of the polythiophene backbone (*vide infra*). For the **P3POET-P3BHOET** precursor series, a less pronounced effect was observed (**Figure 2.6b**), but overall it is clear that more bromine functions lead to more amorphous materials (in film).

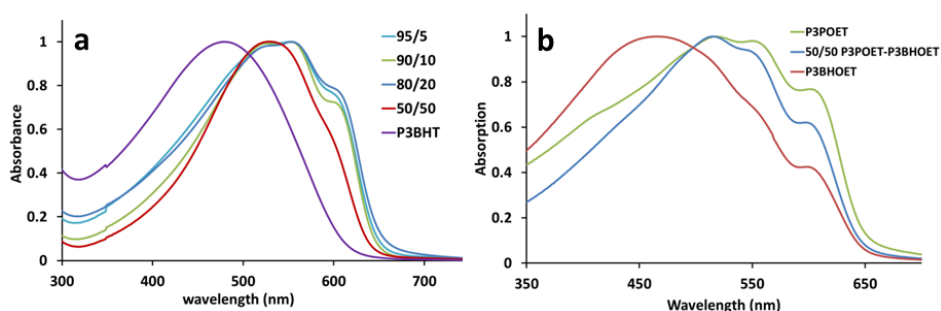


Figure 2.6: Absorption spectra for the different precursor copolymer films of the a) **P3HT-P3BHT** and b) **P3POET-P3BHOET** series.

After functionalization to yield the 5 and 10% **P3HT-P3(MIM)HT-Br** ionic copolymers, the materials were still soluble in chloroform. Therefore it is possible to compare their film-forming properties with those of the precursor polymers casted from the same solvent. Upon comparison of the UV–Vis spectra, a clear difference can be observed (**Figure 2.7**). The vibronic finestructure completely disappeared for the ionic polymer films and only one single band was observed with λ_{\max} around 460–480 nm.

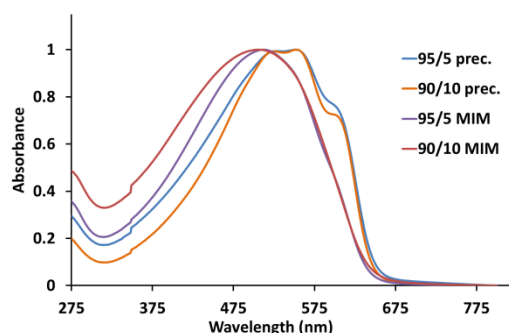


Figure 2.7: Comparison of UV–Vis absorption spectra (in film) as obtained from the **P3HT-P3BHT** and **P3HT-P3(MIM)HT-Br 95/5** and **90/10** copolymers (as casted from CHCl_3).

The polythiophenes with a higher ratio of ionic moieties, such as the **P3HT-P3(MIM)HT-Br 50/50** copolymer and the **P3(MIM)HT-Br** homopolymer, were not soluble in chloroform, impeding facile comparison with the non-ionic precursor polymers, but they could be drop-casted from MeOH. The solid-state absorption spectra were as expected (**Figure 2.8a**), with a narrow band peaking at 473 nm for the **P3(MIM)HT-Br** homopolymer, resembling the non-structured form of P3HT, and a maximum at 515 nm and some distinct shoulders for the **50/50** copolymer, representing the π -stacking of the polythiophene. A strong ‘solvent annealing’ effect was observed for the **P3(MIM)HT-Br** film after treatment of the film with some drops of chloroform (**Figure 2.8b**), with a red-shift toward $\lambda_{\text{max}} = 510$ nm, pointing to structural (re)ordering within the film. On the other hand, a small blue-shift ($\lambda_{\text{max}} = 506$ nm) and disappearance of the fine structure was apparent for the **P3HT-P3(MIM)HT-Br 50/50** film.

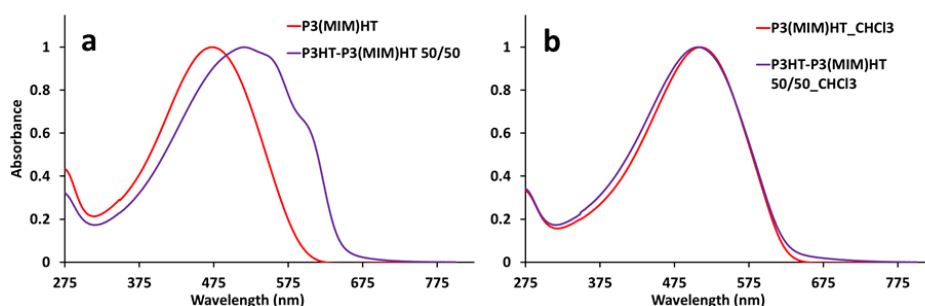


Figure 2.8: UV-Vis spectra for **P3(MIM)HT-Br** and **P3HT-P3(MIM)HT-Br 50/50** films a) as-casted from MeOH solution and b) after chloroform treatment.

This behavior is different from the annealing effect as observed in the **P3POET-P3(MIM)HOET-Br** series. A broad band was seen for the pristine **P3(MIM)HOET-Br** homopolymer film (as casted from MeOH), whereas a finestructure at higher wavelength was visible for the **P3POET-P3(MIM)HOET-Br 50/50** film (**Figure 2.9a**). After treatment with chloroform, both the spectra were red-shifted and the finestructure became more pronounced (**Figure 2.9b**). This difference with the **P3HT-P3(MIM)HT-Br** polymers might be related to a higher mobility of the side chains, a different stacking behavior and/or the lower molecular weights of the **P3POET-P3(MIM)HOET-Br** polymers (**Table 1**).

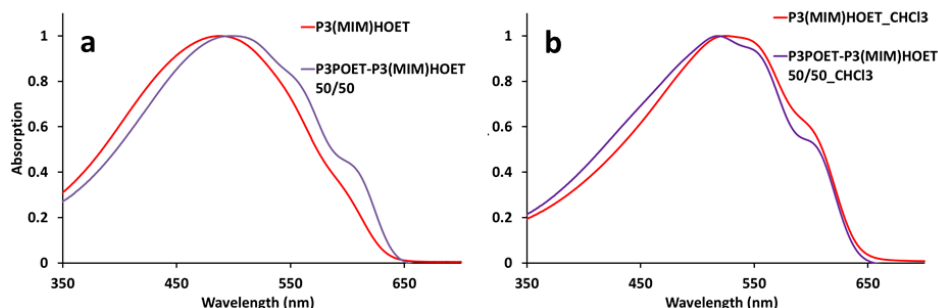


Figure 2.9: UV-Vis spectra for **P3(MIM)HOET-Br** and **P3POET-P3(MIM)HOET-Br 50/50** films a) as casted from MeOH solution and b) after chloroform treatment.

2.2.3.2 Thermal stability

Information regarding thermal stability and crystallinity of active layer materials is of high relevance when looking at applications in organic solar cells. Basic thermal analysis is also a prerequisite to construct phase diagrams of the donor-acceptor active layer blends, from which fundamental understanding of the formation and evolution of the bulk heterojunction blend morphology can be deduced.¹⁸ A thermal stability study using thermogravimetric analysis (TGA) was performed on a selection of the materials described above. The thermal stability of the **P3HT-P3BHT** precursor copolymers was reduced compared to pure P3HT, owing to the loss of the bromine end groups at ~ 240 °C (**Figure 2.10**). **P3BHOET**, **P3POET-P3BHOET 50/50** and **P3MEEET-P3BHOET 70/30** precursor materials all showed a thermal stability similar to **P3BHT**, with a mass loss at ~ 240 °C, although a larger fraction is lost in these materials. After functionalization of the **P3HT-P3BHT** precursors with *N*-methylimidazole, the **P3HT-P3(MIM)HT-Br** material remained stable up to about 280 °C, indicating an increased thermal stability. It should be noted, however, that a small early mass

loss was detected, which can be ascribed to water leaving the material. This confirms the expected hygroscopic properties related to the introduction of the methylimidazole functionality combined with a bromine counter ion. A more dramatic stabilization was found for the **P3(MIM)HOET** homopolymer, which remained stable well over 350 °C.

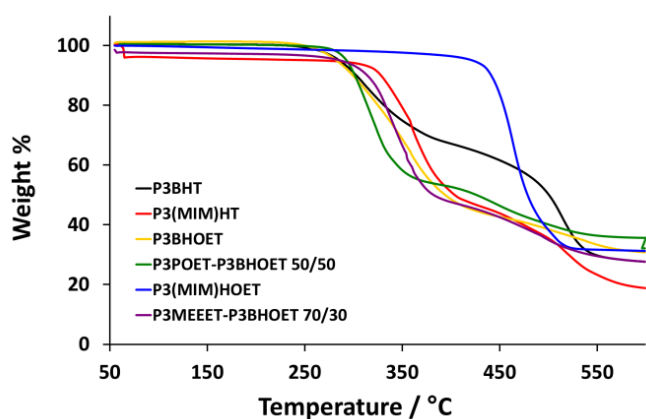


Figure 2.10: TGA curves depicting the mass loss of selected materials at 20 K min⁻¹.

2.2.3.3 Thermal transitions

The **P3HT-P3BHT** precursor materials showed a clear semi-crystalline behavior, with a broad glass transition followed by a double melting peak (**Figure 2.11**, **Table 2.2**). A clear trend could be seen in the crystallinity. When the amount of regular 3-hexylthiophene units increases, higher-melting crystals are formed and a higher degree of crystallinity is reached, as based on the measured melting enthalpy (ΔH_m). This corresponds well with the UV-Vis results of these materials as recorded from thin films (**Figure 2.7a**). The T_g was most pronounced for pure **P3BHT** (less crystalline), with a clear transition between 0 and

40 °C. For the **P3HT-P3BHT** copolymers, accurate determination of the T_g was more difficult and only a gradual transition below 20 °C was seen. It should be noted that in the melting region (and above) of these copolymers, some degradation might occur due to their reduced thermal stability.

The **P3BHOET**-containing precursor polymers are also semi-crystalline (albeit only after a cold-crystallization thermal annealing step for the pure **P3BHOET** homopolymer) (**Figure 2.12, Table 2.2**). For all of the **P3BHOET** copolymers, significantly lower thermal transitions were seen compared to the **P3BHT**-containing precursors described above, which can be attributed to the more flexible side chains present. The T_g around -32 °C for pure **P3BHOET** remained almost unchanged for the **P3POET-P3BHOET 50/50** copolymer. Looking at the **P3MEEET-P3BHOET** copolymers, a further decrease in the T_g was visible, with values around -45 °C. This can be attributed to the even more flexible side chains in the **P3MEEET** repeating units. For both series of **P3BHOET** copolymers, either in combination with **P3POET** or **P3MEEET** units, the melting points and enthalpies increase with decreasing amounts of **P3BHOET**, a similar trend as observed for the **P3HT-P3BHT** copolymers. Combined with the presence of cold crystallization at about 40 °C for the pure **P3BHOET** homopolymer, this seems to indicate that the bromine groups interfere with efficient crystal packing and slow down the crystallization kinetics. This was also seen from the UV–Vis results. A summary of the thermal transitions for the precursor polymers can be found in **Table 2.2**.

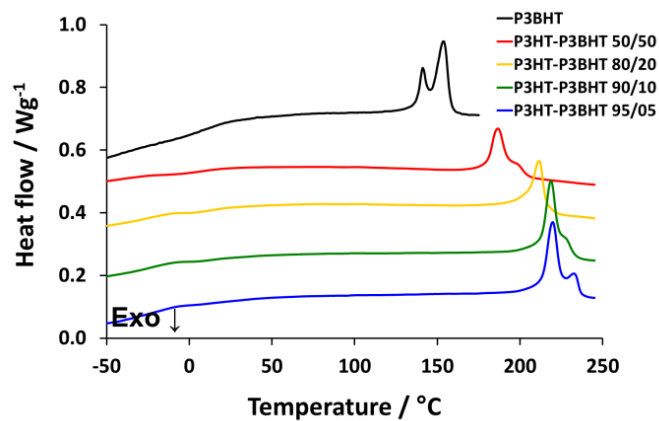


Figure 2.11: DSC thermograms depicting the second heating of **P3BHT** and the **P3HT-P3BHT** copolymers at 10 K min^{-1} . The curves were shifted vertically for clarity.

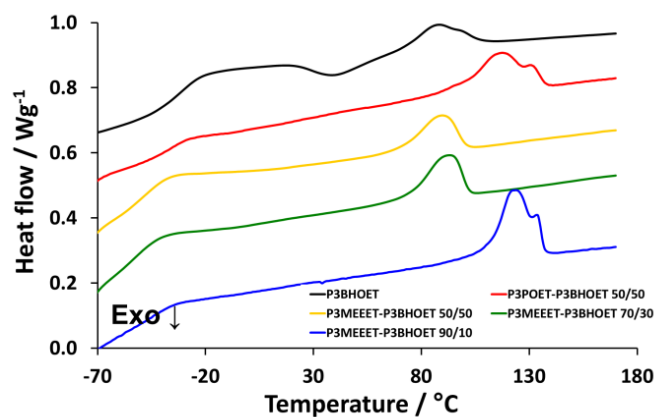


Figure 2.12: DSC thermograms depicting the second heating cycle of **P3BHOET** and the different **P3BHOET**-containing copolymers at 20 K min^{-1} . The curves were shifted vertically for clarity.

Table 2.2: Thermal transitions of selected precursors and **P3(MIM)HT** (co)polymers.

Polymer	T_g (°C)	T_m (°C)	ΔH (J g ⁻¹)
P3HT-P3BHT 95/5	<20 ^a	220	18.0
P3HT-P3BHT 90/10	<20 ^a	219	17.5
P3HT-P3BHT 80/20	<20 ^a	212	12.0
P3HT-P3BHT 50/50	<20 ^a	187	11.7
P3BHT	20	156	9.0
P3POET-P3BHOET 50/50	-35	117	11.3
P3BHOET	-32	85 ^b	4.1 ^b
P3MEEET-P3BHOET 90/10	-44	125	11.9
P3MEEET-P3BHOET 70/30	-49	90	8.0
P3MEEET-P3BHOET 50/50	-48	86	6.8
P3HT-P3(MIM)HT-Br 80/20	43	-	-
P3HT-P3(MIM)HT-Br 50/50	45	-	-
P3(MIM)HT-Br	72	-	-
P3(MIM)HT-TFSI	-15	-	-
P3(MIM)HT-PF₆	58	163 ^b	5.2 ^b

^a The glass transition is difficult to determine due to the high crystallinity of the polymer. ^b After cold-crystallization.

The ionic **P3HT-P3(MIM)HT-Br** copolymers show a very broad endothermic effect after the T_g during the first heating, corresponding to the evaporation of water (**Figure 2.13**). This confirms the hygroscopic character of these materials, which could also be seen in TGA. Fully amorphous behavior was found for all the studied compositions (even

for temperatures up to 250 °C), including the 100% **P3(MIM)HT-Br**, which corresponds to the UV–Vis results in thin film indicating the presence of non-structured chains (**Figure 2.7**). A single broad T_g was detected that increased substantially when the water present was removed after the first heating. The reproducible T_g value found during subsequent heating decreased with increasing 3-hexylthiophene content. This indicates that a homogeneous system is formed, in which the position of the T_g is influenced by the amount of the two repeating units. Interestingly, when the bromine counter ion was exchanged, a different thermal behavior was seen for the 100% **P3(MIM)HT** homopolymers (**Figure 2.14**). When exchanging bromine for TFSI⁻, the T_g was lowered by more than 80 °C. Li-TFSI is sometimes used as a plasticizer, which may explain this effect.¹⁹ Using PF₆⁻ as a counter ion, however, hardly influenced the position of the T_g , but introduced a clearly visible cold-crystallization, followed by melting. Overall, a change in the counter ion seems to have a dramatic effect on the thermal properties. A summary of the thermal transitions for the **P3(MIM)HT** (co)polymers can be found in **Table 2.2**.

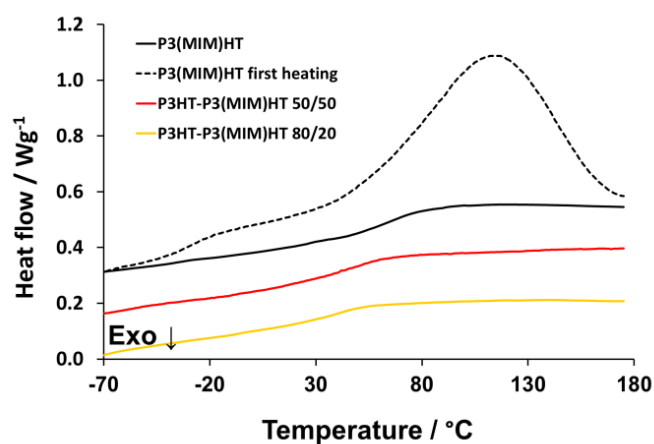


Figure 2.13: DSC thermograms depicting the second heating of **P3HT-P3(MIM)HT-Br** copolymers at 20 K min⁻¹. The dashed line depicts the first heating of the pure **P3(MIM)HT-Br**, where the large endotherm caused by water evaporation is visible. The curves were shifted vertically for clarity.

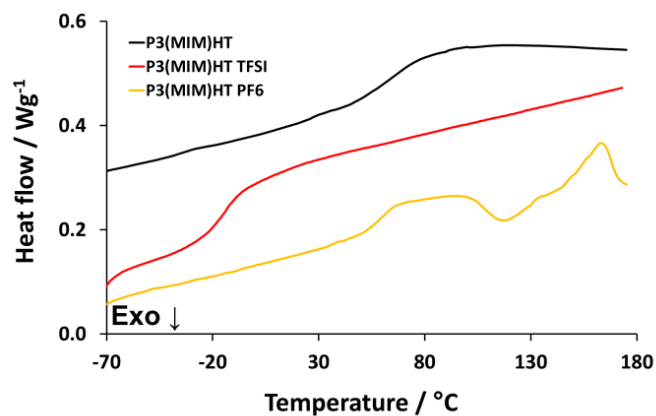


Figure 2.14: DSC thermograms depicting the second heating of **P3(MIM)HT** at 20 K min⁻¹ with either the standard Br, TFSI or PF₆ counter ion. The curves were shifted vertically for clarity.

2.3 Experimental section

2.3.1 General experimental methods

Unless stated otherwise, all reagents and chemicals were obtained from commercial sources and used without further purification. Diethyl ether and THF were dried using a MBraun MB-SPS 800 solvent purification system, operating under N₂ according to the principles described by Pangborn *et al.*²⁰ Microwave synthesis was performed on a CEM Discover SP synthesis platform. NMR chemical shifts (δ , in ppm) were determined relative to the residual ¹H absorption of CHCl₃ (7.26 ppm) or the ¹³C resonance shift of CDCl₃ (77.16 ppm). Gas chromatography-mass spectrometry (GC-MS) analyses were carried out applying Chrompack Cpsil5CB or Cpsil8CB capillary columns. UV-Vis measurements were performed on a VARIAN Cary 500 UV-Vis-NIR spectrophotometer with a scan rate of 600 nm/min in a continuous run from 200 to 800 nm. Analysis of the molecular weights and molecular weight distributions of the polymer samples was performed on a Tosoh EcoSEC System, comprising of an autosampler, a PSS guard column SDV (50 x 7.5 mm), followed by three PSS SDV analytical linear XL columns (5 μ m, 300 x 7.5 mm), a differential refractive index detector (Tosoh EcoSEC RI) and a UV-detector using THF as the eluent at 40 °C with a flow rate of 1.0 mL/min. The SEC system was calibrated using linear narrow polystyrene standards ranging from 474 to 7.5 x 10⁶ g/mol ($K = 14.1 \times 10^{-5}$ dL/g and $\alpha = 0.70$). For the **P3MEEET-P3BHOET** copolymers, purification was performed on a JAI LC-9110 Next recycling preparative HPLC equipped with JAIGEL-2H and 3H columns. DLS experiments were performed on a Malvern CGS-3

apparatus equipped with a He–Ne laser with a wavelength of 632.8 nm and a thermostat. The measurements were performed at 20 °C and at an angle of 90°. In practice, the size distribution histograms were obtained from the auto-correlation curves by the Contin algorithm, a method based on the inverse-Laplace transformation of the DLS data. DSC measurements were performed at 10 or 20 K min⁻¹ in aluminum crucibles on a TA Instruments Q2000 Tzero DSC equipped with a refrigerated cooling system (RCS), using nitrogen (50 mL min⁻¹) as the purge gas. TGA experiments were performed at 20 K min⁻¹ in platinum crucibles on a TA Instruments Q5000 TGA using nitrogen (50 mL min⁻¹) as the purge gas.

2.3.2 Monomer synthesis

2,5-Dibromo-3-(6-bromohexyl)thiophene (**M2**) was prepared using a modified procedure starting from the procedures of Bäuerle²¹ and Miyanishi²². The procedure is outlined in detail in a recently published preceding paper.^{3e} Two other monomers, 2,5-dibromo-3-(2-((6-bromohexyl)oxy)ethyl)thiophene (**M3**) and 2,5-dibromo-3-(2-(pentyloxy)ethyl)thiophene (**M4**) were prepared using a slightly modified procedure as reported by Yassar *et al.*²³ 2,5-Dibromo-3-(2-(2-(2-methoxyethoxy)ethoxy)ethyl)thiophene (**M5**) was prepared using modified standard reaction procedures. More detailed information on the monomer syntheses and experimental data can be found in the SI.

2.3.3 Precursor polymer synthesis

2.3.3.1 P3HT-P3BHT series

Homopolymer synthesis: P3BHT

2,5-Dibromo-3-(6-bromohexyl)thiophene (**M2**) (0.86 g, 2.12 mmol) was added to a flame-dried three-neck flask and dissolved in dry THF (25 mL). The reaction mixture was put under inert atmosphere and cooled down to 0 °C. An *i*-PrMgCl.LiCl solution (1.3 M in THF, 1.63 mL, 2.12 mmol, 1 equiv) was added and the mixture was stirred for 30 min at 0 °C. To start the polymerization, 0.8 mol% of Ni(dppp)Cl₂ catalyst (9 mg, 0.017 mmol) was added and the mixture was stirred for 2 h at 40 °C. The polymer was precipitated into an ice-cold HCl/MeOH (5%) mixture and filtered off on a PTFE membrane (47 mm/0.45 μm). The polymer was purified using soxhlet extraction for 24 h with methanol, *n*-hexane and chloroform, respectively. After evaporation of the solvent, the residue was redissolved in chloroform and precipitated again from methanol, filtered, washed with methanol and dried, affording **P3BHT** as a black powder (0.331 g, 64%). ¹H NMR (400 MHz, CDCl₃): δ = 6.96 (s, 1H), 3.41 (t, *J* = 6.8 Hz, 2H), 2.81 (t, *J* = 7.4 Hz, 2H), 1.88 (q, *J* = 6.6 Hz, 2H), 1.71 (q, *J* = 7.4 Hz, 2H), 1.55–1.39 (m, 4H); UV–Vis (CHCl₃, nm): λ_{max} = 447, UV–Vis (film, nm): λ_{max} = 479; SEC (THF, PS standards): *M*_n = 3.0 × 10⁴ g/mol, *M*_w = 4.0 × 10⁴ g/mol, PDI = 1.34.

General random copolymer synthesis: P3HT-P3BHT 50/50

The two monomers, 2,5-dibromo-3-hexylthiophene (**M1**) (0.269 g, 0.825 mmol) and 2,5-dibromo-3-(6-bromohexyl)thiophene (**M2**) (0.334 g, 0.825 mmol), were added to a flame-dried three-neck flask and dissolved

in dry THF (15 mL). The reaction mixture was put under inert atmosphere and cooled down to 0 °C. An *i*-PrMgCl.LiCl solution (1.3 M in THF, 1.269 mL, 1.65 mmol, 1 equiv) was added and the mixture was stirred for 30 min at 0 °C. To start the polymerization, 0.8 mol% of Ni(dppp)Cl₂ catalyst (7 mg, 0.013 mmol) was added and the mixture was stirred for 2 h at 40 °C and 12 h at room temperature. The polymer was precipitated into an ice cold HCl/MeOH (5%) mixture and filtered off on a PTFE membrane (47 mm/0.45 μm). The polymer was purified using soxhlet extraction for 24 h with methanol, *n*-hexane and chloroform, respectively. After evaporation of the solvent, the residue was redissolved in chloroform and precipitated again from methanol, filtered, washed with methanol and dried, affording the 50% random copolymer **P3HT-P3BHT 50/50** as a black powder (0.193 g, 57%). ¹H NMR (300 MHz, CDCl₃): δ = 6.96 (s, 2H), 3.41 (t, *J* = 6.7 Hz, 2H), 2.79 (br, 4H), 1.88 (q, *J* = 6.4 Hz, 2H), 1.69 (br, 4H), 1.56–1.22 (m, 10H), 0.90 (br, 3H); UV–Vis (CHCl₃, nm): λ_{max} = 442, UV–Vis (film, nm): λ_{max} = 525; SEC (THF, PS standards): *M*_n = 2.9 x 10⁴ g/mol, *M*_w = 3.2 x 10⁴ g/mol, PDI = 1.13; calculated monomer ratio via NMR = 52/48. Other random **P3HT-P3BHT x/y** copolythiophenes were prepared using the same procedure.

P3HT-P3BHT 25/75

M1 (0.096 g, 0.294 mmol) and **M2** (0.304 g, 0.750 mmol) were added together and dissolved in dry THF (10 mL). An *i*-PrMgCl.LiCl solution (1.3 M in THF, 0.8 mL, 1.04 mmol, 1 equiv) was added and the polymerization was started by adding 0.8 mol% of catalyst (5.4 mg,

0.008 mmol). The copolymer was obtained as a black powder (98 mg, 53%). ^1H NMR (300 MHz, CDCl_3): δ = 6.96 (s), 3.41 (t, J = 6.9 Hz), 2.81 (br), 1.88 (br), 1.71 (br), 1.55–1.30 (m), 0.90 (br); UV–Vis (CHCl_3 , nm): λ_{max} = 443; SEC (THF, PS standards): M_n = 1.5×10^4 g/mol, M_w = 2.5×10^4 g/mol, PDI = 1.7; calculated ratio via NMR = 22/78. As this experiment was conducted as one of the first trials, the molecular weight and PDI are not optimized.

P3HT-P3BHT 80/20

M1 (0.590 g, 1.8 mmol) and **M2** (0.180 g, 0.444 mmol) were added together and dissolved in dry THF (20 mL). An *i*-PrMgCl.LiCl solution (1.3 M in THF, 1.73 mL, 2.24 mmol, 1 equiv) was added and the polymerization was started by adding 0.8 mol% of catalyst (9.7 mg, 0.018 mmol). The copolymer was obtained as a black powder (281 mg, 68%). ^1H NMR (300 MHz, CDCl_3): δ = 6.96 (s), 3.40 (t, J = 6.7 Hz), 2.79 (br), 1.87 (br), 1.69 (br), 1.55–1.20 (m), 0.90 (br); UV–Vis (CHCl_3 , nm): λ_{max} = 443, UV–Vis (film, nm): λ_{max} = 552; SEC (THF, PS standards): M_n = 3.3×10^4 g/mol, M_w = 5.6×10^4 g/mol, PDI = 1.7; calculated ratio via NMR = 77/23.

P3HT-P3BHT 90/10

M1 (0.550 g, 1.69 mmol) and **M2** (0.076 g, 0.187 mmol) were added together and dissolved in dry THF (15 mL). An *i*-PrMgCl.LiCl solution (1.3 M in THF, 1.44 mL, 1.88 mmol, 1 equiv) was added and the polymerization was started by adding 0.8 mol% of catalyst (8 mg, 0.015 mmol). The copolymer was obtained as a black powder (206 mg, 63%).

^1H NMR (300 MHz, CDCl_3): δ = 6.96, 3.40 (t, J = 6.8 Hz), 2.79 (br), 1.88 (br), 1.69 (br), 1.55–1.21 (m), 0.89 (br); UV–Vis (CHCl_3 , nm): λ_{max} = 449, UV–Vis (film, nm): λ_{max} = 552; SEC (THF, PS standards): M_n = 2.8×10^4 g/mol, M_w = 4.0×10^4 g/mol, PDI = 1.46; calculated ratio via NMR = 85/15.

P3HT-P3BHT 95/5

M1 (0.681 g, 2.0 mmol) and **M2** (0.049 g, 0.12 mmol) were added together and dissolved in dry THF (20 mL). An *i*-PrMgCl.LiCl solution (1.3 M in THF, 1.63 mL, 2.12 mmol, 1 equiv) was added and the polymerization was started by adding 0.8 mol% of catalyst (8.7 mg, 0.016 mmol). The copolymer was obtained as a black powder (254 mg, 68%). ^1H NMR (400 MHz, CDCl_3): δ = 6.96 (s), 3.40 (t, J = 6.8 Hz), 2.79 (br), 1.88 (br), 1.69 (br), 1.47–1.21 (m), 0.89 (br); UV–Vis (CHCl_3 , nm): λ_{max} = 448, (film, nm): λ_{max} = 552; SEC (THF, PS standards): M_n = 2.3×10^4 g/mol, M_w = 2.9×10^4 g/mol, PDI = 1.25.

2.3.3.2 P3POET-P3BHOET series

Homopolymer synthesis: P3BHOET

2,5-Dibromo-3-(2-((6-bromohexyl)oxy)ethyl)thiophene (**M3**) (0.750 g, 1.67 mmol) was added to a flame-dried three-neck flask and dissolved in dry THF (15 mL). The reaction mixture was put under inert atmosphere and cooled to 0 °C. An *i*-PrMgCl.LiCl solution (1.3 M in THF, 1.3 mL, 1.67 mmol, 1 equiv) was added and the mixture was stirred for 30 min at 0 °C. To start the polymerization, 1 mol% of Ni(dppp)Cl₂ catalyst (9 mg, 0.0167 mmol) was added and the mixture was stirred for 16 h at 75 °C. The polymer was precipitated into an ice cold HCl/MeOH (5%) mixture

and filtered off on a PTFE membrane (47 mm/0.45 μm). The polymer was purified using soxhlet extraction for 24 h with methanol, *n*-hexane and chloroform, respectively. After evaporation of the solvent, the residue was redissolved in chloroform and precipitated again from methanol, filtered, washed with methanol and dried, affording the homopolymer **P3BHOET** as a black powder (0.272 g, 57%). ^1H NMR (300 MHz, CDCl_3): δ = 7.06 (s, 1H), 3.69 (t, J = 7.0 Hz, 2H), 3.49-3.44 (m, 2H), 3.35 (t, J = 6.7 Hz, 2H), 3.07 (t, J = 6.5 Hz, 2H), 1.82 (q, J = 7.2 Hz, 2H), 1.59 (q, J = 6.7 Hz, 2H), 1.49–1.26 (m, 4H); UV–Vis (CHCl_3 , nm): λ_{max} = 434; SEC (THF, PS standards): M_n = 1.8×10^4 g/mol, M_w = 3.1×10^4 g/mol, PDI = 1.75.

Random copolymer synthesis: P3POET-P3BHOET 50/50

The two monomers, 2,5-dibromo-3-(2-(pentyloxy)ethyl)thiophene (**M4**) (0.450 g, 1.26 mmol) and 2,5-dibromo-3-(2-((6-bromohexyl)oxy)ethyl)thiophene (**M3**) (0.550 g, 1.22 mmol), were added to a flame-dried three-neck flask and dissolved in dry THF (25 mL). The reaction mixture was put under inert atmosphere and cooled to 0 °C. An *i*-PrMgCl.LiCl solution (1.3 M in THF, 1.92 mL, 2.49 mmol, 1 equiv) was added and the mixture was stirred for 90 min at 0 °C. To start the polymerization, 0.8 mol% of Ni(dppp)Cl₂ catalyst (10 mg, 0.0187 mmol) was added and the mixture was stirred for 12 h at 40 °C. The polymer was precipitated into an ice cold HCl/MeOH (5%) mixture and filtered off on a PTFE membrane (47 mm/0.45 μm). The polymer was purified using soxhlet extraction for 24 h with methanol, *n*-hexane and chloroform, respectively. After evaporation of the solvent, the residue

was redissolved in chloroform and precipitated again from methanol, filtered, washed with methanol and dried, affording the random copolymer as a black powder (0.291 g, 48%). ^1H NMR (300 MHz, CDCl_3): δ = 7.06 (s, 2H), 3.69 (t, J = 7.0 Hz, 4H), 3.46 (t, J = 6.4 Hz, 4H), 3.35 (t, J = 6.9 Hz, 2H), 3.07 (t, J = 6.9 Hz, 4H), 1.82 (q, J = 7.2 Hz, 2H), 1.67–1.48 (m, 4H), 1.47–1.26 (m, 8H), 0.87 (br, 3H); UV–Vis (CHCl_3 , nm): λ_{max} = 435; SEC (THF, PS standards): M_n = 1.1×10^4 g/mol, M_w = 1.9×10^4 g/mol, PDI = 1.7; calculated ratio via NMR = 53/47.

2.3.3.3 P3MEEET/P3BHOET series

General random copolymer synthesis: P3MEEET/P3BHOET 50/50

The two monomers, 2,5-dibromo-3-(2-(2-(2-methoxyethoxy)ethoxy)ethyl)thiophene (**M5**) (0.216 g, 0.56 mmol) and 2,5-dibromo-3-(2-((6-bromohexyl)oxy)ethyl)thiophene (**M3**) (0.238 g, 0.53 mmol), were added to a flame-dried three-neck flask and dissolved in dry THF (10 mL). The reaction mixture was put under inert atmosphere and cooled to 0 °C. An *i*-PrMgCl.LiCl solution (1.3 M in THF, 0.84 mL, 1.09 mmol, 1 equiv) was added and the mixture was stirred for 90 min at 0 °C. To start the polymerization, 0.8 mol% of Ni(dppp)Cl₂ catalyst (5 mg, 0.009 mmol) was added and the mixture was stirred for 2 h at 40 °C. The polymer was precipitated into an ice cold HCl/MeOH (5%) mixture and was filtered off on a PTFE membrane (47 mm/0.45 μm). The polymer was purified using soxhlet extraction for 24 h with methanol, *n*-hexane and dichloromethane, respectively. After evaporation of the solvent, the residue was redissolved in chloroform and precipitated again from methanol, filtered,

washed with methanol and dried, affording the random copolymer as a black powder (0.153 g, 55%). ^1H NMR (300 MHz, CDCl_3): $\delta = 7.09\text{--}7.03$ (m, 2H), 3.79–3.43 (m, 14H), 3.35 (t, $J = 6.4$ Hz, 2H), 3.34 (s, 3H), 3.14–3.01 (m, 4H), 1.82 (q, $J = 6.9$ Hz, 2H), 1.67–1.50 (m, 2H), 1.47–1.32 (m, 4H); UV–Vis (CHCl_3 , nm): $\lambda_{\text{max}} = 439$; SEC (THF, PS standards): $M_n = 3.4 \times 10^4$ g/mol, $M_w = 6.4 \times 10^4$ g/mol, PDI = 1.8.

Other random **P3MEEET/P3BHOET** *x/y* copolythiophenes were prepared using the same procedure.

P3MEEET/P3BHOET 70/30

M5 (0.308 g, 0.79 mmol) and **M3** (0.112 g, 0.34 mmol) were added together and dissolved in dry THF (10 mL). An *i*-PrMgCl.LiCl solution (1.3 M in THF, 0.87 mL, 1.13 mmol, 1 equiv) was added and the polymerization was started by adding 0.8 mol% of catalyst (0.005 g, 0.009 mmol). The copolymer was obtained as a black powder (58 mg, 23%). ^1H NMR (300 MHz, CDCl_3): $\delta = 7.08\text{--}7.03$ (m), 3.79–3.43 (m), 3.39–3.32 (m), 3.13–3.02 (m), 1.82 (q, $J = 7.0$ Hz), 1.67–1.51 (m), 1.47–1.32 (m); UV–Vis (CHCl_3 , nm): $\lambda_{\text{max}} = 438$; SEC (THF, PS standards): $M_n = 3.3 \times 10^4$ g/mol, $M_w = 4.5 \times 10^4$ g/mol, PDI = 1.4.

P3MEEET/P3BHOET 90/10

M5 (0.726 g, 1.87 mmol) and **M3** (0.105 g, 0.234 mmol) were added together and dissolved in dry THF (20 mL). An *i*-PrMgCl.LiCl solution (1.3 M in THF, 1.62 mL, 2.1 mmol, 1 equiv) was added and the polymerization was started by adding 1 mol% of catalyst (0.011 g, 0.02 mmol). The copolymer was obtained as a black powder (153 mg, 68%).

¹H NMR (300 MHz, CDCl₃): δ = 7.10–7.03 (m), 3.75 (t, J = 6.9 Hz), 3.70–3.48 (m), 3.38–3.32 (m), 3.09 (t, J = 7.0 Hz), 1.82 (q, J = 6.7 Hz), 1.64–1.53 (m), 1.47–1.32 (m); UV–Vis (CHCl₃, nm): λ_{max} = 436; SEC (THF, PS standards): M_n = 2.0 x 10⁴ g/mol, M_w = 2.4 x 10⁴ g/mol, PDI = 1.2.

2.3.3.4 General procedure for polymer functionalization with *N*-methylimidazole^{3e,6e}

P3BHT (0.250 g, M_n = 3.0 x 10⁴ g/mol, PDI = 1.34) was suspended in acetonitrile (2 mL) in a 10 mL microwave vial and *N*-methylimidazole (3 mL) was added. The vial was filled with argon and closed. The reaction mixture was heated in the microwave at 100 °C for 4 h (with maximum power of 200 W and a maximum pressure of 17 bar). After cooling down, the reaction mixture was added drop wise to Et₂O and a dark precipitate was obtained. The polymer was filtered off using a PTFE membrane (47 mm/0.45 μ m) and (freeze-)dried carefully, affording **P3(MIM)HT-Br** as a purple-black powder (0.295 g, 88%). ¹H NMR (400 MHz, DMSO-*d*₆): δ = 9.30 (s, 1H), 7.83 (s, 1H), 7.72 (s, 1H), 7.18 (s, 1H), 4.18 (t, J = 6.9 Hz, 2H), 3.84 (s, 3H), 2.86–2.65 (m, 2H), 1.85–1.71 (br, 2H), 1.69–1.54 (m, 2H), 1.45–1.17 (m, 4H); UV–Vis (MeOH, nm): λ_{max} = 444.

P3HT-P3(MIM)HT-Br 25/75

P3HT-P3BHT-Br 25/75 (0.09 g, M_n = 1.5 x 10⁴ g/mol, PDI = 1.69); purple-black powder (0.105 g, 94%); ¹H NMR (400 MHz, DMSO-*d*₆): δ = 9.29 (s), 7.83 (s), 7.75 (s), 7.20 (s), 4.20 (br), 3.86 (s), 2.79 (br), 1.81

(br), 1.64 (br), 1.49–1.18 (m), 0.87 (br); UV–Vis (MeOH, nm): λ_{\max} = 445.

P3HT-P3(MIM)HT-Br 50/50

P3HT-P3BHT 50/50 (0.150 g, $M_n = 2.9 \times 10^4$ g/mol, PDI = 1.13); purple-black powder (0.176 g, 98%); ^1H NMR (300 MHz, DMSO- d_6): δ = 9.19 (s, 1H), 7.79 (s, 1H), 7.72 (s, 1H), 7.18 (s, 2H), 4.17 (br, 2H), 3.84 (s, 3H), 2.80 (br, 4H), 1.80 (br, 2H), 1.65 (br, 2H), 1.49–1.18 (m, 8H), 0.87 (br, 3H); UV–Vis (MeOH, nm): λ_{\max} = 446.

P3HT-P3(MIM)HT-Br 80/20

P3HT-P3BHT 80/20 (0.050 g, $M_n = 3.3 \times 10^4$ g/mol, PDI = 1.7); purple-black powder (0.049 g, 90%); ^1H NMR (300 MHz, CDCl_3 - CD_3OD): δ = 9.53 (br), 7.19 (br), 6.62 (s), 3.94 (br), 3.65 (br), 2.45 (br), 1.56 (br), 1.34 (br), 1.18–0.87 (m), 0.55 (br); UV–Vis (CHCl_3 , nm): λ_{\max} = 446.

P3HT-P3(MIM)HT-Br 90/10

P3HT-P3BHT 90/10 (0.070 g, $M_n = 2.8 \times 10^4$ g/mol, PDI = 1.46); purple-black powder (0.065 g, 89%); ^1H NMR (300 MHz, CDCl_3): δ = 6.96 (s), 4.30 (br), 4.08 (br), 3.47 (s), 2.79 (br), 1.93 (br), 1.69 (br), 1.57–1.21 (m), 0.96–0.82 (m); UV–Vis (CHCl_3 , nm): λ_{\max} = 449.

P3HT-P3(MIM)HT-Br 95/5

P3HT-P3BHT 95/5 (0.070 g, $M_n = 2.3 \times 10^4$ g/mol, PDI = 1.25); purple-black powder (0.058 g, 81%); ^1H NMR (300 MHz, CDCl_3): δ =

6.96 (s), 4.29 (br), 4.06 (br), 3.47 (s), 2.79 (br), 1.93 (br), 1.70 (br), 1.49–1.21 (m), 0.98–0.80 (m); UV–Vis (CHCl₃, nm): λ_{\max} = 448.

P3(MIM)HOET-Br

P3BHOET (0.050 g, M_n = 1.8 x 10⁴ g/mol, D = 1.7); purple-black powder (0.051 g, 79%); ¹H NMR (300 MHz, DMSO-*d*₆): δ = 9.28 (s, 1H), 7.78 (s, 1H), 7.71 (s, 1H), 7.27 (s, 1H), 4.13 (br, 2H), 3.83 (s, 3H), 3.65 (br, 2H), 3.40 (br, 2H), 2.99 (br, 2H), 1.74 (br, 2H), 1.48 (br, 2H), 1.36–1.13 (m, 4H); UV–Vis (MeOH, nm): λ_{\max} = 439.

P3POET-P3(MIM)HOET-Br 50/50

P3POET-P3BHOET 50/50 (0.070 g, M_n = 1.1 x 10⁴ g/mol, PDI = 1.7); purple-black powder (0.054 g, 66%); ¹H NMR (300 MHz, DMSO-*d*₆): δ = 9.11 (s, 1H), 7.73 (s, 1H), 7.67 (s, 1H), 7.25 (s, 2H), 4.10 (br, 4H), 3.81 (s, 2H), 3.64 (br, 3H), 3.39 (br, 4H), 2.99 (br, 4H), 1.72 (br, 2H), 1.47 (br, 4H), 1.35–1.15 (m, 8H), 0.80 (br, 3H); UV–Vis (MeOH, nm): λ_{\max} = 439.

P3MEEET/P3(MIM)HOET-Br 50/50

P3MEEET/P3BHOET 50/50 (0.150 g, M_n = 3.4 x 10⁴ g/mol, PDI = 1.8); purple-black powder (0.156 g, 90%); ¹H NMR (300 MHz, DMSO-*d*₆): δ = 9.17 (br, 1H), 7.75 (s, 1H), 7.71 (s, 1H), 7.30 (s, 2H), 4.13 (br, 2H), 3.84 (s, 3H), 3.79–3.62 (m, 2H), 3.61–3.28 (m, 12H), 3.18 (s, 3H), 3.02 (br, 4H), 1.83–1.68 (m, 2H), 1.58–1.42 (m, 2H), 1.39–1.17 (m, 4H); UV–Vis (MeOH, nm): λ_{\max} = 443.

2.3.3.5 General procedure for counter ion exchange

P3(MIM)HT-TFSI

P3(MIM)HT (0.100 g) was dissolved in distilled water (20 mL) and a solution of Li-TFSI (0.5 g, 1.7 mmol) in distilled water (1 mL) was added drop wise. A precipitate was immediately formed and the mixture was stirred for another 8 h at rt. The sticky precipitate was filtered off on a regenerated cellulose membrane (47 mm/0.45 μm) and dried under vacuum, affording **P3(MIM)HT-TFSI** as a sticky black powder (85 mg, 53%). ^1H NMR (400 MHz, $\text{DMSO-}d_6$): $\delta = 9.07$ (s, 1H), 7.72 (s, 1H), 7.68 (s, 1H), 7.15 (s, 1H), 4.13 (br, 2H), 3.83 (s, 3H), 2.77 (br, 2H), 1.79 (br, 2H), 1.63 (br, 2H), 1.47–1.18 (m, 4H); UV–Vis (MeOH, nm): $\lambda_{\text{max}} = 443$.

P3(MIM)HT-PF₆

P3(MIM)HT (0.100 g) was dissolved in distilled water (20 mL) and a solution of Li-PF₆ (0.2 g, 1.3 mmol) in distilled water (1 mL) was added drop wise. A precipitate was immediately formed and the mixture was stirred for another 8 h at rt. The precipitate was filtered off on a regenerated cellulose membrane (47 mm/0.45 μm) and dried under vacuum, affording **P3(MIM)HT-PF₆** as a red-black powder (97 mg, 81%). ^1H NMR (300 MHz, $\text{DMSO-}d_6$): $\delta = 9.07$ (s, 1H), 7.71 (s, 1H), 7.67 (s, 1H), 7.17 (s, 1H), 4.13 (br, 2H), 3.82 (s, 3H), 2.76 (br, 2H), 1.86–1.71 (m, 2H), 1.71–1.52 (m, 2H), 1.44–1.22 (m, 4H); UV–Vis (TFP, nm) $\lambda_{\text{max}} = 444$.

P3(MIM)HOET-TFSI was prepared in a similar way as the **P3(MIM)HT-TFSI** analogue. sticky black powder (88 mg, 57%); ^1H NMR (400 MHz, $\text{DMSO-}d_6$): $\delta = 9.09$ (s, 1H), 7.71 (s, 1H), 7.68 (s, 1H), 7.27 (s, 1H), 4.11 (t, $J = 7.3$ Hz, 2H), 3.83 (s, 3H), 3.67 (br, 2H), 3.46–3.31 (br, 2H), 3.01 (br, 2H), 1.81–1.68 (m, 2H), 1.56–1.42 (m, 2H), 1.39–1.16 (m, 4H); UV–Vis (MeOH, nm): $\lambda_{\text{max}} = 441$.

P3MEEET-P3(MIM)HOET-TFSI 50/50 was prepared in a similar way as the **P3(MIM)HT-TFSI** analogue. sticky black powder (125 mg, 78%); ^1H NMR (400 MHz, $\text{DMSO-}d_6$): $\delta = 9.06$ (s, 1H), 7.71 (s, 1H), 7.67 (s, 1H), 7.28 (s, 2H), 4.11 (t, $J = 6.8$ Hz, 2H), 3.82 (s, 3H), 3.78–3.62 (m, 2H), 3.61–3.27 (m, 12H), 3.18 (s, 3H), 3.02 (br, 4H), 1.80–1.69 (m, 2H), 1.56–1.44 (m, 2H), 1.38–1.18 (m, 4H); UV–Vis (MeOH, nm): $\lambda_{\text{max}} = 443$.

2.4 Conclusions

The GRIM polymerization procedure is demonstrated to be a versatile method to synthesize a broad range of bromine-functionalized statistical polythiophene copolymers. Postpolymerization modification of these copolythiophenes with *N*-methylimidazole via microwave activation resulted in smooth and efficient conversion to the ionic copolymers. The ionic materials are in general better soluble in polar solvents and some of them even in water. Dynamic light scattering was used to get more insight in the size of formed aggregates in solution. In good agreement with UV–Vis studies, DLS confirmed that the **P3HT-P3(MIM)HT-Br 50/50** copolymer forms aggregates in water-rich solvent mixtures. Although it is quite clear that structures are formed in solution, the system is too complicated to give a clear view on the formed aggregates in solution. From thermal analysis experiments it can be concluded that all the synthesized precursor polymers are semi-crystalline. For all of these materials, a larger amount of bromine-functionalized repeating units leads to melting at lower temperatures. The semi-crystalline behavior changes to fully amorphous for the **P3(MIM)HT-Br** polymers, where only a glass transition is seen. This lack of order confirms the findings from UV–Vis results on thin films of the ionic materials. In both DSC and TGA it could be seen that the latter materials are hygroscopic. A striking change in the thermal behavior of the imidazolium-substituted polythiophenes was seen when the bromine counter ion was replaced by either TFSI or PF₆. In the former case, a strong plasticizing effect was observed, while in the latter case the polymer could easily get semi-crystalline (after a cold-crystallization

thermal annealing step). The presented ionic (co-polythiophenes will be investigated as suitable materials for bulk heterojunction polymer solar cells, notably to analyze structure-performance relationships when applying them as electron transport layers to improve the efficiency of said devices.^{6e} Preliminary probing of the morphological and local electrical properties by AFM techniques seems to point to a different coverage of the active layer depending on the polymer structure.

2.5 References

- 1 (a) Kippelen, B.; Brédas, J.-L. *Energy Environ. Sci.* **2009**, 251-261; (b) Brédas, J.-L.; Norton, J. E.; Cornil, J.; Coropceanu, V. *Acc. Chem. Res.* **2009**, 1691-1699; (c) Kumar, P.; Chand, S. *Prog. Photovolt: Res. Appl.* **2012**, 20, 377-415; (e) Mishra, A.; Bäuerle, P. *Angew. Chem. Int. Ed.* **2012**, 51, 2020-2067; (f) Hardin, B. E.; Snaith, H. J.; McGehee, M. D. *Nat. Photonics* **2012**, 162-169.
- 2 (a) Günes, S.; Neugebauer, H.; Sariciftci, N. S. *Chem. Rev.* **2007**, 107, 1324-1338; (b) Brabec, C. J.; Gowrisanker, S.; Halls, J. J. M.; Laird, D.; Jia, S.; Williams, S. P. *Adv. Mater.* **2010**, 22, 3839-3856; (c) Heeger, A. J. *Chem. Soc. Rev.* **2010**, 39, 2354-2371; (d) Delgado, J. L.; Bouit, P.-A.; Filippone, S.; Herranz, M. A.; Martin, N. *Chem. Commun.* **2010**, 46, 4853-4865; (e) Boudreault, P.-L. T.; Najari, A.; Leclerc, M. *Chem. Mater.* **2011**, 23, 456-469; (f) Thompson, B.; Khlyabich, P.; Burkhart, B.; Aviles, A.; Rudenko, A.; Shultz, G.; Christi, F.; Mangubat, L. *Green* **2011**, 1, 29-54; (g) Nelson, J. *Mater. Today* **2011**, 14, 462-470; (h) Zhou, H.; Yang, L.; You, W. *Macromolecules* **2012**, 45, 607-632; (i) Jørgensen, M.; Norrman, K.; Gevorgyan, S. A.; Tromholt, T.; Andreasen, B.; Krebs, F. C. *Adv. Mater.* **2012**, 24, 580-612; (j) Søndergaard, R.; Hösel, M.; Angmo, D.; Larsen-Olsen, T. T.; Krebs, F. C. *Mater. Today* **2012**, 15, 36-49; (k) Li, G.; Zhu, R.; Yang, Y. *Nat. Photonics* **2012**, 6, 153-161; (l) Bian, L.; Zhu, E.; Tang, J.; Tang, W.; Zhang, F. *Prog. Polym. Sci.* **2012**, 37, 1292-1331.
- 3 (a) Vandenbergh, J.; Dergent, J.; Conings, B.; Krishna, G. T.V.V.; Maes, W.; Cley, T. J.; Lutsen, L.; Manca, J.; Vanderzande, D. J. M. *Eur. Polym. J.* **2011**, 1827-1835; (b) Andersen, T. R., Larsen-Olsen, T. T., Andreasen, B., Böttiger, A. P. L., Carlé, J. E., Helgesen, M., Bundgaard, E., et al. *ACS Nano* **2011**, 5, 4188-4196; (c) Baeten, L., Conings, B., D'Haen, J., Hardy, A., Manca, J. V., & Van Bael, M. K. *Sol. Energy Mater. Sol. Cells* **2012**, 107, 230-235; (d) Wei, H.; Zhang, H.; Sun, H.; Yang, B. *Nano Today* **2012**, 7, 316-326; (e) Ghoos, T.; Malinkiewicz, O.; Lutsen, L.; Vanderzande, D. J.; Bolink, H. J.; Maes, W. *RSC Adv.*, manuscript submitted.

- 4 (a) Chayer, M.; Faïd, K.; Leclerc, M. *Chem. Mater.* **1997**, *9*, 2902-2905; (b) Ho, H. A.; Leclerc, M. *J. Am. Chem. Soc.* **2003**, *125*, 4412-4413; (c) Liu, B., Wang, S., Bazan, G. C., & Mikhailovsky, A. *J. Am. Chem. Soc.* **2003**, *125*, 13306-13307; (d) Elbing, M.; Garcia, A.; Urban, S.; Nguyen, T.-Q.; Bazan, G. C. *Macromolecules*, **2008** *41*, 9146-9155; (e) Ying, L.; Zalar, P.; Collins, S. D.; Chen, Z.; Mikhailovsky, A. A.; Nguyen, T.-Q.; Bazan, G. C. *Adv. Mater.* **2012**, *24*, 6496-6501.
- 5 (a) Koster, L. J. A.; Shaheen, S. E.; Hummelen, J. C. *Adv. Energy Mater.*, **2012**, *2*, 1246-1253; (b) Chiechi, R. C.; Hummelen, J. C. *ACS Macro Lett.*, **2012**, *1*, 1180-1183.
- 6 (a) Wu, H.; Huang, F.; Mo, Y.; Yang, W.; Wang, D.; Peng, J.; Cao, Y. *Adv. Mater.* **2004**, *16*, 1826-1830; (b) Seo, J. H.; Gutacker, A.; Sun, Y. M.; Wu, H. B.; Huang, F.; Cao, Y.; Scherf, U.; Heeger, A. J.; Bazan, G. C. *J. Am. Chem. Soc.*, **2011**, *133*, 8416-8419; (c) Lee, W.; Choi, H.; Hwang, S.; Kim, J. Y.; Woo, H. Y. *Chemistry*, **2012**, *18*, 2551-2558; (d) Chen, Y.; Jiang, Z.; Gao, M.; Watkins, S. E.; Lu, P.; Wang, H.; Chen, X. *Appl. Phys. Lett.*, **2012**, *100*, 203304; (e) Kesters, J.; Ghoos, T.; Penxten, H.; Drijkoningen, J.; Vangerven, T.; Lyons, D. M.; Verreert, B.; Aernouts, T.; Lutsen, L.; Vanderzande, D.; Manca, J.; Maes, W. *Adv. Energy Mater.* **2013**, doi: 10.1002/aenm.201300049.
- 7 (a) Wang, S.; Bazan, G. C. *Chem. Commun.* **2004**, 2508-2509; (b) Knaapila, M.; Evans, R. C.; Garamus, V. M.; Almasy, L.; Szekely, N. K.; Gutacker, A.; Scherf, U.; Burrows, H. D. *Langmuir*, **2010**, *26*, 15634-15643; (c) Hoeben, F. J. M.; Jonkheijm, P.; Meijer, E. W.; Schenning, A. P. H. J. *Chemical reviews*, **2005**, *105*, 1491-1546.
- 8 (a) Dang, M. T.; Hirsch, L.; Wantz, G. *Adv. Mater.* **2011**, *23*, 3597-3602; (b) Marrocchi, A.; Lanari, D.; Facchetti, A.; Vaccaro, L. *Energy Environ. Sci.* **2012**, *5*, 8457-8474.
- 9 (a) Miyanishi, S.; Tajima, K.; Hashimoto, K. *Macromolecules*, **2009**, *42*, 1610-1618; (b) Bumjoon, J. K.; Miyamoto, Y.; Ma B.; Fréchet, J. M. J. *Adv. Funct. Mater.* **2009**, *19*, 2273-2281; (c) Smeets, A.; Willot, P.; Winter, J. D.; Gerbaux, P.; Verbiest, T.; Koeckelberghs, G. *Macromolecules* **2011**, *44*, 6017-6025; (d)

- Tanenbaum, D. M.; Hermenau, M.; Voroshazi, E.; Lloyd, M. T.; Galagan, Y.; Zimmermann, B.; Hösel, M.; Dam, H. F.; Jørgensen, M.; Gevorgyan, S. A.; Kudret, S.; Maes, W.; Lutsen, L.; Vanderzande, D.; Würfel, U.; Andriessen, R.; Rösch, R.; Hoppe, H.; Lira-Cantu, M.; Rivaton, A.; Uzunoğlu, G. Y.; Germack, D.; Andreasen, B.; Madsen, M. V.; Norrman, K.; Krebs, F. C. *RSC Adv.* **2012**, *2*, 882-893; (e) Oosterhout, S. D.; Koster, L. J. A.; van Bavel, S. S.; Loos, J.; Stenzel, O.; Thiedmann, R.; Schmidt, V.; Campo, B.; Cleij, T. J.; Lutsen, L.; Vanderzande, D.; Wienk, M. M.; Janssen, R. A. J. *Adv. Energy Mater.*, **2011**, *1*, 90-96; (f) Kim, H. J.; Han, A.-R.; Cho, C.-H.; Kang, H.; Cho, H.-H.; Lee, M. Y.; Fréchet, J. M. J.; Oh, J. H.; Kim, B. J. *Chem. Mater.*, **2012**, *24*, 215-221; (g) Lin, Y.; Lim, J. A.; Wei, Q.; Mannsfeld, S. C. B.; Briseno, A. L.; Watkins, J. J. *Chem. Mater.*, **2012**, *24*, 622-632; (h) Lobež, J. M.; Andrew, T. L.; Bulovic, V.; Swager, T. M. *ACS Nano*, **2012**, *6*, 3044-3056; (i) Campo, B.; Bevk, D.; Kesters, J.; Gilot, J.; Bolink, H. J.; Zhao, J.; Bolsée, J.-C.; Oosterbaan, W. D.; Bertho, S.; Ruttens, B.; D'Haen, J.; Manca, J.; Lutsen, L.; Van Assche, G.; Maes, W.; Janssen, R. A. J.; Vanderzande, D. *Org. Electron.*, **2013**, *14*, 523-534; (j) Bertho, S.; Campo, B.; Piersimoni, F.; Spoltore, D.; D'Haen, J.; Lutsen, L.; Maes, W.; Vanderzande, D.; Manca, J. *Sol. Energy Mater. Sol. Cells* **2013**, *110*, 69-76.
- 10 (a) Ho, H. A.; Leclerc, M. *J. Am. Chem. Soc.* **2003**, *125*, 4412-4413; (b) Bondarev, D.; Zednik, J.; Sloufova, I.; Sharf, A.; Prochazka, M.; Pflieger J.; Vohlidal, J. *J. Polym. Sci., Part A: Polym. Chem.*, **2010**, *48*, 3073-3081; (c) Kazim, S.; Pflieger, J.; Prochazka, M.; Bondarev D.; Vohlidal, J. *J. Colloid Interface Sci.*, **2011**, *354*, 611-619; (d) Knaapila, M.; Evans, R. C.; Gutacker, A.; Garamus, V. M.; Székely, N. K.; Scherf U.; Burrows, H. D. *Soft Matter*, **2011**, *7*, 6863-6872; (e) Richter, T. V.; Bühler C.; Ludwigs, S.; *J. Am. Chem. Soc.*, **2012**, *134*, 43-46.
- 11 (a) Loewe, R. S.; Ewbank, P. C.; Liu, J.; Zhai, L.; McCullough, R. D. *Macromolecules*, **2001**, *34*, 4324-4333; (b) Miyakoshi, R.; Yokoyama, A.; Yokozawa, T. *Macromol. Rapid Commun.* **2004**, *25*, 1663-1666; (c) Stefan, M. C.; Bhatt, M. P.; Sista, P.; Magurudeniya, H. D. *Polym. Chem.*, **2012**, *3*, 1693-

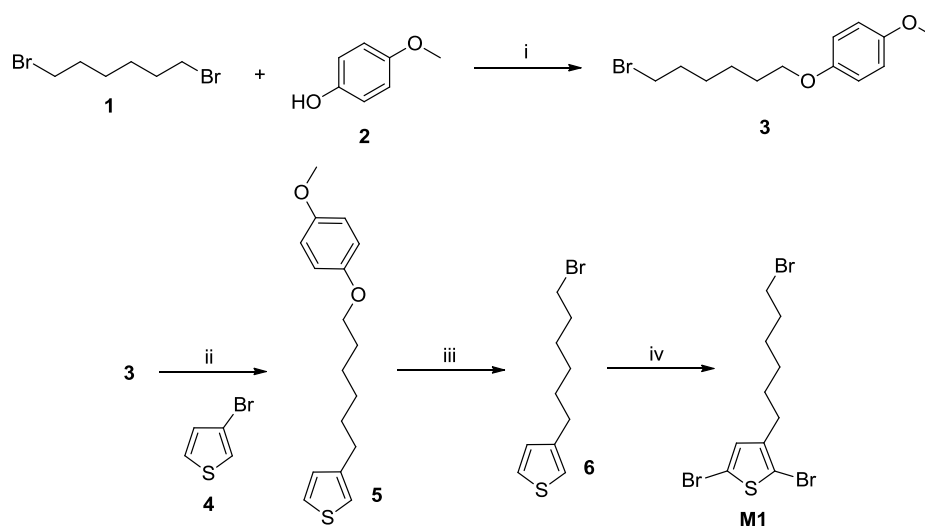
- 1701; (d) Geng, Y.; Huang, L.; Wu, S.; Wang, F. *Sci. China: Chem.* **2010**, *53*, 1620-1633.
- 12 Yuan, J.; Antonietti, M. *Polymer*, **2011**, *52*, 1469–1482.
- 13 (a) Marcilla, R.; Blazquez, J. A.; Rodriguez, J.; Pomposo, J. A.; Mecerreyes, D. *J. Polym. Sci., Part A: Polym. Chem.*, **2004**, *42*, 208–212; (b) Green, M. D.; Long, T. E. *Polym. Rev.* **2009**, *49*, 291-314; (c) Green, O.; Grubjesic, S.; Lee, S.; Firestone, M. A. *Polym. Rev.* **2009**, *49*, 339-360.
- 14 (a) Lenes, M.; Bolink, H. J. *ACS Appl. Mater. Interfaces* **2010**, *12*, 3664; (b) Hany, R.; Fan, B.; Araujo de Castro, F.; Heier, J.; Kylberg, W.; Nuesch, F. *Prog. Photovolt. Res. Appl.* **2011**, *19*, 851; (c) Malinkiewicz, O.; Grancha, T.; Molina-Ontoria, A.; Soriano, A.; Brine, H.; Bolink, H. J. *Adv. Ener. Mater.* **2013**, *3*, 472-477.
- 15 (a) Hoeben, F. J. M.; Jonkheijm, P.; Meijer, E. W.; Schenning, A. P. H. J. *Chem. Rev.* **2005**, *105*, 1491-1546; (b) Gutacker, A.; Adameczyk, S.; Helfer, A.; Garner, L. E.; Evans, R. C.; Fonseca, S. M.; Knaapila, M.; Bazan, G. C.; Burrows, H. D.; Scherf, U. *J. Mater. Chem.* **2010**, *20*, 1423-1430; (c) Hammer, B. a. G.; Bokel, F. a.; Hayward, R. C.; Emrick, T. *Chem. Mater.* **2011**, *23*, 4250-4256.
- 16 McCullough, R. D.; Tristram-Nagle, S.; Williams, S. P.; Lowe, R. D.; Jayaraman, M. *J. Am. Chem. Soc.*, **1993**, *115*, 4910-4911.
- 17 (a) Vandeleene, S.; Van den Bergh, K.; Verbiest, T.; Koeckelberghs, G. *Macromolecules*, **2008**, *41*, 5123–5131; (b) Babudri, F.; Colangiuli, D.; Di Bari, L.; Farinola, G. M.; Hassan Omar, O.; Naso, F.; Pescitelli, G. *Macromolecules*, **2006**, *39*, 5206–5212.
- 18 Zhao, J.; Swinnen, A.; Van Assche, G.; Manca, J.; Vanderzande, D.; Van Mele, B. *J. Phys. Chem. B* **2009**, *113*, 1587-1591.
- 19 Cui, Y.; Zhang, J.; Wang, P.; Zhang, X.; Zheng, J.; Sun, Q.; Feng, J.; Zhu, Y. *Electrochim. Acta* **2012**, *74*, 194-200.
- 20 Pangborn, A. B.; Giardello, M. A.; Grubbs, R. H.; Rosen, R. K.; Timmers, F.J. *Organometallics*, **1996**, *15*, 1518-1520.
- 21 Bäuerle, P.; Würthner, F.; Heid, S. *Angew. Chem., Int. Ed. Engl.*, **1990**, *29*, 419-420.

Chapter 2

- 22 Miyanishi, S.; Tajima, K.; Hashimoto, K. *Macromolecules*, **2009**, 42, 1610-1618.
- 23 Suspène, C.; Miozzo, L.; Choi, J.; Gironda, R.; Geffroy, B.; Tondelier, D.; Bonnassieux, Y.; Horowitz, G.; Yassar, A. *J. of Mater. Chem.*, **2012**, 22, 4511-4518.

2.6 Supporting information

2.6.1 Details on the monomer synthesis



Scheme S2.1. Synthesis of 2,5-dibromo-3-(6-bromohexyl)thiophene (**M1**): i. KO^tBu, MeOH/acetone, reflux; ii. a) Mg, Et₂O, b) **4**, Ni(dppp)Cl₂, Et₂O; iii. HBr, Ac₂O; iv. NBS, THF.

1-(6-Bromohexyloxy)-4-methoxybenzene (3).¹ 4-Methoxyphenol (**2**) (20.0 g, 161 mmol) and potassium *tert*-butoxide (21.7 g, 193 mmol, 1.2 equiv) were dissolved in a mixture of MeOH (80 mL) and acetone (80 mL) and stirred for 30 min at rt. The reaction mixture was then added dropwise to a solution of 1,6-dibromohexane (**1**) (77.9 g, 322 mmol, 2 equiv) in acetone (80 mL) at reflux temperature, and the reaction was further heated at reflux temperature until completion (as analyzed by TLC). The mixture was cooled down to rt and water was added. The product was extracted with diethyl ether and the organic layer was

¹ Toyoshima, R.; Narita, M.; Akagi, K.; Shirakawa, H. *Synthetic Metals*, **1995**, 69, 289–290.

washed with brine. The organic layer was dried with MgSO_4 , filtered and evaporated to dryness under reduced pressure. The unreacted 1,6-dibromohexane was removed by vacuum distillation. The pure product was recrystallized from MeOH and the resulting white crystals were dried under vacuum (32.6 g, 71%). ^1H NMR (300 MHz, CDCl_3): δ = 6.83 (s, 4H), 3.91 (t, J = 6.4 Hz, 2H), 3.77 (s, 3H), 3.43 (t, J = 6.7 Hz, 2H), 1.89 (q, J = 7.0 Hz, 2H), 1.77 (q, J = 6.7 Hz, 2H), 1.54–1.46 (m, 4H); ^{13}C NMR (75 MHz, CDCl_3) δ = 154.4, 153.9, 116.1 (CH), 115.3 (CH), 69.0 (CH_2), 56.4 (CH_3), 34.6 (CH_2), 33.4 (CH_2), 29.9 (CH_2), 28.6 (CH_2), 26.0 (CH_2); MS (EI): m/z = 286/288 (M^+).

3-[6-(4-Methoxyphenoxy)hexyl]thiophene (5). 1-(6-Bromohexyloxy)-4-methoxybenzene (**3**) (10.57 g, 36.8 mmol, 1 equiv), dissolved in a minimum amount of anhydrous diethyl ether (50 mL), was added under inert atmosphere to a suspension of Mg turnings (0.97 g, 40 mmol, 1.3 equiv) in anhydrous diethyl ether (10 mL) at reflux temperature. The reaction mixture was further refluxed for 1 h. The Grignard solution was cooled down to rt and then transferred dropwise via a cannula to an ice-cooled mixture of $\text{Ni}(\text{dppp})\text{Cl}_2$ (4 mol%) and 3-bromothiophene (5.0 g, 30.7 mmol) in dry diethyl ether (15 mL). The reaction mixture was refluxed for 12–15 h and afterwards hydrolyzed with a mixture of HCl (10 mL of a 1 M solution) and ice-water (20 mL), followed by extraction with several portions of Et_2O . Drying of the combined organic phases with MgSO_4 , filtration and removal of the solvent under reduced pressure afforded an orange oil which solidified upon standing. The product was purified by crystallization from hexane to provide an off-

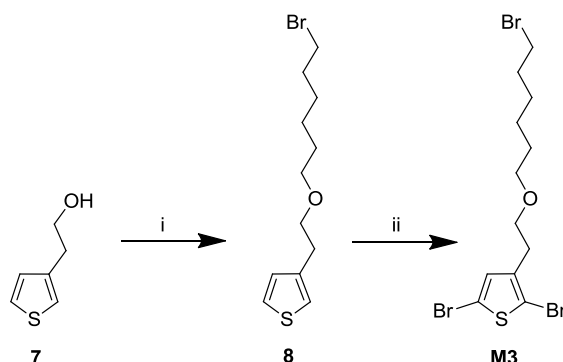
white solid. The filtrate was evaporated and additionally purified via column chromatography (silica) with a 50/50 hexanes/CH₂Cl₂ eluent mixture. Removal of the solvent gave the product as an off-white solid (overall yield 6.14 g, 69%). ¹H NMR (300 MHz, CDCl₃) δ = 7.23 (dd, *J* = 4.9 Hz and 3.0 Hz, 1H), 6.93–6.89 (m, 2H), 6.82 (s, 4H), 3.89 (t, *J* = 6.5 Hz, 2H), 3.75 (s, 3H), 2.63 (t, *J* = 7.6 Hz, 2H), 1.82–1.30 (m, 8H); ¹³C NMR (75 MHz, CDCl₃) δ = 154.3, 153.9, 143.7, 128.9 (CH), 125.8 (CH), 120.5 (CH), 116.1 (CH), 115.2 (CH), 69.2 (CH₂), 56.4 (CH₃), 31.1 (CH₂), 30.8 (CH₂), 29.9 (CH₂), 29.7 (CH₂), 26.5 (CH₂); MS (EI): *m/z* = 290 (M⁺).

3-(6-Bromohexyl)thiophene (6). Procedure as reported by Bäuerle et al.² ¹H NMR (300 MHz, CDCl₃) δ = 7.22 (dd, *J* = 4.8 and 2.9 Hz, 1H), 6.93–6.88 (m, 2H), 3.39 (t, *J* = 6.7 Hz, 2H), 2.62 (t, *J* = 7.7 Hz, 2H), 1.84 (q, *J* = 7.0 Hz, 2H), 1.62 (q, *J* = 7.6 Hz, 2H), 1.52–1.21 (m, 4H); ¹³C NMR (75 MHz, CDCl₃) δ = 143.5, 128.9 (CH), 125.8 (CH), 120.6 (CH), 34.7 (CH₂), 33.4 (CH₂), 31.0 (CH₂), 30.8 (CH₂), 29.0 (CH₂), 28.6 (CH₂); MS (EI): *m/z* = 246/248 (M⁺).

2,5-Dibromo-3-(6-bromohexyl)thiophene (M1). 3-(6-Bromohexyl)thiophene (**6**) (2.62 g, 10.6 mmol) was dissolved in THF (100 mL), cooled to 0 °C and protected from light. NBS (4.34 g, 24.4 mmol, 2.3 equiv) was added portion wise and the mixture was stirred further at rt for 8 h in the absence of light. The reaction mixture was quenched by pouring it into an ice-cold solution of 1 M NaOH and the product was

² Bäuerle, P.; Wurthner, F.; Heid, S. *Angew. Chem., Int. Ed. Engl.* **1990**, *29*, 419-420.

extracted with Et₂O. The organic layer was dried with MgSO₄, filtered and the solvent was evaporated under reduced pressure. The residue was purified on a silica plug with 50/50 hexanes/CH₂Cl₂ as the eluent. The pure fractions were collected and the solvent was removed under reduced pressure affording a colourless oil (3.9 g, 91%). ¹H NMR (300 MHz, CDCl₃): δ = 6.75 (s, 1H), 3.38 (t, *J* = 6.9 Hz, 2H), 2.49 (t, *J* = 7.7 Hz, 2H), 1.84 (q, *J* = 7.2 Hz, 2H), 1.54 (q, *J* = 7.7 Hz, 2H), 1.48–1.38 (m, 2H), 1.38–1.25 (m, 2H); ¹³C NMR (75 MHz, CDCl₃) δ = 143.2, 131.4 (CH), 111.0, 108.6, 34.4 (CH₂), 33.1 (CH₂), 29.9 (CH₂), 29.8 (CH₂), 28.7 (CH₂), 28.4 (CH₂); MS (EI): *m/z* = 402/404/406/408 (M⁺).



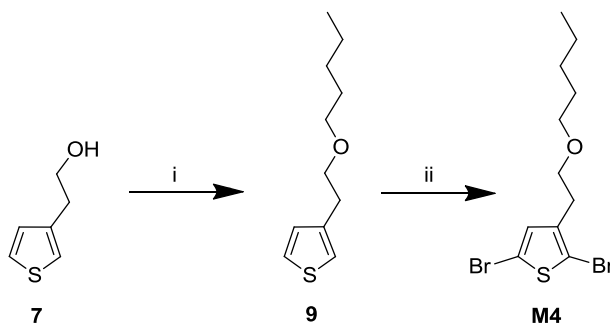
Scheme S2.2: Synthesis of 2,5-dibromo-3-{2-[(6-bromohexyl)oxy]ethyl}thiophene (**M3**): i. NaH, 1,6-dibromohexane, DMSO, 40 °C; ii. NBS, THF.

3-{2-[(6-bromohexyl)oxy]ethyl}thiophene (8). 1,6-Dibromohexane (76.1 g, 312 mmol) was dissolved in DMSO (150 mL), NaH (60% dispersion in mineral oil, 4.68 g, 117 mmol) was added and this suspension was heated at 40 °C under inert atmosphere. 2-(Thiophen-3-yl)ethanol (**7**) (10.0 g, 78 mmol) was dissolved in DMSO (50 mL) and

added dropwise. The reaction mixture was stirred for 4 h at 40 °C before it was cooled down to room temperature. The reaction was quenched by the addition of a saturated NH₄Cl solution (50 mL), water was added and the reaction mixture was extracted several times with diethyl ether. The organic layer was dried with MgSO₄, filtered and evaporated under reduced pressure. The residue was purified on a silica column with an eluent gradient from pure *n*-hexane to 75/25 *n*-hexane/DCM. The pure fractions were collected and evaporated, yielding a colorless oil (10.9 g, 48%). ¹H NMR (300 MHz, CDCl₃): δ = 7.27 (dd, *J* = 4.9 and 2.9 Hz, 1H), 7.05–7.02 (m, 1H), 7.00 (dd, *J* = 4.9 and 1.2 Hz, 1H), 3.65 (t, *J* = 7.1 Hz, 2H), 3.46 (t, *J* = 6.4 Hz, 2H), 3.42 (t, *J* = 6.4 Hz, 2H), 2.93 (t, *J* = 7.0 Hz, 2H), 1.88 (q, *J* = 6.6 Hz, 2H), 1.61 (q, *J* = 6.9 Hz, 2H), 1.52–1.32 (m, 4H); ¹³C NMR (75 MHz, CDCl₃) δ = 140.0, 129.2 (CH), 125.8 (CH), 121.7 (CH), 71.66 (CH₂), 71.4 (CH₂), 34.6 (CH₂), 33.4 (CH₂), 31.4 (CH₂), 30.2 (CH₂), 28.6 (CH₂), 26.1 (CH₂); MS (EI): *m/z* = 292/290 (M⁺).

2,5-Dibromo-3-{2-[(6-bromohexyl)oxy]ethyl}thiophene (M3). Similar to the synthesis of **M2** with following quantities: **8** (10.93 g, 37.5 mmol) was dissolved in dry THF (250 mL) and NBS (14.68 g, 82.5 mmol, 2.2 equiv) was added. The product was obtained as a pale yellow oil (10.75 g, 64%). ¹H NMR (300 MHz, CDCl₃): δ = 6.83 (s, 1H), 3.51 (t, *J* = 6.7 Hz, 2H) 3.38 (t, *J* = 6.6 Hz, 2H), 3.37 (t, *J* = 6.6 Hz, 2H) 2.75 (t, *J* = 6.7 Hz, 2H), 1.82 (q, *J* = 6.7 Hz, 2H), 1.54 (q, *J* = 6.9 Hz, 2H), 1.46–1.26 (m, 4H); ¹³C NMR (75 MHz, CDCl₃): δ = 139.7, 131.4 (CH), 110.3,

109.0, 70.8 (CH₂), 69.4 (CH₂), 33.9 (CH₂), 32.8 (CH₂), 30.1 (CH₂), 29.5 (CH₂), 27.9 (CH₂), 25.4 (CH₂); MS (EI): $m/z = 446/448/450/452$ (M⁺).

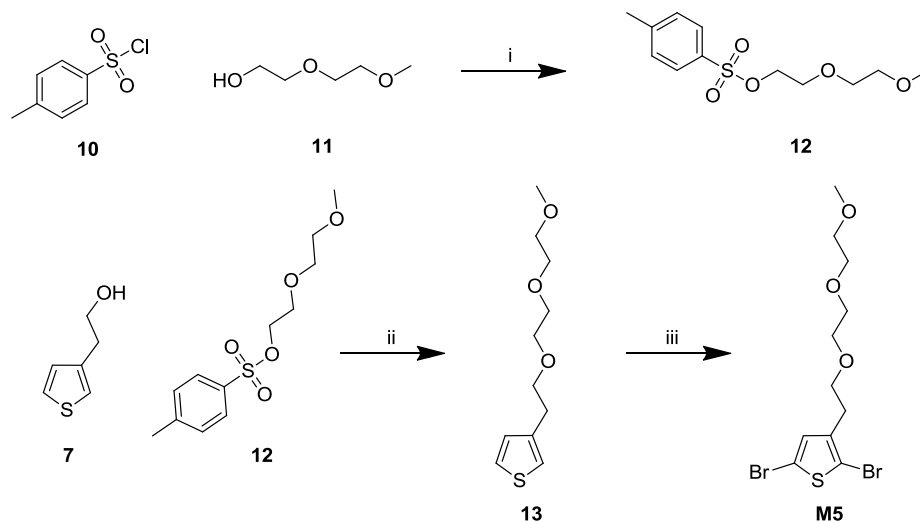


Scheme S2.3: Synthesis of 2,5-dibromo-3-[2-(pentyloxy)ethyl]thiophene (**M4**): i. NaH, 1-bromopentane, DMSO, 40 °C; ii. NBS, THF.

3-[2-(Pentyloxy)ethyl]thiophene (9). 2-(Thiophen-3-yl)ethanol (**7**) (5.0 g, 39 mmol) was dissolved in DMSO (150 mL), NaH (60% dispersion in mineral oil, 3.12 g, 78 mmol) was added and this suspension was stirred at room temperature for 30 min. 1-Bromopentane (11.8 g, 78 mmol) was added drop wise and the mixture was stirred for 8 h at room temperature. The reaction was quenched by the addition of a saturated NH₄Cl solution (50 mL), water was added and the reaction mixture was extracted several times with diethyl ether. The organic layer was dried with MgSO₄, filtered and evaporated under reduced pressure. The residue was purified on a silica column with an eluent gradient from pure *n*-hexane to 75/25 *n*-hexane/DCM. The pure fractions were collected and evaporated, yielding a colorless oil (7.24 g, 94%). ¹H NMR (300 MHz, CDCl₃): δ = 7.23 (dd, *J* = 5.1 and 3.0 Hz, 1H), 7.02–6.99 (m, 1H), 6.97 (dd, *J* = 4.9 and 1.3 Hz, 1H), 3.62 (t, *J* = 7.2 Hz, 2H), 3.43 (t, *J* = 6.9 Hz, 2H), 2.90

(t, $J = 7.0$ Hz, 2H), 1.58 (q, $J = 6.9$ Hz, 2H), 1.36–1.24 (m, 4H), 0.92–0.86 (m, 3H); ^{13}C NMR (75 MHz, CDCl_3): $\delta = 140.0, 129.2$ (CH), 125.8 (CH), 121.7 (CH), 71.8 (CH_2), 71.6 (CH_2), 31.4 (CH_2), 30.1 (CH_2), 29.0 (CH_2), 23.2 (CH_2), 14.7 (CH_3); MS (EI): $m/z = 198$ (M^+).

2,5-Dibromo-3-[2-(pentyloxy)ethyl]thiophene (M4). Similar to the synthesis of **M2** with following quantities: 10 (7.24 g, 36.5 mmol) was dissolved in dry THF (150 mL) and NBS (14.3 g, 80.3 mmol, 2.3 equiv) was added. The product was obtained as a colorless oil (12.0 g, 92%). ^1H NMR (300 MHz, CDCl_3): $\delta = 6.84$ (s, 1H), 3.52 (t, $J = 6.9$ Hz, 2H) 3.39 (t, $J = 6.7$ Hz, 2H), 2.76 (t, $J = 6.7$ Hz, 2H), 1.54 (q, $J = 6.9$ Hz, 2H), 1.33–1.21 (m, 4H), 0.87 (t, $J = 6.9$ Hz, 3H); ^{13}C NMR (75 MHz, CDCl_3): $\delta = 140.4, 132.2$ (CH), 111.1, 109.6, 71.8 (CH_2), 70.1 (CH_2), 30.8 (CH_2), 30.1 (CH_2), 29.1 (CH_2), 23.3 (CH_2), 14.8 (CH_2); MS (EI): $m/z = 354/356/358$ (M^+).



Scheme S2.4: Synthesis of 2,5-dibromo-3-{2-[2-(2-methoxyethoxy)ethoxy]ethyl}thiophene (**M5**): i. pyridine, DCM, rt ; ii. NaH, THF/DMSO, rt – 40 °C iii. NBS, THF.

2-(2-Methoxyethoxy)ethyl tosylate (12). A solution of 2-(2-methoxyethoxy)ethanol (**11**) (30.3 g, 252 mmol) in DCM (50 mL) was added drop wise to a solution of tosylchloride (**10**) (50 g, 260 mmol) and pyridine (59 g, 750 mmol) in DCM (300 mL) at room temperature. The reaction mixture was stirred at room temperature for 2 h. A solution of NH_4Cl (100 mL, 2 M) was added, the organic layer was separated and the water layer was extracted twice with DCM. The combined organic layers were washed once with a 20% aq NaCl-solution, dried over MgSO_4 and evaporated. The residue was purified on a silica plug with an eluent gradient from 100% DCM to 95/5 DCM/EtOH. The product fractions were collected and evaporated (30.0 g, 43%). ^1H NMR (300 MHz, CDCl_3): δ = 7.80 (d, J = 8.3 Hz, 2H), 7.34 (dd, J = 8.5 and 0.7 Hz, 2H), 4.20–4.15 (m, 2H), 3.72–3.66 (m, 2H), 3.61–3.46 (m, 4H), 3.35 (s,

3H), 2.45 (s, 3H); ^{13}C NMR (75 MHz, CDCl_3): $\delta = 145.5, 133.5, 130.5$ (CH), 128.6 (CH), 72.4 (CH_2), 71.3 (CH_2), 69.9 (CH_2), 69.3 (CH_2), 59.7 (CH_3), 22.3 (CH_3); MS (EI): $m/z = 274$ (M^+).

3-{2-[2-(2-Methoxyethoxy)ethoxy]ethyl}thiophene (13). To a solution of 2-(3-thienyl)ethanol (**7**) (10 g, 78 mmol) in a mixture of THF (150 mL) and DMSO (50 mL), NaH (60% in mineral oil, 3.8 g, 93 mmol) was added portion wise. This mixture was stirred at room temperature for 30 min before a solution of 2-(2-methoxyethoxy)ethyl tosylate (**12**) in THF (100 mL) was added drop wise. The reaction mixture was stirred at room temperature for 2 h, and then at 40 °C for 8 h. The reaction was quenched with a saturated NH_4Cl solution (100 mL), the phases were separated and the water layer was extracted several times with EtOAc. The combined organic layers were subsequently washed with a NH_4Cl and a NaCl solution, dried with MgSO_4 and evaporated. The residue was purified on a silica plug with 70/30 hexane/EtOAc as the eluent. The product fractions were collected and evaporated to dryness (16.5 g, 92%). ^1H NMR (300 MHz, CDCl_3): $\delta = 7.21$ (dd, $J = 4.9$ and 3.0 Hz, 1H), 7.00 (dd, $J = 3.0$ and 1.2 Hz, 1H), 6.96 (dd, $J = 4.9$ and 1.2 Hz, 1H), 3.67 (t, $J = 7.0$ Hz, 2H) 3.63–3.51 (m, 8H) 3.36 (s, 3H) 2.9 (t, $J = 7.0$ Hz, 2H); ^{13}C NMR (75 MHz, CDCl_3): $\delta = 139.8, 129.2$ (CH), 125.8 (CH), 121.8 (CH), 72.6 (CH_2), 72.3 (CH_2), 71.3 (CH_2), 71.2 (CH_2), 70.9 (CH_2), 59.7 (CH_3), 31.3 (CH_2); MS (EI): $m/z = 230$ (M^+).

2,5-Dibromo-3-{2-[2-(2-methoxyethoxy)ethoxy]ethyl} thiophene (M5).

Similar to the synthesis of **M2** with following quantities: **13** (16.5 g, 71.6 mmol) was dissolved in dry THF (250 mL) and NBS (26.8 g, 150.4 mmol) was added. The residue was purified on a silica plug with an eluent mixture 70/30 hexane/EtOAc (19.4 g, 70%). ¹H NMR (300 MHz, CDCl₃): δ = 6.87 (s, 1H), 3.63–3.53 (m, 10H) 3.36 (s, 3H) 2.78 (t, *J* = 6.7 Hz, 2H); ¹³C NMR (100 MHz, CDCl₃): δ = 139.5, 131.5 (CH), 110.4, 109.0, 71.9 (CH₂), 70.6 (CH₂), 70.3 (CH₂), 69.9 (CH₂), 59.0 (CH₂), 29.9 (CH₃); MS (EI): *m/z* = 389 (M⁺).

Chapter 3

Solution-processed bi-layer polythiophene-fullerene organic solar cells

Ghoos, T.; Malinkiewicz, O.; Lutsen, L.; Vanderzande, D. J.; Bolink, H. J.; Maes, W.
manuscript submitted to RSC Advances.

3.1 Introduction

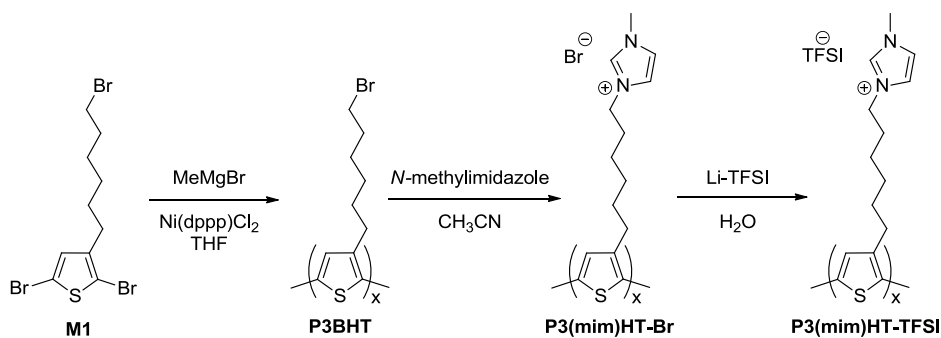
Organic photovoltaic cells (OPVs) have attracted a lot of attention in the last years, not in the least due to significant breakthroughs in device efficiencies.¹⁻⁶ Most of the best performing cells rely on bulk heterojunctions (BHJs), optimized for maximum light absorption and efficient charge generation. Less attention has been paid to the much simpler planar heterojunctions in bi-layer OPVs. Although bi-layer cells have lower efficiencies as a consequence of the use of thinner active layers (imposed by the limited exciton diffusion lengths), they still possess very interesting features which make them excellent platforms for the screening of new materials and for fundamental studies. Thanks to the planar structure (one organic layer on top of another) the charges generated at the interface are spatially separated which means that holes are confined within the donor layer while the electrons are confined within the acceptor layer. Since recombination between free charges is practically eliminated, it is possible to obtain information on physical phenomena such as exciton diffusion length, efficiency of charge transfer etc. in a straightforward way.⁷ Most bi-layer devices studied up to now were prepared by vacuum sublimation.⁸⁻¹⁰ This had led to a wealth of information, yet it is limited to materials that can be sublimed, excluding polymeric and ionic materials.^{7,10-13} The preparation of neat bi-layers from solution, however, is not trivial, not in the least as both donor and acceptor materials are frequently soluble in the same common solvents.¹⁴ Therefore, alternative deposition techniques such as film-transfer have been explored to allow the study of polymer-fullerene bi-layer OPVs.¹⁵ A few works were published in which bi-layer planar

Solution-processed bi-layer polythiophene-fullerene organic solar cells

heterostructures were prepared from solution using ionic donor molecules in combination with evaporated acceptor molecules.¹⁶⁻¹⁹ Recently it was also demonstrated that a bi-layer inverted OPV could be prepared using a low impact solution coating technique referred to as meniscus coating.^{20,21}

Among the organic molecules applied as donor materials in OPVs, poly(3-hexylthiophene) or P3HT is without any doubt the most commonly applied.^{1,22,23} More advanced polythiophene derivatives, e.g. end-group or side-chain functionalized and block copolymer structures, have been synthesized towards morphology control and stability.²⁴⁻³¹ Bi-layer devices using P3HT and PC₆₁BM ([6,6]-phenyl-C61-butyric acid methyl ester) have been reported, yet due to the similar solubility of these materials the PC₆₁BM molecules diffuse into the P3HT layer generating concentration gradients in the vertical direction. In this way power conversion efficiencies are obtained that are rather similar to BHJ devices.^{32,33} To prevent the intermixing of the two materials upon solution processing, chemically modified or modifiable polythiophenes should be used.²⁵ Conjugated polyelectrolytes based on ionic polythiophenes, obtained via the introduction of pendant ionic functionalities on the alkyl side chains, have shown large potential as interlayer materials in OPVs.³⁴ These materials have a very different solubility than their neutral counterparts. Therefore, ionic P3HT derivatives are of particular appeal for the preparation of neat bi-layer OPVs, as they allow processing from orthogonal and environmentally friendly solvents (e.g. alcohols).³⁵⁻³⁹

Here we present a solution-processed neat planar heterojunction OPV system using an ionic poly(3-alkylthiophene) (i-P3AT) (**Scheme 3.1**) as the donor material and PC₆₁BM or PC₇₁BM (**Figure 3.1**) as the acceptor. Due to the ionic nature of the polythiophene donor material it is completely insoluble in chlorobenzene, used to deposit the fullerene acceptor layer. This, together with the high film qualities obtained by meniscus coating (the deposition technique used in this work) allowed for the preparation of neat bi-layer devices. The best performing devices with active layers of 40 nm using PC₇₁BM as the acceptor exhibited power conversion efficiencies (PCE) in excess of 1.5% (1.9% best device).



Scheme 3.1: Polymerization and functionalization protocol towards ionic polythiophene **P3(mim)HT-TFSI**.

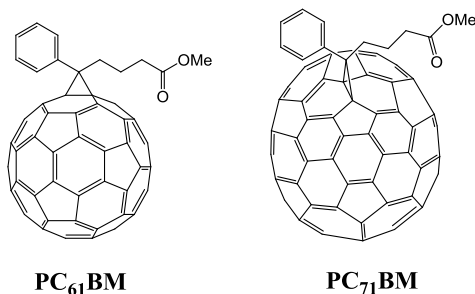


Figure 3.1: PC₆₁BM and PC₇₁BM fullerene acceptors.

3.2 Experimental section

3.2.1 Synthesis and characterization

Unless stated otherwise, all reagents and chemicals were obtained from commercial sources and used without further purification. Diethyl ether and tetrahydrofuran (THF) were dried using a MBraun MB-SPS 800 solvent purification system, operating under N₂ according to the principles described by Pangborn et al.⁴⁰ NMR chemical shifts (δ , in ppm) were determined relative to the residual ¹H absorption of CHCl₃ (7.26 ppm) or the ¹³C resonance shift of CDCl₃ (77.16 ppm). Gas chromatography-mass spectrometry (GC-MS) analyses were carried out applying Chrompack Cpsil5CB or Cpsil8CB capillary columns. UV-Vis measurements of the polymers in solution were performed with a scan rate of 600 nm/min in a continuous run from 200 to 800 nm. Molecular weights and molecular weight distributions were determined relative to polystyrene standards (Polymer Labs) by size exclusion chromatography (SEC). Analysis of the molecular weight and molecular weight distribution of the precursor polymer was performed on a Tosoh EcoSEC System, comprising of an auto sampler, a PSS guard column SDV (50 x 7.5 mm), followed by three PSS SDV analytical linear XL

columns (5 μm , 300 x 7.5 mm), and a differential refractive index detector (Tosoh EcoSEC RI) and a UV detector using THF as the eluent at 40 $^{\circ}\text{C}$ with a flow rate of 1.0 mL/min. The SEC system was calibrated using linear narrow polystyrene standards ranging from 474 to 7.5×10^6 g/mol ($K = 14.1 \times 10^{-5}$ dL/g and $\alpha = 0.70$). Polymer concentrations were in the range of 3–5 mg/mL. The ionic polythiophenes were analyzed on a 1260 infinity SEC system from Agilent Technologies with UV (200 nm) and RI detector, Zorbax PSM Bimodal column (6.2 x 250 mm, 5 μm) at 30 $^{\circ}\text{C}$, hexafluoroisopropanol (HFIP) with potassium trifluoroacetate (0.1 M) as the eluent, 1 mL/min elution speed, calibrated with linear PMMA standards from Agilent (Polymer Laboratories).

3.2.2 Monomer synthesis

2,5-Dibromo-3-(6-bromohexyl)thiophene (**M1**) was prepared using a modified procedure based on literature protocols by Bäuerle⁴¹ and Miyanishi.²⁵ More detailed information is provided in the Supporting Information (SI)

3.2.3 Polymer synthesis: poly(3-(6-bromohexyl)thiophene) or P3BHT²⁵

The monomer, 2,5-dibromo-3-(6-bromohexyl)thiophene (**M1**) (0.51 g, 1.27 mmol), was added to a flame-dried three-neck flask and dissolved in dry THF (15 mL). The reaction mixture was put under inert atmosphere and heated to reflux temperature. A MeMgBr solution (0.65 M in THF, 1.96 mL, 1.27 mmol, 1 equiv) was added and the mixture was stirred for 1 h at reflux temperature. To start the polymerization, 0.8

Solution-processed bi-layer polythiophene-fullerene organic solar cells

mol% of Ni(dppp)Cl₂ (5.5 mg, 0.01 mmol) was added and the mixture was stirred for 2 h at reflux temperature. The polymer was precipitated into an ice cold HCl/MeOH (5%) mixture and the precipitated polymer was filtered off on a PTFE membrane (47 mm/0.45 μm). The polymer was purified using Soxhlet extraction for 24 h with methanol, n-hexane and chloroform, respectively. After evaporation of the solvent, the polymer was redissolved in chloroform and precipitated again from methanol, filtered, washed with methanol and dried, affording **P3BHT** as a black powder (0.153 g, 49%). ¹H NMR (300 MHz, CDCl₃): δ = 6.96 (s, 1H), 3.41 (t, J = 6.7 Hz, 2H), 2.81 (t, J = 7.3 Hz, 2H), 1.88 (q, J = 6.8 Hz, 2H), 1.71 (br, 2H), 1.56–1.41 (m, 4H); UV-Vis (CHCl₃, nm) λ_{max} 440; SEC (THF, PS standards) M_n = 1.2 x 10⁴ g/mol, M_w = 3.5 x 10⁴ g/mol, D = 3.1.

3.2.4 Polymer functionalization with N-methylimidazole: poly[3-(6-(1-methylimidazolium-3-yl)hexyl)thiophene] bromide or P3(mim)HT-Br

P3BHT (0.050 g, M_n = 1.2 x 10⁴ g/mol, PDI = 3.1) was suspended in acetonitrile (1 mL) in a 10 mL vial and N-methylimidazole (1 mL) was added. The vial was filled with argon and closed. The suspension was heated at 70 °C for 48 h in the dark before it was added dropwise to Et₂O and a dark red precipitate was obtained. The precipitated polymer was filtered off using a PTFE membrane (47 mm/0.45 μm) and (freeze-)dried carefully, affording **P3(mim)HT-Br** as a purple-black powder (0.061 g, 91%). ¹H NMR (300 MHz, DMSO-d₆): δ = 9.39 (s, 1H), 7.85 (s, 1H), 7.75 (s, 1H), 7.21 (s, 1H), 4.21 (br, 2H), 3.87 (s, 3H), 2.78 (br, 2H), 1.81

(br, 2H), 1.64 (br, 2H), 1.46–1.24 (m, 4H); UV-Vis (MeOH, nm) λ_{\max} 442; SEC (HFIP, PMMA standards) $M_n = 1.9 \times 10^4$ g/mol, $M_w = 6.6 \times 10^4$ g/mol, $D = 3.5$.

3.2.5 Counter ion exchange: poly[3-(6-(1-methylimidazolium-3-yl)hexyl)thiophene] bis(trifluorosulfonyl)imide or P3(mim)HT-TFSI

P3(mim)HT-Br (0.040 g) was dissolved in distilled water (4 mL) and a solution of Li-TFSI (0.4 g, 1.4 mmol) in distilled water (1 mL) was added dropwise. A precipitate was immediately formed and the mixture was stirred for another 8 h at rt. The sticky precipitate was filtered off on a regenerated cellulose membrane (47 mm/0.45 μm) and dried under vacuum, affording **P3(mim)HT-TFSI** as a sticky black powder (54 mg, 84%). ^1H NMR (300 MHz, DMSO- d_6): $\delta = 9.06$ (s, 1H), 7.71 (s, 1H), 7.67 (s, 1H), 7.15 (s, 1H), 4.13 (br, 2H), 3.82 (s, 3H), 2.77 (br, 2H), 1.78 (br, 2H), 1.63 (br, 2H), 1.44–1.22 (m, 4H); UV-Vis (MeOH, nm) λ_{\max} 443; SEC (HFIP, PMMA standards) $M_n = 1.6 \times 10^4$ g/mol, $M_w = 8.4 \times 10^4$ g/mol, $D = 5.4$.

3.2.6 Device fabrication

Devices were prepared using the meniscus coating technique (**Figure 3.2**).^{20,21} The choice for this non-standard technique was based on the high quality of the solution-processed films that can be obtained by this method²⁰ and the extremely low material usage.⁴²

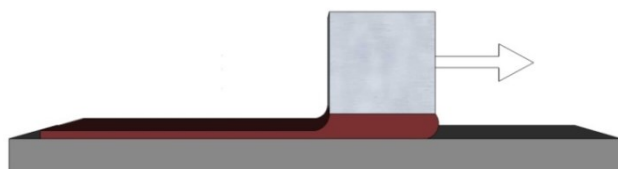


Figure 3.2: Schematic drawing of the meniscus coating technique.

A drop of solution is placed in between the substrate and the bottom of a flat blade (3 by 20 mm). Because the distance between the blade and the substrate is small (0.2 mm), the drop is maintained within the gap by capillary forces creating the so-called meniscus. When moving the blade over the substrate, this meniscus is stretched, leaving behind a thin film of the organic material. The resulting dry film thickness is primarily determined by the drawing speed of the blade and its distance to the substrate.^{20,43}

Pre-patterned ITO-covered glass substrates (www.naranjosubstrates.com) were first pre-cleaned by a standard procedure in detergent (5 min), deionized water (5 min) and isopropanol (5 min) using an ultrasonic bath. Then the samples were transferred to a UV-ozone lamp for 15 min and 70 nm of PEDOT:PSS (CLEVIOS™ P VP AI 4083, aqueous dispersion, 1.3–1.7% solid content, Heraeus) was spin-coated immediately after the ozone treatment. The residual water was removed from the PEDOT:PSS layer by annealing at 150 °C for 10 min. Then approx. 50 nm of the **P3(mim)HT-TFSI** polymer was deposited from 2,2,3,3-tetrafluoro-1-propanol (TFP; 10 mg/mL) solution using the meniscus coating technique (**Figure 3.2**). For a 50 nm thick

P3(mim)HT-TFSI film, the drawing speed of the blade was 20 mm/s, and the gap between the blade and the substrate was 0.2 mm, corresponding to approximately 43 μL of solution. After deposition, the polymer layer was left to dry for approx. 1 min and 40 nm of PC₆₁BM (Solenne) was deposited on top from a chlorobenzene solution (20 mg/mL) by the same technique. The drawing speed of the blade in the case of the fullerene film was varied from 20 mm/s up to 40 mm/s, resulting in film thicknesses between 30 and 60 nm. To complete the devices, samples were transferred into a nitrogen-filled glove box (1 ppm O₂ and <0.1 ppm H₂O) where 5 nm of Ba and 70 nm of Ag were evaporated as a cathode (<5 x 10⁻⁶ mbar). Solar cells (active area 9 mm²) were illuminated by a white light halogen lamp in combination with interference filters for the EQE (external quantum efficiency) and J–V measurements (MiniSun simulator by ECN, the Netherlands). An estimation of the short-circuit current density (J_{sc}) under standard test conditions was calculated by convolving the EQE spectrum with the AM1.5G reference spectrum, using the premise of a linear dependence of J_{sc} on light intensity. J–V characteristics of the solar cells were recorded using a Keithley 2400 Source Meter. All characterization was performed in a nitrogen-filled glove box (1 ppm O₂ and <0.1 ppm H₂O) without device encapsulation.

3.3 Results and discussion

3.3.1 Polymer synthesis and characterization

In order to synthesize the desired ionic polythiophenes, a highly regioregular (rr) precursor (homo)polymer was prepared first using the

standard Grignard metathesis (GRIM) polymerization protocol (**Scheme 3.1**).^{23,40–42} The isolated yield for the polymerization of 2,5-dibromo-3-(6-bromohexyl)thiophene (**M1**) towards **P3BHT**^{24,36–38} was ~50% (not including the 15–25% loss of the non-selective transmetalation), with molecular weight averages $M_n = 1.2 \times 10^4$ and $M_w = 3.5 \times 10^4$. The rather broad distribution ($D = 3.1$) is mainly due to the high sensitivity of the GRIM method to traces of moisture in the reaction mixture and impurities in the monomer solution. Functionalization of the precursor polymer with *N*-methylimidazole was performed over 48 h to ensure complete conversion to the ionic polythiophene derivative **P3(mim)HT-Br** (**Scheme 3.1**).^{35–39} The polymer was precipitated in the non-solvent diethyl ether, washed several times with ether and used without any further purification. The resulting ionic polymer was soluble in polar solvents such as water, methanol, DMF and DMSO. UV-Vis absorption spectra of the polymer material in solution showed a distinct broadening and red-shift in water, compared to the absorbance in methanol and DMF (**Figure S3.1**).¹³ In methanol and DMSO the polymer seems molecularly dissolved, but some problems were encountered upon filtration of the solutions before preparing the devices (*vide infra*). The bromide counter ions of **P3(mim)HT-Br** were then exchanged for more apolar bis(trifluorosulfonyl)-imide (TFSI) organic counter ions (Scheme 1) to render the polymer less hygroscopic and more soluble in solvents suitable for bi-layer processing.⁴⁴ After anion exchange, the **P3(mim)HT-TFSI** polymer was not soluble anymore in water (nor in THF, chloroform or chlorobenzene), but it was still soluble in acetone, acetonitrile and 2,2,3,3-tetrafluoro-1-propanol (TFP). This solubility

behaviour enables to use this ionic polymer for the construction of bi-layer devices. TFP was chosen since it is a good and environmentally acceptable solvent for film casting.

From ^1H NMR characterization of the obtained polymers (**Figure S3.2**), one can easily see that the substitution protocol was successful, by following the shift of the protons on the side-chain carbon atoms next to the end groups, going from 3.41 ppm (in CDCl_3) for the **P3BHT** polymer to 4.21 ppm (in $\text{DMSO-}d_6$) for **P3(mim)HT-Br** and 4.13 ppm (in $\text{DMSO-}d_6$) for the final **P3(mim)HT-TFSI** polymer. The aromatic protons of the imidazole moiety also showed a shift when the counter ion was exchanged. The exchange was quantitative (within the NMR detection limit) as no residual peaks of **P3(mim)HT-Br** were found in the **P3(mim)HT-TFSI** spectrum.

3.3.2 Device construction and analysis

The ionic polythiophenes were then applied as donor materials together with PC_{61}BM fullerene as the acceptor material in a simple bi-layer configuration, as is shown in **Figure 3.3**.

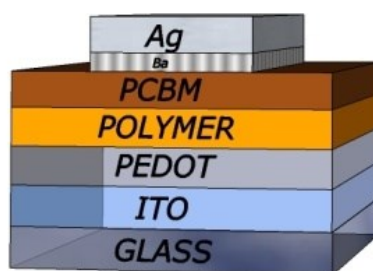


Figure 3.3: Bilayer device layout.

Solution-processed bi-layer polythiophene-fullerene organic solar cells

The film absorption spectrum of **P3(mim)HT-TFSI** (as casted from TFP) is blue-shifted with respect to that of a film of rr-P3HT (Rieke metals, 4002-EE) (**Figure 3.4**).

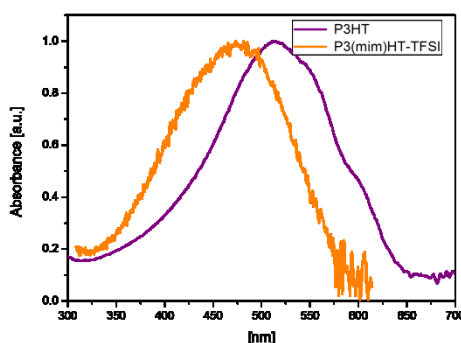


Figure 3.4: Absorption spectra of P3HT and **P3(mim)HT-TFSI** in a thin film configuration.

The origin of this blue-shift is not completely clear but it can indicate a poor packing of the chains, and as a consequence the typical absorption band around 600 nm is not observed. Yet, the absence of the higher wavelength absorption leads to a slightly higher bandgap for the **P3(mim)HT-TFSI** material. Additionally, it was observed that, keeping the same thickness of the polythiophene layers, the **P3(mim)HT-TFSI** absorbs less light compared to the non-ionic polymer. The difference in absorbance is due to the slightly lower density of the conjugated polythiophene part due to the addition of bulky ionic groups at the periphery of the polymer chains.

To find optimal thicknesses of the layers a series of device experiments was performed in which the polymer layer thickness was kept constant (between 45–50 nm) and the PC₆₁BM layer thickness was varied from 30 to 60 nm. **Figure 3.5** and **Table 3.1** show the average output

Chapter 3

parameters collected from approximately four solar cells for each PC₆₁BM film thickness. The best values in the series were obtained for a PC₆₁BM layer of 40 nm, resulting in an average PCE of 0.5%. This optimum PC₆₁BM thickness was then used for the remaining experiments described below.

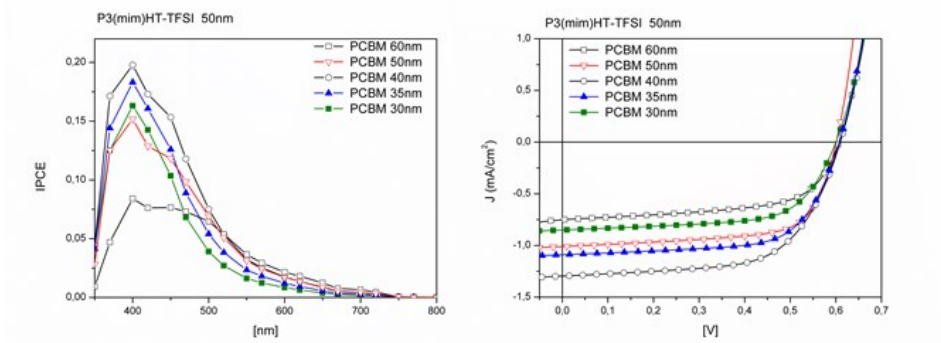


Figure 3.5: Typical IPCE versus wavelength (left) and current density versus voltage curves (right) for solar cells with different PC₆₁BM film thicknesses.

Table 3.1: Bi-layer device optimization (PC₆₁BM thickness).

P3(mim)- HT-TFSI [nm]	PC₆₁BM [nm]	IPCE_{max} [%]	PCE [%]	FF [%]	V_{oc} [V]	J_{sc} [mA/cm²]
50	30	16	0.32	61	0.6	0.9
50	35	18	0.4	63	0.6	1.1
50	40	19	0.49	62	0.61	1.3
50	50	15	0.41	65	0.6	1
50	60	8	0.27	60	0.61	0.72

To ensure that there was no intermixing between the active layers, a series of simple experiments was performed. First, the absorption of a

Solution-processed bi-layer polythiophene-fullerene organic solar cells

thin layer of **P3(mim)HT-TFSI** was determined. The absorption of the thin film was also repeatedly determined after subsequent washing steps with chlorobenzene. No notable changes were observed after as much as 10 washing steps (**Figure S3.3**). These results showed that no **P3(mim)HT-TFSI** was removed by exposure to chlorobenzene. To verify if the PC₆₁BM did not diffuse into the **P3(mim)HT-TFSI** layer, a PC₆₁BM layer was deposited on top of the ionic polymer layer, dried either at room temperature or at 150 °C, and then removed by washing with chlorobenzene. After the washing step, the absorption spectrum for both experiments was identical to the pristine **P3(mim)HT-TFSI** layer, suggesting that all PC₆₁BM material was removed from the layer and that no PC₆₁BM had diffused into the donor layer.

For the optimized bi-layer solar cells the incident photon to current efficiencies (IPCE) versus wavelength were determined (**Figure 3.6a**). The highest efficiencies were obtained close to 400 nm where the principal absorber is PC₆₁BM. The **P3(mim)HT-TFSI** polymer has an absorption maximum at ~450 nm, which is in agreement with the secondary maximum visible in the IPCE curve around that wavelength. The corresponding current density-voltage (*J-V*) curves were reasonably rectangular, resulting in good fill factors (~60%). The V_{oc} for these cells is rather typical (~0.6 V). The current density is significantly lower than observed for P3HT/PCBM BHJ devices, due to the limited interface in these planar cells and additionally due to the lower light absorption in the **P3(mim)HT-TFSI** layer. The finding that no increase of the current was observed with increasing layer thickness is an additional indication that the bi-layers formed are “neat”, without intermixing at the interface.

If such intermixing would occur, the current would increase proportionally to the active layer thickness, as is usually observed in BHJ devices.¹⁴

To put the key performance characteristics of the solution-processed devices in perspective they were compared to those obtained from cells prepared via the dry film transfer method recently published by Tada et al. (**Table 3.2**).¹⁵ The results obtained from the solution-processed bi-layer cells are comparable with those obtained from the dry transfer method. The slightly lower current observed in the solution-processed layer is compensated for by a slightly higher V_{oc} .^{15,25,32,33} It should be noted as well that all devices presented were very reproducible, even if repeated after some period of time and using different batches of the same polymer (see SI, **Tables S3.1** and **S3.2**).

Table 3.2: Comparison between an optimized bi-layer device, a PC₆₁BM-only device and a device with an ultra-thin P3(mim)HT-TFSI donor layer.

	PC ₆₁ BM [nm]	polymer [nm]	IPCE _{max} [%]	PCE [%]	FF [%]	V_{oc} [V]	J_{sc} [mA/cm ²]
PC ₆₁ BM- only	50	-	4.5	0.05	33	0.7	1.3
P3(mim)HT- TFSI (thin)	40	20	10.5	0.33	58	0.67	1.1
P3(mim)HT- TFSI	40	50	19	0.48	62	0.61	0.9
Non-ionic (lit ¹⁵)	45	40	-	0.4	53	0.5	1

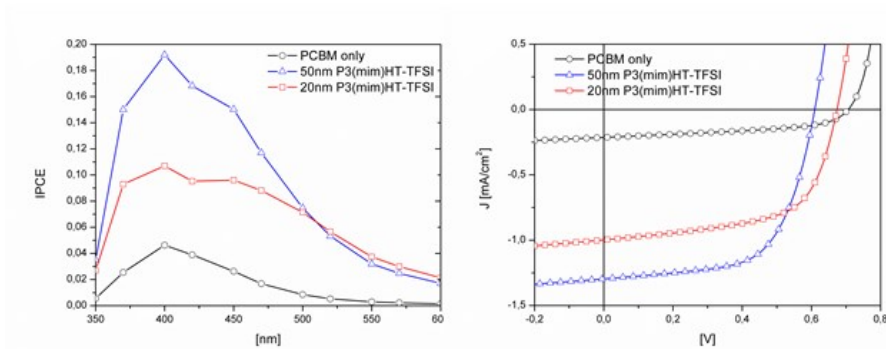


Figure 3.6: Typical IPCE versus wavelength (left) and current density versus voltage curves (right) for devices using different **P3(mim)HT-TFSI** thicknesses, including a fullerene-only device.

Even though the absorbance of the **P3(mim)HT-TFSI** polymer is blue-shifted and partially overlapping with that of PC₆₁BM, its presence in the device is important, as is shown below. To this extent a PC₆₁BM-only device (ITO/PEDOT-70 nm/PC₆₁BM-50 nm/Ba-5 nm/Ag-70 nm) was prepared and compared with devices with a very thin **P3(mim)HT-TFSI** layer (~5 nm). In the double layer devices with the thin **P3(mim)HT-TFSI** layer, the absorption of the polymer is negligible. Using meniscus coating it was possible to prepare very high quality PC₆₁BM films, as evidenced by the reasonable *J-V* curve for a PC₆₁BM film of only 50 nm thickness. It is clear from **Figure 3.6** and the values reported in **Table 3.2** that without the polymer layer the excitons created within the PC₆₁BM layer do not contribute to the current. With the addition of a thin layer of **P3(mim)HT-TFSI**, the excitons can efficiently dissociate at the interface leading to a reasonable current flow in the device. Moreover, the high fill factors of the cells (over 60%) reveal excellent film-forming properties of the ionic polymer.

Chapter 3

Finally, since a significant part of the current of the cell originates from the fullerene layer, we decided to switch from PC₆₁BM to PC₇₁BM (**Figure 3.1**), which has a much broader absorption. The comparison between bi-layer cells using the different fullerenes as acceptor layers is shown in **Figure 3.7** and **Table 3.3**. As expected, the current of the cells increased significantly, improving the cell efficiency up to 1.6%, which is a good value for this type of structures.

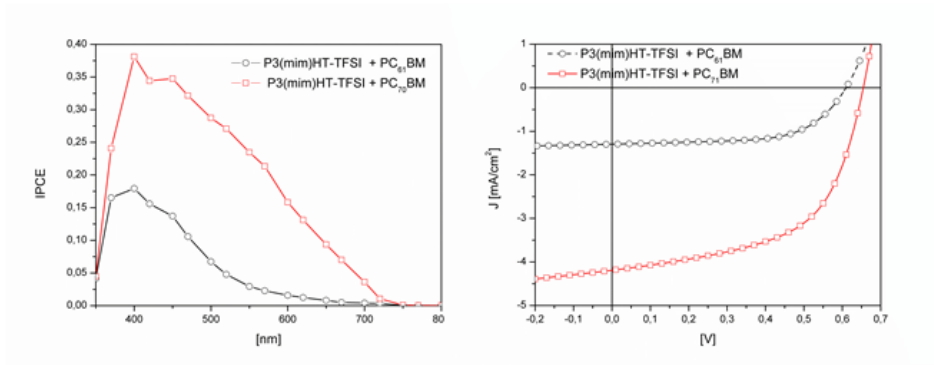


Figure 3.7: Typical IPCE versus wavelength (left) and current density versus voltage curves (right) for devices using PC₆₁BM or PC₇₁BM as the material for the acceptor layers.

Table 3.3: PC₆₁BM device vs. PC₇₁BM device for a 50 nm layer of **P3(mim)HT-TFSI**.

	[nm]	IPCE _{max} [%]	PCE [%]	FF [%]	V _{oc} [V]	J _{sc} [mA/cm ²]
PC ₆₁ BM	40	19	0.5	62	0.61	1.3
PC ₇₁ BM	40	38	1.6	57	0.65	4.3

3.4 Conclusions

In conclusion, we report on polar polythiophenes with pendant ionic liquid-like side chains as a promising class of materials for organic solar cells. The main difference between a non-ionic and an ionic polythiophene is the fact that the latter one is not soluble in chlorobenzene, thus enabling processing of bi-layer configurations from solution. We have shown that our modified **P3(mim)HT-TFSI** polymer shows the same or even slightly superior performance as compared to standard P3HT in a bi-layer configuration. We underline that the novel ionic P3HT derivative synthesized in this work shows excellent film-forming properties and devices were highly reproducible. Using it in combination with PC₇₁BM as the acceptor, power conversion efficiencies of 1.6% were achieved for these simple solution-processed bi-layer solar cells.

3.5 References

- 1 M. Helgesen, R. Søndergaard, and F. C. Krebs, *Journal of Materials Chemistry*, 2010, **20**, 36.
- 2 B. C. Thompson, P. P. Khlyabich, B. Burkhart, A. E. Aviles, A. Rudenko, G. V. Shultz, C. F. Ng, and L. B. Mangubat, *Green*, 2011, **1**, 29–57.
- 3 P. Kumar and S. Chand, *Progress in Photovoltaics*, 2012, **20**, 377–415.
- 4 M. Mayukh, I. H. Jung, F. He, and L. P. Yu, *Journal of Polymer Science Part B-Polymer Physics*, 2012, **50**, 1057–1070.
- 5 G. Li, R. Zhu, and Y. Yang, *Nature Photonics*, 2012, **6**, 153–161.
- 6 A. Mishra and P. Bäuerle, *Angew Chem Int Ed Engl*, 2012, **51**, 2020–2067.
- 7 C. Uhrich, D. Wynands, S. Olthof, M. K. Riede, K. Leo, S. Sonntag, B. Maennig, and M. Pfeiffer, *Journal of Applied Physics*, 2008, **104**, 043107.
- 8 M. Riede, T. Mueller, W. Tress, R. Schueppel, and K. Leo, *Nanotechnology*, 2008, **19**, 424001.
- 9 I. Kim, H. M. Haverinen, Z. Wang, S. Madakuni, Y. Kim, J. Li, and G. E. Jabbour, *Chemistry of Materials*, 2009, **21**, 4256–4260.
- 10 J. Wagner, M. Gruber, A. Wilke, Y. Tanaka, K. Topczak, A. Steindamm, U. Hörmann, A. Opitz, Y. Nakayama, H. Ishii, J. Pflaum, N. Koch, and W. Brütting, *Journal of Applied Physics*, 2012, **111**, 054509.
- 11 A. Foertig, A. Wagenpfahl, T. Gerbich, D. Cheyns, V. Dyakonov, and C. Deibel, *Advanced Energy Materials*, 2012, **2**, 1483–1489.
- 12 S. Yoo, W. J. Potscavage, B. Domercq, S.-H. Han, T.-D. Li, S. C. Jones, R. Szoszkiewicz, D. Levi, E. Riedo, S. R. Marder, and B. Kippelen, *Solid-State Electronics*, 2007, **51**, 1367–1375.
- 13 Y. Zang, J. Yu, J. Huang, R. Jiang, and G. Huang, *Journal of Physics D: Applied Physics*, 2012, **45**, 175101.
- 14 V. S. Gevaerts, L. J. A. Koster, M. M. Wienk, and R. a J. Janssen, *ACS applied materials & interfaces*, 2011, **3**, 3252–5.
- 15 A. Tada, Y. Geng, Q. Wei, K. Hashimoto, and K. Tajima, *Nature materials*, 2011, **10**, 450–5.

Solution-processed bi-layer polythiophene-fullerene organic solar cells

- 16 H. Benmansour, F. A. Castro, M. Nagel, J. Heier, R. Hany, and F. Nüesch, *CHIMIA International Journal for Chemistry*, 2007, **61**, 787–791.
- 17 B. Fan, F. Araujo de Castro, B. T.-T. Chu, J. Heier, D. Opris, R. Hany, and F. Nüesch, *Journal of Materials Chemistry*, 2010, **20**, 2952.
- 18 M. Lenes and H. J. Bolink, *ACS Appl Mater Interfaces*, 2010, **2**, 3664–3668.
- 19 O. Malinkiewicz, T. Grancha, A. Molina-Ontoria, A. Soriano, H. Brine, and H. J. Bolink, *Advanced Energy Materials*, 2012, 10.1002/aenm.201200764.
- 20 O. Malinkiewicz, M. Lenes, H. Brine, and H. J. Bolink, *RSC Advances*, 2012, **2**, 3335.
- 21 B. Park and M.-Y. Han, *Optics express*, 2009, **17**, 13830–40.
- 22 M. T. Dang, L. Hirsch, and G. Wantz, *Advanced Materials*, 2011, **23**, 3597–3602.
- 23 A. Marrocchi, D. Lanari, A. Facchetti, and L. Vaccaro, *Energy & Environmental Science*, 2012, **5**, 8457–8474.
- 24 S. Miyanishi, K. Tajima, and K. Hashimoto, *Macromolecules*, 2009, **42**, 1610–1618.
- 25 B. J. Kim, Y. Miyamoto, B. Ma, and J. M. J. Fréchet, *Advanced Functional Materials*, 2009, **19**, 2273–2281.
- 26 A. Smeets, P. Willot, J. De Winter, P. Gerbaux, T. Verbiest, G. Koeckelberghs, and A. Polythiophenes, 2011, 6017–6025.
- 27 D. M. Tanenbaum, M. Hermenau, E. Voroshazi, M. T. Lloyd, Y. Galagan, B. Zimmermann, M. Hösel, H. F. Dam, M. Jørgensen, S. a. Gevorgyan, S. Kudret, W. Maes, L. Lutsen, D. Vanderzande, U. Würfel, R. Andriessen, R. Rösch, H. Hoppe, G. Teran-Escobar, M. Lira-Cantu, A. Rivaton, G. Y. Uzunoğlu, D. Germack, B. Andreasen, M. V. Madsen, K. Norrman, and F. C. Krebs, *RSC Advances*, 2012, **2**, 882.
- 28 S. D. Oosterhout, L. J. A. Koster, S. S. van Bavel, J. Loos, O. Stenzel, R. Thiedmann, V. Schmidt, B. Campo, T. J. Cleij, L. Lutzen, D. Vanderzande, M. M. Wienk, and R. a. J. Janssen, *Advanced Energy Materials*, 2011, **1**, 90–96.
- 29 H. J. Kim, A. R. Han, C.-H. Cho, H. Kang, H.-H. Cho, M. Y. Lee, J. M. J. Fréchet, J. H. Oh, and B. J. Kim, *Chemistry of Materials*, 2012, **24**, 215–221.

Chapter 3

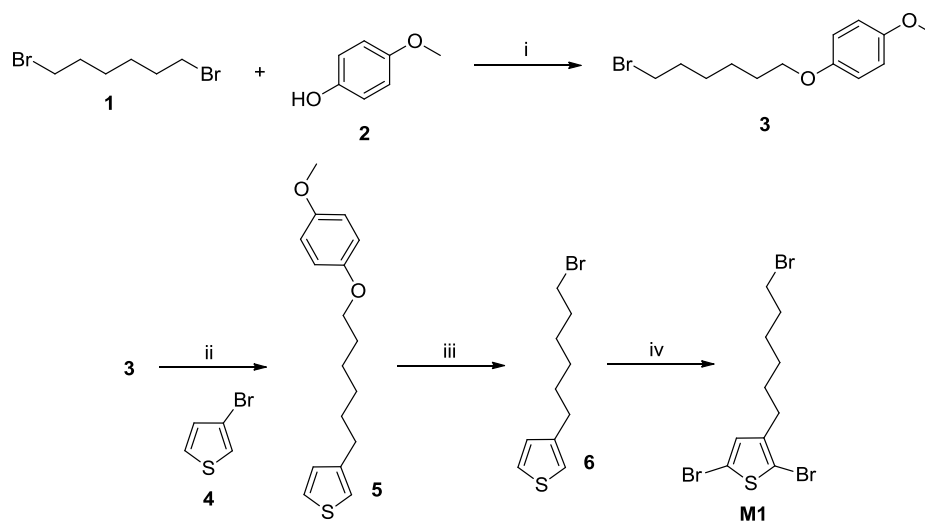
- 30 Y. Lin, J. A. Lim, Q. Wei, S. C. B. Mannsfeld, A. L. Briseno, and J. J. Watkins, *Chemistry of Materials*, 2012, **24**, 622–632.
- 31 J. M. Lobež, T. L. Andrew, V. Bulović, and T. M. Swager, *ACS nano*, 2012, **6**, 3044–56.
- 32 D. H. Wang, H. K. Lee, D.-G. Choi, J. H. Park, and O. O. Park, *Applied Physics Letters*, 2009, **95**, 043505.
- 33 V. Vohra, G. Arrighetti, L. Barba, K. Higashimine, W. Porzio, and H. Murata, *The Journal of Physical Chemistry Letters*, 2012, **3**, 1820–1823.
- 34 J. H. Seo, A. Gutacker, Y. M. Sun, H. B. Wu, F. Huang, Y. Cao, U. Scherf, A. J. Heeger, and G. C. Bazan, *Journal of the American Chemical Society*, 2011, **133**, 8416–8419.
- 35 H. A. Ho and M. Leclerc, *Journal of the American Chemical Society*, 2003, **125**, 4412–3.
- 36 D. Bondarev, J. Zednik, I. Sloufova, A. Sharf, M. Prochazka, J. Pfleger, and J. Vohlidal, *Journal of Polymer Science Part a-Polymer Chemistry*, 2010, **48**, 3073–3081.
- 37 S. Kazim, J. Pfleger, M. Prochazka, D. Bondarev, and J. Vohlidal, *J Colloid Interface Sci*, 2011, **354**, 611–619.
- 38 M. Knaapila, R. C. Evans, A. Gutacker, V. M. Garamus, N. K. Székely, U. Scherf, and H. D. Burrows, *Soft Matter*, 2011, **7**, 6863.
- 39 T. V Richter, C. Bühler, and S. Ludwigs, *Journal of the American Chemical Society*, 2012, **134**, 43–6.
- 40 A. B. Pangborn, M. A. Giardello, R. H. Grubbs, R. K. Rosen, and F. J. Timmers, *Organometallics*, 1996, **15**, 1518–1520.
- 41 P. Bauerle, F. Wurthner, and S. Heid, *Angewandte Chemie-International Edition in English*, 1990, **29**, 419–420.
- 42 F. Nickel, C. Sprau, M. F. G. Klein, P. Kapetana, N. Christ, X. Liu, S. Klinkhammer, U. Lemmer, and A. Colmann, *Solar Energy Materials and Solar Cells*, 2012, **104**, 18–22.
- 43 F. C. Krebs, *Solar Energy Materials and Solar Cells*, 2009, **93**, 394–412.

Solution-processed bi-layer polythiophene-fullerene organic solar cells

- 44 K. Vijayakrishna, D. Mecerreyes, Y. Gnanou, and D. Taton, *Macromolecules*, 2009, **42**, 5167–5174.

3.6 Supporting information

3.6.1 Details on the monomer synthesis



Scheme S3.1: Synthesis of 2,5-dibromo-3-(6-bromohexyl)thiophene (**M1**): i. KO^tBu, MeOH/acetone, reflux; ii. a) Mg, Et₂O, b) **4**, Ni(dppp)Cl₂, Et₂O; iii. HBr, Ac₂O; iv. NBS, THF.

1-(6-Bromohexyloxy)-4-methoxybenzene (3).³ 4-Methoxyphenol (**2**) (20.0 g, 161 mmol) and potassium *tert*-butoxide (21.7 g, 193 mmol, 1.2 equiv) were dissolved in a mixture of MeOH (80 mL) and acetone (80 mL) and stirred for 30 min at rt. The reaction mixture was then added dropwise to a solution of 1,6-dibromohexane (**1**) (77.9 g, 322 mmol, 2 equiv) in acetone (80 mL) at reflux temperature, and the reaction was further heated at reflux temperature until completion (as analyzed by TLC). The mixture was cooled down to rt and water was added. The product was extracted with diethyl ether and the organic layer was

³ Toyoshima, R.; Narita, M.; Akagi, K.; Shirakawa, H. *Synthetic Metals*, **1995**, 69, 289–290.

Solution-processed bi-layer polythiophene-fullerene organic solar cells

washed with brine. The organic layer was dried with MgSO₄, filtered and evaporated to dryness under reduced pressure. The unreacted 1,6-dibromohexane was removed by vacuum distillation. The pure product was recrystallized from MeOH and the resulting white crystals were dried under vacuum (32.6 g, 71%). ¹H NMR (300 MHz, CDCl₃): δ = 6.83 (s, 4H), 3.91 (t, *J* = 6.4 Hz, 2H), 3.77 (s, 3H), 3.43 (t, *J* = 6.7 Hz, 2H), 1.89 (q, *J* = 7.0 Hz, 2H), 1.77 (q, *J* = 6.7 Hz, 2H), 1.54–1.46 (m, 4H); ¹³C NMR (75 MHz, CDCl₃) δ = 154.4, 153.9, 116.1 (CH), 115.3 (CH), 69.0 (CH₂), 56.4 (CH₃), 34.6 (CH₂), 33.4 (CH₂), 29.9 (CH₂), 28.6 (CH₂), 26.0 (CH₂); MS (EI): *m/z* = 286/288 (M⁺).

3-[6-(4-Methoxyphenoxy)hexyl]thiophene (5). 1-(6-Bromohexyloxy)-4-methoxybenzene (**3**) (10.57 g, 36.8 mmol, 1 equiv), dissolved in a minimum amount of anhydrous diethyl ether (50 mL), was added under inert atmosphere to a suspension of Mg turnings (0.97 g, 40 mmol, 1.3 equiv) in anhydrous diethyl ether (10 mL) at reflux temperature. The reaction mixture was further refluxed for 1 h. The Grignard solution was cooled down to rt and then transferred dropwise via a cannula to an ice-cooled mixture of Ni(dppp)Cl₂ (4 mol%) and 3-bromothiophene (5.0 g, 30.7 mmol) in dry diethyl ether (15 mL). The reaction mixture was refluxed for 12–15 h and afterwards hydrolyzed with a mixture of HCl (10 mL of a 1 M solution) and ice-water (20 mL), followed by extraction with several portions of Et₂O. Drying of the combined organic phases with MgSO₄, filtration and removal of the solvent under reduced pressure afforded an orange oil which solidified upon standing. The product was purified by crystallization from hexane to provide an off-

white solid. The filtrate was evaporated and additionally purified via column chromatography (silica) with a 50/50 hexanes/CH₂Cl₂ eluent mixture. Removal of the solvent gave the product as an off-white solid (overall yield 6.14 g, 69%). ¹H NMR (300 MHz, CDCl₃) δ = 7.23 (dd, *J* = 4.9 Hz and 3.0 Hz, 1H), 6.93–6.89 (m, 2H), 6.82 (s, 4H), 3.89 (t, *J* = 6.5 Hz, 2H), 3.75 (s, 3H), 2.63 (t, *J* = 7.6 Hz, 2H), 1.82–1.30 (m, 8H); ¹³C NMR (75 MHz, CDCl₃) δ = 154.3, 153.9, 143.7, 128.9 (CH), 125.8 (CH), 120.5 (CH), 116.1 (CH), 115.2 (CH), 69.2 (CH₂), 56.4 (CH₃), 31.1 (CH₂), 30.8 (CH₂), 29.9 (CH₂), 29.7 (CH₂), 26.5 (CH₂); MS (EI): *m/z* = 290 (M⁺).

3-(6-Bromohexyl)thiophene (6). Procedure as reported by Bäuerle et al.⁴ ¹H NMR (300 MHz, CDCl₃) δ = 7.22 (dd, *J* = 4.8 and 2.9 Hz, 1H), 6.93–6.88 (m, 2H), 3.39 (t, *J* = 6.7 Hz, 2H), 2.62 (t, *J* = 7.7 Hz, 2H), 1.84 (q, *J* = 7.0 Hz, 2H), 1.62 (q, *J* = 7.6 Hz, 2H), 1.52–1.21 (m, 4H); ¹³C NMR (75 MHz, CDCl₃) δ = 143.5, 128.9 (CH), 125.8 (CH), 120.6 (CH), 34.7 (CH₂), 33.4 (CH₂), 31.0 (CH₂), 30.8 (CH₂), 29.0 (CH₂), 28.6 (CH₂); MS (EI): *m/z* = 246/248 (M⁺).

2,5-Dibromo-3-(6-bromohexyl)thiophene (M1). 3-(6-Bromohexyl)thiophene (**6**) (2.62 g, 10.6 mmol) was dissolved in THF (100 mL), cooled to 0 °C and protected from light. NBS (4.34 g, 24.4 mmol, 2.3 equiv) was added portion wise and the mixture was stirred further at rt for 8 h in the absence of light. The reaction mixture was quenched by pouring it into an ice-cold solution of 1 M NaOH and the product was

⁴ Bäuerle, P.; Wurthner, F.; Heid, S. *Angew. Chem., Int. Ed. Engl.* **1990**, *29*, 419-420.
116

Solution-processed bi-layer polythiophene-fullerene organic solar cells

extracted with Et₂O. The organic layer was dried with MgSO₄, filtered and the solvent was evaporated under reduced pressure. The residue was purified on a silica plug with 50/50 hexanes/CH₂Cl₂ as the eluent. The pure fractions were collected and the solvent was removed under reduced pressure affording a colourless oil (3.9 g, 91%). ¹H NMR (300 MHz, CDCl₃): δ = 6.75 (s, 1H), 3.38 (t, *J* = 6.9 Hz, 2H), 2.49 (t, *J* = 7.7 Hz, 2H), 1.84 (q, *J* = 7.2 Hz, 2H), 1.54 (q, *J* = 7.7 Hz, 2H), 1.48–1.38 (m, 2H), 1.38–1.25 (m, 2H); ¹³C NMR (75 MHz, CDCl₃) δ = 143.2, 131.4 (CH), 111.0, 108.6, 34.4 (CH₂), 33.1 (CH₂), 29.9 (CH₂), 29.8 (CH₂), 28.7 (CH₂), 28.4 (CH₂); MS (EI): *m/z* = 402/404/406/408 (M⁺).

3.6.2 UV-Vis spectra of the ionic polythiophenes

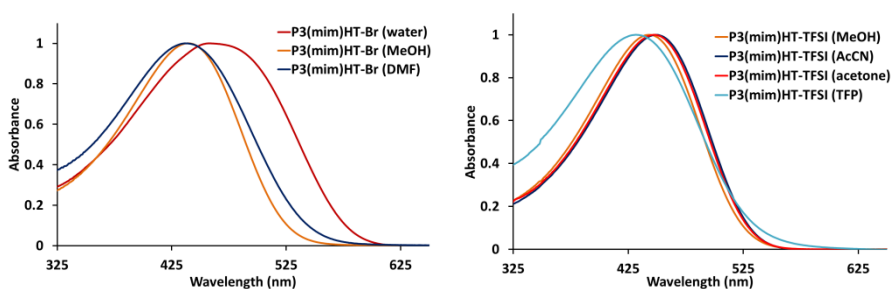


Figure S3.1: UV-Vis spectra of the ionic polythiophenes.

3.6.3 ^1H NMR spectra of the ionic polythiophenes

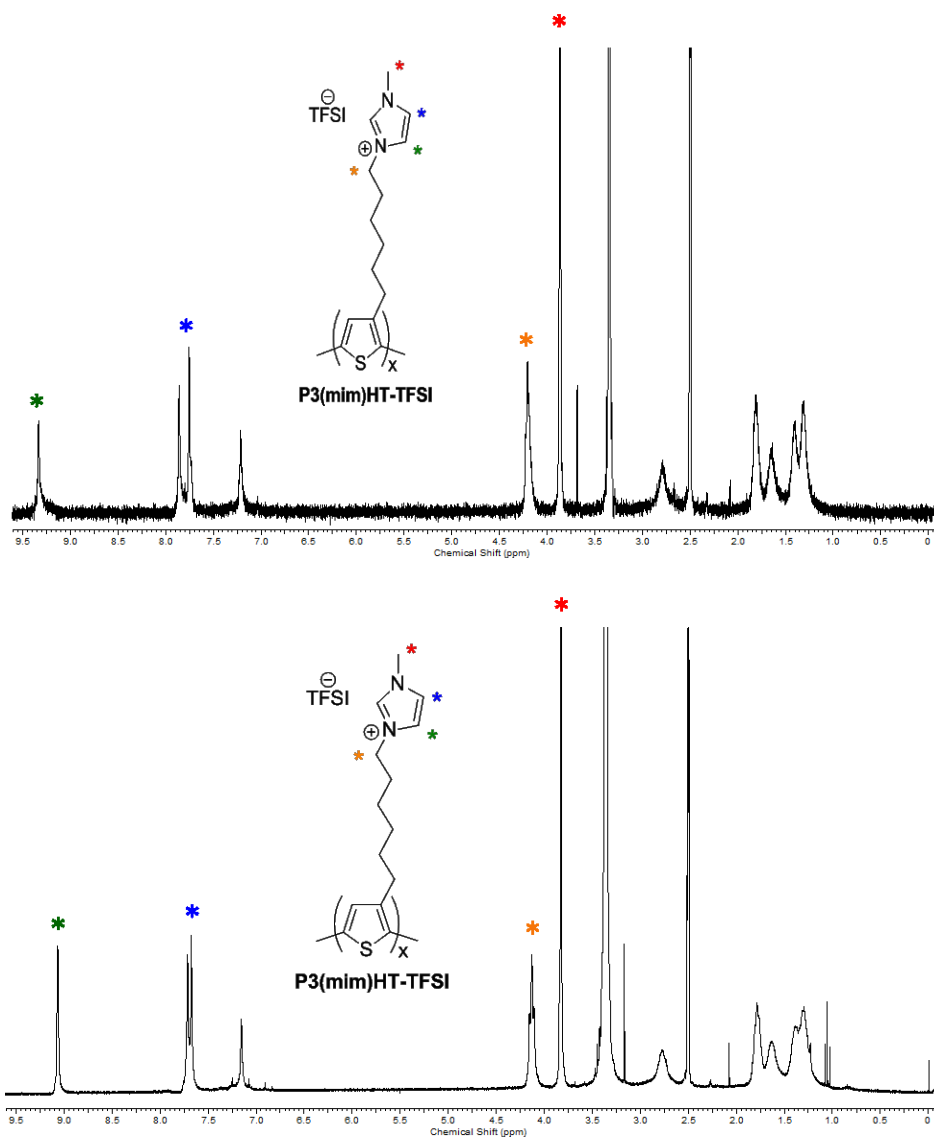


Figure S3.2: ^1H NMR spectra of the ionic polythiophenes.

3.6.4 Bi-layer integrity study

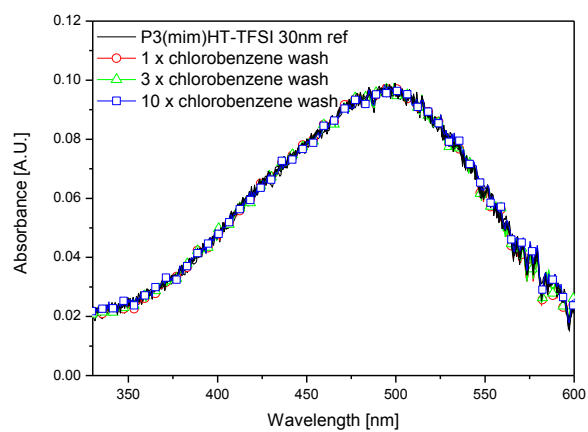


Figure S3.3: Absorption spectrum of the **P3(mim)HT-TFSI** layer before and after chlorobenzene washes.

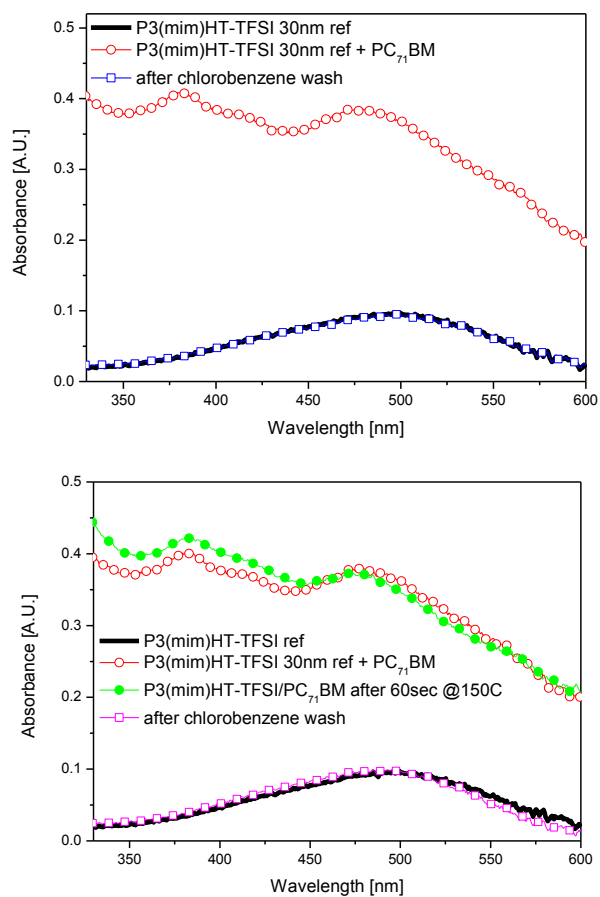


Figure S3.4: Absorption spectra of **P3(mim)HT-TFSI** alone, **P3(mim)HT-TFSI** with **PC₇₁BM** on top, and the same **P3(mim)HT-TFSI** after removal of the **PC₇₁BM** layer by a chlorobenzene wash, either without heating step (top) or with short annealing of the **P3(mim)HT-TFSI/PC₇₁BM** bi-layer (bottom).

3.6.5 Reproducibility data for bi-layer devices based on P3(mim)HT-TFSI

Table S3.1: Reproducibility data for P3(mim)HT-TFSI/PC₆₁BM bi-layer devices.

P3(mim) HT-TFSI [nm]	PC ₆₁ BM [nm]	PCE [%]	FF [%]	V _{oc} [V]	J _{sc} [mA/cm ²]
50	40	0.49	61	0.61	1.3
50	40	0.45	63	0.61	1.2
50	40	0.54	63	0.61	1.4
50	40	0.47	62	0.61	1.3
50*	40*	0.49*	62*	0.61*	1.3*
50	35	0.42	62	0.61	1.1
50	35	0.4	64	0.6	1
50	35	0.41	65	0.6	1.1
50	35	0.35	62	0.6	1
50*	35*	0.4*	63*	0.6*	1.1*
50	30	0.3	61	0.59	0.85
50	30	0.33	61	0.6	0.9
50*	30*	0.32*	61*	0.6*	0.9*
50	50	0.41	64	0.6	1.1
50	50	0.42	66	0.59	1
50*	50*	0.41*	65*	0.6*	1*
50	60	0.23	60	0.61	0.61
50	60	0.31	60	0.61	0.84
50*	60*	0.27*	60*	0.61*	0.72*

* Average values.

Table S3.2: Reproducibility data for **P3(mim)HT-TFSI/PC₇₁BM** bi-layer devices.

P3(mim) HT-TFSI [nm]	PC₇₁BM [nm]	PCE [%]	FF [%]	V_{oc} [V]	J_{sc} [mA/cm²]
40	40	1.5	55	0.65	4.3
40	40	1.3	56	0.66	3.5
40	40	1.8	55	0.64	5.2
40	40	1.6	56	0.65	4.3
40	40	1.7	59	0.65	4.5
40	40	1.5	60	0.65	3.9
40	40	1.6	57	0.64	4.4
40	40	1.5	60	0.65	3.9
40	40	1.5	56	0.66	4
40	40	1.4	57	0.66	3.8
40	40	1.9	57	0.65	5.1
40	40	1.6	56	0.66	4.2
40*	40*	1.6*	57*	0.65*	4.26*

* Average values.

Chapter 4

Imidazolium-substituted polythiophenes as efficient electron transport layers improving photovoltaic performance

Kesters, J.; Ghoo, T.; Penxten, H.; Drijkoningen, J.; Vangerven, T.; Lyons, D. M.; Verreert, B.; Aernouts, T.; Lutsen, L.; Vanderzande, D. J.; Manca J.; Maes, W. *Adv. Energy. Mater.*, **2013**, DOI: 10.1002/aenm.201300049

4.1 Introduction

The field of organic photovoltaics (OPV) has experienced a tremendous growth over the past few years. This is a direct consequence of the potential commercial value of this type of technology, exhibiting specific desirable properties such as simple preparation, novel aesthetical possibilities, mechanical flexibility, semi-transparency, better performance in diffuse light and reduced weight, which makes OPV particularly attractive for portable or wearable electronics and building-integrated photovoltaics (BIPV). Moreover, in contrast to traditional Si-based solar cells, solution-processability allows low cost large-area thin film fabrication by e.g. roll-to-roll (R2R) printing. Currently, single junction OPV power conversion efficiencies (PCEs) of up to 9.2% have been reported,¹ and further improvements are constantly on the horizon.² Up till now, the active layer materials comprising the bulk heterojunction (BHJ) have been the main focus point, with a special emphasis on low bandgap conjugated polymers and small donor molecules.³ However, as overall performance is determined by the entire device built-up, a closer inspection and optimization of the other cell components can also lead to noticeable improvements, e.g. better interfaces between the various layers in the solar cell stack lead to a reduction of loss-mechanisms due to an improvement of the charge extraction pathways.²

At present, a number of different device architectures have been reported for BHJ polymer solar cells (PSCs). Besides the standard ‘sandwich’ structure, inverted solar cells,^{1,4} generally leading to enhanced lifetimes, and tandem devices,⁵ in which two separate cells are stacked one upon

Imidazolium-substituted PTs as efficient electronic transport layers

another and connected in series or parallel (affording record efficiencies up to 10.7%), are the most effective and most widely applied architectures to date. Insertion of additional charge transporting layers has been proposed as an effective mean to further optimize device performance by diminishing detrimental factors such as leakage current, bad interface tuning, charge recombination, etc. To facilitate electron transport and collection (and block hole transport), various electron transport layers (ETLs) have been introduced at metal/active layer (standard cell) or metal oxide/active layer (inverted cell) interfaces, e.g. LiF, Cs₂CO₃, fullerene derivatives and notably conjugated polyelectrolytes (CPEs), affording remarkable improvements in device parameters (V_{oc} , J_{sc} , FF) and final PCEs.^{1,6,7} The additional layer creates a more hydrophilic surface and dipole alignment at the interface, resulting in a higher built-in potential (and hence V_{oc}), while electron transport and collection are facilitated (causing more balanced charge injection and hence an increase in FF) by affecting the effective work function of the cathode, providing better energy alignment and minimizing contact resistance.⁶ Hydrophilic polymers are particularly attractive as they allow low-temperature solution processing and afford air-stable films. Mainly inspired by parallel efforts in the field of polymer light-emitting diodes (PLEDs), the number of CPE structures explored to date is rather limited and CPE synthesis has only been exploited for a limited number of conjugated polymers. Most of the ultrathin CPE interlayers that have been reported are thiophene- or fluorene-based (co)polymers with appended polar amines or ionic ammonium moieties.^{6,7} Moreover, the influence of the chemical nature

of the CPE and the underlying BHJ blend is still poorly understood, leaving lots of opportunities for improvements by interdisciplinary work of synthetic material chemists and device physicists.

In this work, we report on the implementation of a specific type of electron transport layer, i.e. a CPE layer based on an amphiphilic polythiophene with appended ionic liquid-like polar groups, to boost the internal cell parameters of devices based on PCDTBT:PC₇₁BM and PCPDT-DTTzTz:PC₇₁BM photoactive layers (**Figure 4.1**).⁸ The addition of this CPE layer between the active layer and the electron collecting Al cathode (replacing the air sensitive Ca layer) has a positive influence on the internal voltage as well as on the leakage current, and an efficiency increase of 20% (up to an average PCE of 6.2% for PCDTBT:PC₇₁BM devices) was achieved with one of the ETL materials. Upon comparison with an analogous polythiophene-based CPE recently reported by Bazan *et al.*^{6b} or the widely used PFN,⁹ the novel interlayer material is more effective. Additionally, the molecular weight of the hydrophilic polymer was identified as an important factor determining the overall performance.

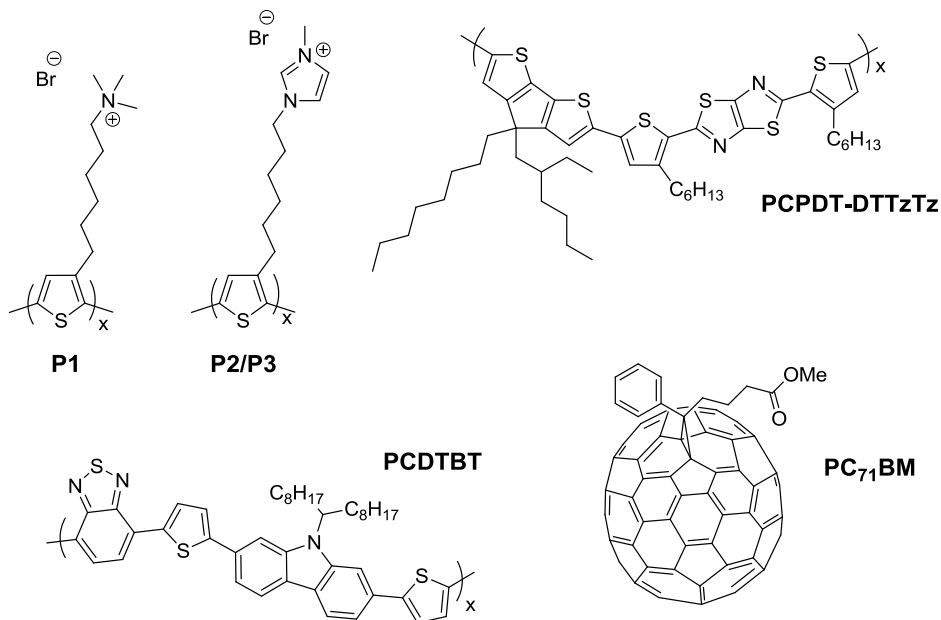


Figure 4.1: Trimethylamine-functionalized polythiophene **P1**, imidazole-functionalized polythiophenes **P2** and **P3**, the **PCDTBT** and **PCPDT-DTTzTz** donor polymers, and **PC₇₁BM**.

4.2 Experimental section

Trimethylamine-functionalized polythiophene **P1** (**P3(TMA)HT**) (**Figure 4.1**), used as a reference interlayer, was prepared by a literature procedure as reported by Bazan *et al.*¹⁰ Imidazolium-substituted polythiophenes **P2** and **P3** were prepared according to a recently reported method.¹¹ Details on the synthetic procedures and characterization data are provided as supplementary material.

The reference BHJ solar cells were fabricated using the traditional glass/ITO/PEDOT-PSS/active layer/Ca/Al architecture. To investigate the impact of the CPE layers, the Ca layer was replaced by a CPE in this architecture. A control device without a CPE or Ca layer was included as

an additional reference. Before device processing, the indium tin oxide (ITO, Kintec, 100 nm, 20 Ohm/sq) containing substrates were cleaned using soap, demineralized water, acetone, isopropanol and a UV/O₃ treatment. Subsequently, the ITO substrates were covered by a ~30 nm thick layer of PEDOT-PSS (poly(3,4-ethylenedioxythiophene)-poly(styrenesulfonic acid), Heraeus Clevios) by spin-coating. Further processing was performed under nitrogen atmosphere in a glove box, starting off with an annealing step at 130 °C for 15 min to remove any residual water. The PCDTBT (poly[[9-(1-octylnonyl)-9*H*-carbazole-2,7-diyl]-2,5-thiophenediyl-2,1,3-benzothiadiazole-4,7-diyl-2,5-thiophenediyl]) donor polymer was obtained from SolarisChem ($M_n = 79$ kDa, $D = 2.4$), and used as received. PCPDT-DTTzTz (poly([4-(2'-ethylhexyl)-4-octyl-4*H*-cyclopenta[2,1-*b*:3,4-*b'*]dithiophene-2,6-diyl]-*alt*-[2,5-di(3'-hexylthiophen-2'-yl)thiazolo[5,4-*d*]-thiazole-5',5''-diyl])) was synthesized according to a previously reported method.⁸ The active layer consisting of PCDTBT:PC₇₁BM ([6,6]-phenyl C₇₁ butyric acid methyl ester) (Solenne) was spin-coated with a thickness of ~65 nm. Blend solutions were prepared in a 1:4 ratio, with PCDTBT concentrations of 5 mg/mL, using chlorobenzene:1,2-dichlorobenzene (1:3) as a solvent mixture.^{6b} For the devices containing PCPDT-DTTzTz:PC₇₁BM as the active layer, a thickness of ~70 nm was obtained through spin-coating. Blend solutions were prepared in a 1:3 ratio, with PCPDT-DTTzTz concentrations of 5 mg/mL, using chlorobenzene as a solvent.⁸ The layer thickness obtained after spincoating was ~70 nm. The active layer deposition step was followed by spin-coating of the CPE interlayers, aiming for thicknesses of ~5-10

Imidazolium-substituted PTs as efficient electronic transport layers

nm (as confirmed by DEKTAK). The CPE solutions were prepared in concentrations of 0.01, 0.02 and 0.04 w/v% in methanol. Finally, the devices were finished off with Al as the top electrode, with a thickness of ~80 nm. Thicknesses of the top electrodes of the reference device containing Ca/Al were ~20 and 80 nm, respectively. In the standard cell configuration, an active area of 25 mm² was obtained. To provide a better assessment of the value of the in-house prepared CPE's, the more commonly used interlayer material PFN (poly[(9,9-bis(3'-(*N,N*-dimethylamino)propyl)-2,7-fluorene)]) was used as well.

Device characterization: The PCEs of the BHJ solar cells were measured using a Newport class A solar simulator (model 91195A) calibrated with a silicon solar cell to give an AM 1.5g spectrum. For AFM imaging, a Bruker Multimode 8 AFM was used in PeakForce tapping mode, employing ScanAsyst. The images were produced with a silicon tip on a nitride lever with a spring constant of 4 N/m.

EQE and reflection measurements: A commercial set-up (Bentham) was used to measure the EQE. Light from a Xe arc lamp (300–670 nm) and a quartz halogen lamp (670–900 nm) is chopped, coupled into a monochromator and aimed at the device. The resulting current is sent through a Bentham477 current pre-amplifier, then arriving in the Bentham485 lock-in amplifier. Calibration is done with a certificated Si cell. The integration of these EQEs over the solar spectrum is listed in Table S2 as J_{EQE} . The same optics and measurement setup is used with a DTR6 integrating sphere to determine the reflection.

4.3 Results and discussion

To render conjugated polymers soluble in more environmentally benign solvents (rather than chlorobenzene etc.), which are highly desirable toward high-throughput OPV solution processing, several synthetic strategies can be adopted. Introduction of ionic moieties as side chains on the polymer backbone affords CPEs applicable either as active light-harvesting materials or as interlayers in the solar cell stack. Ongoing synthetic efforts have been directed toward the preparation of a wide range of cationic polythiophene (co)polymers with appended ‘ionic liquid-like’ *N*-methylimidazole moieties, through substitution on the bromohexyl-substituted precursor polymers, considerably facilitated by employing microwave heating.^{11,12} The versatility of the GRIM polymerization route¹³ allows straightforward tuning of the molecular weight, the built-in monomer ratio, the side chain pattern and the polymer architecture (random *vs* block copolymers), combined with narrow polydispersities and high regioregularities, while the counter ion can be readily exchanged on the final polymer stage.¹¹

For this interlayer work, one particular ionic imidazolium-functionalized polythiophene homopolymer (with Br⁻ counter ion) was initially selected. Two batches with varying molecular weight (**P2** and **P3**, with $M_n = 11.2$ kDa and 32.6 kDa, respectively, for the non-ionic precursor polymers) and narrow polydispersity ($D = 1.6$) were prepared. These materials were first evaluated as interlayer materials on top of an active layer comprising of PCDTBT, one of the current state-of-the-art low bandgap donor polymers,¹⁴ and PC₇₁BM (**Figure 4.1**). The PCDTBT:PC₇₁BM combination combines high efficiency and long

operating lifetimes.^{14c} To enable comparison with the ETL material introduced by Bazan *et al.*,^{6b} trimethylamine-functionalized polythiophene **P1**¹⁰ was prepared as well ($M_n = 32.6$ kDa) as a reference material (**Figure 4.1**). Additionally, PFN was also included as an additional ETL material in the device set. For ionic polythiophenes **P1–P3**, complete functionalization and material purity were confirmed by ¹H NMR (**Figure S4.1**).¹¹ The optical absorption spectra show typical polythiophene features, with a small red shift (in film) for **P2** and **P3** ($\lambda_{max} = 504$ nm) compared to **P1** ($\lambda_{max} = 482$ nm) (**Table S4.1**). ‘P3HT-like’ electrochemical behavior was observed for all three materials by cyclic voltammetry (**Table S4.1**), the main difference being located at the reduction onset. The presence of the ionic groups in these hydrophilic polymers makes them soluble in alcohols, hence enabling processing from more benign non-chlorinated solvents. Moreover, as orthogonal solvents are applied for the photoactive layer and CPE interlayer, integrity problems due to redissolution of the underlying BHJ layer are readily avoided.

For the evaluation of the ETL features of the novel ionic polythiophenes, the standard solar cell stack glass/ITO/PEDOT-PSS/polymer:PC₇₁BM/CPE/Al was employed.^{6b} In a first experiment, the optimal concentration of the CPE materials (in methanol) was investigated for PCDTBT:PC₇₁BM active layers (data not shown). The optimum was found around 0.02 w/v% and hence all further experiments were performed using this concentration.^{6b} Next, the devices with interfacial charged polymer layers were compared to cells with traditional Ca/Al electrodes (**Table 4.1**). Ca is commonly applied as a

low work function metal to optimize electrical contact but suffers from high air sensitivity and is therefore increasingly replaced by solution-processed metal oxides (ZnO, TiO_x). The overall increase in PCE due to the ETL materials could mainly be attributed to an increase in short-circuit current density (J_{sc}), with only minor contributions from open-circuit voltage (V_{oc}) and fill factor (FF) (**Figure 4.2**). Comparing the three interlayer materials, the novel high- M_n ionic polythiophene **P3** afforded the best results, with a top PCE at 6.7% (average 6.2%). Compared to the reference ETL material **P1** reported by Bazan *et al.*, derived from the same precursor batch, there is an increase in PCE of ~0.2% (both for the best and average PCE). In comparison with the device utilizing Ca, J_{sc} increased from 10.7 mA cm⁻² to 12.1 mA cm⁻², which is an increase of roughly 20%. The increase in J_{sc} was confirmed by extracting the currents from external quantum efficiency (EQE) measurements (**Figure S4.2**, **Table S4.2**). The enhanced current can partly be explained by increased reflection upon removing the Ca layer (which shows some ‘parasitic’ absorption; **Figure S4.3**).¹⁵ The addition of the CPE layers seems to provide an optimal balance between improved ohmic contact and mirror effects.

Utilizing the same ionic polythiophene material with a lower M_n (**P2**) resulted in a clearly lower performance, indicating that the efficiency of the interlayer is highly dependent on the molecular weight of the interfacial polymer. Ionic polythiophene **P3** also showed a noticeable improvement when compared with the widely used PFN interlayer material (on average 5.96% vs. 6.22%). Finally, a reference device for which pure methanol was spin-coated on top of the active layer was

Imidazolium-substituted PTs as efficient electronic transport layers

produced (**Table 4.1**, indicated as .../MeOH/Al, **Figure S4.4**) to investigate whether the beneficial factor leading to improved device performance was not originating from the solvent only. From the data in **Table 4.1** we can observe a noticeable improvement with respect to the reference device utilizing the traditional Ca/Al electrode. This observation has been made before, leading to the statement that the methanol treatment results in the formation of an interface dipole between the active layer and the metal layer.^{6,16} The incorporation of the CPE layers did, however, result in further improvements in J_{sc} , resulting in higher overall PCEs. This suggests that, on top of the formation of an interface dipole, the presence of the CPE layer leads to additional beneficial factors improving charge extraction.

Table 4.1: Photovoltaic performance of PCDTBT:PC₇₁BM BHJ devices with and without the addition of CPE layers.^a

Layer Sequence	V_{oc} (V)	J_{sc} (mA cm ⁻²) ^b	FF	Average η (%)	Best η (%)
.../Al	0.73	11.36	0.41	3.39 ± 0.36	3.82
.../Ca/Al	0.87	10.66	0.57	5.23 ± 0.33	5.71
.../P1/Al	0.88	11.82	0.58	6.03 ± 0.46	6.48
.../P2/Al	0.84	11.67	0.55	5.32 ± 0.24	5.57
.../P3/Al	0.87	12.05	0.59	6.22 ± 0.43	6.69
.../PFN/Al	0.88	11.84	0.58	5.96 ± 0.42	6.33
.../MeOH/Al	0.88	11.68	0.57	5.81 ± 0.17	5.99

^a Stack: glass/ITO/PEDOT-PSS/PCDTBT:PC₇₁BM/X/Al with X = Ca or CPE. ^b Uncorrected data

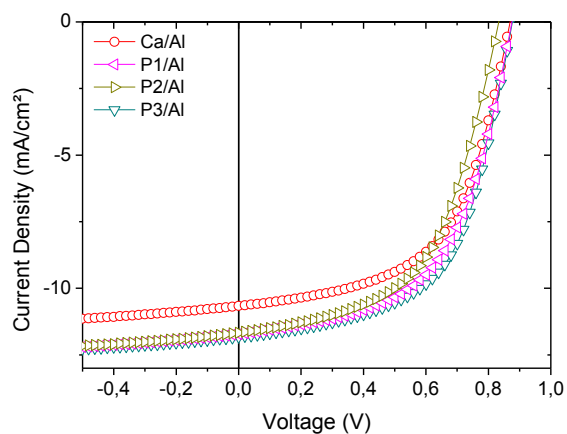


Figure 4.2: J - V curves under illumination of PCDTBT:PC₇₁BM BHJ photovoltaic devices with and without additional CPE layers (averaged results).

In a follow-up experiment, the highest performing ETL material **P3** was also tested on top of an active layer comprising of a different low bandgap polymer, i.e. PCPDT-DTTzTz. As can clearly be seen from the data in **Table 4.2** (J - V curves in **Figure S4.5**), the results confirmed the beneficial effect of the novel CPE layer, with an increase in J_{sc} and FF leading to a similar overall PCE improvement. It has to be noted here that the efficiency obtained for the reference device (4.78% best, 4.50% average) is the highest PCE reported for this donor polymer (4.03% before).

Imidazolium-substituted PTs as efficient electronic transport layers

Table 4.2: Photovoltaic performance of PCPDT-DTTzTz:PC₇₁BM BHJ devices with and without the addition of CPE layers.^a

Layer Sequence	V_{oc} (V)	J_{sc} (mA cm ⁻²) ^b	FF	Average η (%)	Best η (%)
.../PCPDT- DTTzTz:PC ₇₁ BM/Ca/Al	0.68	12.2	0.54	4.50 ± 0.2	4.78
.../PCPDT- DTTzTz:PC ₇₁ BM/ P3 /Al	0.68	12.9	0.55	4.86 ± 0.4	5.43

^a Stack: glass/ITO/PEDOT-PSS/PCPDT-DTTzTz:PC₇₁BM/X/Al with X = Ca or CPE. ^b Uncorrected data

To get a more clear view on the potential loss mechanisms in the devices, dark J - V curves were measured, revealing information on the series and shunt resistances (R_s and R_{sh}). **Figure 4.3** shows the dark curves for the best performing CPE material **P3** and for the reference devices with solely Al and Ca/Al as top electrodes. Utilizing **P3** as a CPE resulted in a strong increase of R_{sh} in comparison to the two reference devices. As for R_s , there was a slight improvement when comparing the CPE-containing device with the Ca/Al reference. However, compared with the Al reference, R_s was much lower. Moreover, in the negative half of the x-axis, the photovoltaic device with a **P3** ETL layer showed much less leakage current, confirming the positive influence of the interlayer on the performance of the solar cell device.

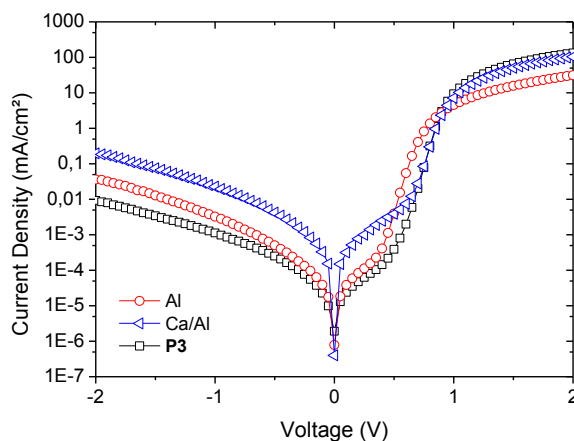


Figure 4.3: J - V curves of PCDTBT-based BHJ photovoltaic devices under dark conditions with and without additional CPE layers.

AFM measurements were performed to investigate the interlayers when deposited on top of the PCDTBT:PC₇₁BM active layer (**Figure 4.4**). The roughness in all cases increased compared to non-covered PCDTBT:PC₇₁BM films. The ETL materials **P1–P3** do not completely cover the active layer surface. The calculated surface coverage seemed to be similar for all ETLs (~55%), but the observed morphology was noticeably different. **Figure 4.4a–c** show the topography, whereas **Figure 4.4d–f** reveal the adhesion images, reflecting the ‘sticking’ of the AFM tip to the surface (additional images can be found in **Figure S4.6** and **Figure S4.7**). The topography images (a–c) show the presence of rather large ‘holes’ (average diameter 110 nm) for **P1**, whereas for **P3** a much finer and more random network is formed. From the adhesion images (d–f) it can be seen that the regions with low adhesion (dark spots) correspond with the higher topography features, and the regions with high adhesion (bright spots) correspond with the lower features on

Imidazolium-substituted PTs as efficient electronic transport layers

the height image. From these observations, it looks like the active layer is not completely covered and is directly exposed by the presence of holes in the ETL material. The density of these holes can possibly be correlated to the final device performance.

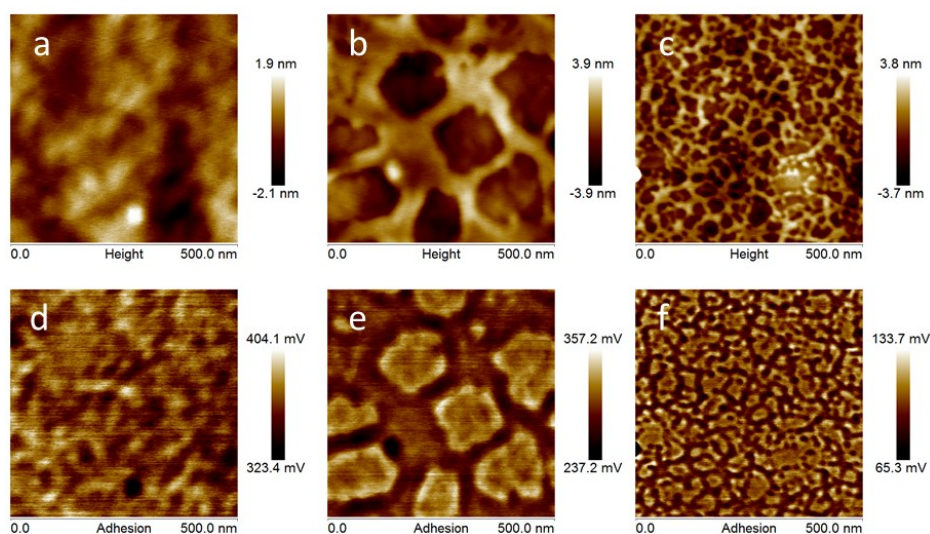


Figure 4.4: AFM (a,b,c: topography; d,e,f: adhesion) images ($500 \times 500 \text{ nm}^2$) of layer stacks with and without additional CPE materials: a,d) PCDTBT:PC₇₁BM, b,e) PCDTBT:PC₇₁BM/P1, c,f) PCDTBT:PC₇₁BM/P3.

The presented study confirms that high-efficiency polymer solar cells can be prepared by insertion of appropriate ionic polymer materials at the electrode/active layer interface. Interface engineering provides a simple pathway to BHJ OPV efficiency improvement, but its full potential has yet to be explored. The imidazole-substituted ionic polythiophene introduced here combines a number of features that favor this ETL material above most competitive polymer and/or fullerene materials. It is a simple polythiophene derivative, prepared via the

Chapter 4

straightforward GRIM polymerization method – providing structural versatility and scalability – and its stability and alcohol solubility enable easy processing from environmentally acceptable solvents. The material also seems to be applicable to different polymer:fullerene active layers. Moreover, by tuning the chemical structure of the ionic polythiophene, further improvement is conceivable, e.g. by varying the density and organization of ionic groups at the surface.

4.4 Conclusions

In conclusion, we have shown that the device performance of polymer solar cells can be remarkably improved by incorporation of a thin electron transport layer based on an imidazolium-substituted ionic polythiophene (20% increase in PCE up to an average value of 6.2% for PCDTBT:PC₇₁BM). The beneficial effect is notably higher than for previously reported materials such as an analogous trimethylamine-functionalized ionic polythiophene or PFN. Best results were obtained for the highest molecular weight ETL material, pointing to an important influence of polymer chain length on ETL performance. Remaining questions on the exact influence of polymer molecular weight (and its relation to active layer coverage) and the polythiophene backbone need to be addressed in future work.

4.5 References

- 1 He, Z.; Zhong, C.; Su, S.; Xu, M.; Wu, H.; Cao, Y. *Nat. Photonics*, **2012**, *6*, 591.
- 2 (a) Brabec, C. J.; Gowrisanker, S.; Halls, J. J. M.; Laird, D.; Jia, S.; Williams, S. P. *Adv. Mater. (Deerfield Beach, Fla.)*, **2010**, *22*, 3839; (b) Nelson, J.; *Mater. Today*, **2011**, *14*, 462; (c) Koster, L. J. A.; Shaheen, S. E.; Hummelen, J. C. *Adv. Energy Mater.*, **2012**, *2*, 1246; (d) Kumar, P.; Chand, S. *Prog. Photovoltaics*, **2012**, *20*, 377; (e) Li, G.; Zhu, R.; Yang, Y. *Nat. Photonics*, **2012**, *6*, 153; (f) Jørgensen, M.; Norrman, K.; Gevorgyan, S.; Tromholt, T.; Andreasen, B.; Krebs, F. C. *Adv. Mater. (Deerfield Beach, Fla.)*, **2012**, *24*, 580.
- 3 (a) Heeger, A. J.; *Chem. Soc. Rev.*, **2010**, *39*, 2354; (b) Delgado, J. L.; Bouit, P. -A.; Filippone, S.; Herranz, M. A.; Martín, N. *Chem. Commun. (Cambridge, U.K.)*, **2010**, *46*, 4853; (c) Boudreault, P. -L. T.; Najari, A.; Leclerc, M. *Chem. Mater.*, **2011**, *23*, 456; (d) Facchetti, A. *Chem. Mater.*, **2011**, *23*, 733; (e) Bian, L.; Zhu, E.; Tang, J.; Tang, W.; Zhang, F. *Prog. Polym. Sci.*, **2012**, *37*, 1292; (f) Zhou, H.; Yang, L.; You, W. *Macromolecules*, **2012**, *45*, 607; (g) Mishra, A.; Bäuerle, P. *Angew. Chem., Int. Ed. Engl.*, **2012**, *51*, 2020.
- 4 (a) Ferreira, S. R.; Davis, R. J.; Lee, Y.; Lu, P.; Hsu, J. W. P. *Org. Electron.*, **2011**, *12*, 1258; (b) Sun, Y.; Takacs, C. J.; Cowan, S. R.; Seo, J. H.; Gong, X.; Roy, A.; Heeger, A. J. *Adv. Mater.*, **2011**, *23*, 2226; (c) Zhang, F.; Xu, X.; Tang, W.; Zhang, J.; Zhuo, Z.; Wang, J.; Wang, J.; Zheng, X.; Wang, Y. *Sol. Energy Mater. Sol. Cells*, **2011**, *95*, 1785; (d) Liu, J.; Shao, S.; Fang, G.; Meng, B.; Xie, Z.; Wang, L. *Adv. Mater.*, **2012**, *24*, 2774.
- 5 (a) Sista, S.; Hong, Z.; Chen, L. -M.; Yang, Y. *Energy Environ. Sci.*, **2011**, *4*, 1606; (b) Dou, L.; You, J.; Yang, J.; Chen, C.; He, Y.; Murase, S.; Moriarty, T.; Emery, K.; Li, G.; Yang, Y. *Nat. Photonics*, **2012**, *6*, 356; (c) Gevaerts, V. S.; Furlan, A.; Wienk, M. M.; Turbiez, M.; Janssen, R. A. J. *Adv. Mater. (Deerfield Beach, Fla.)*, **2012**, *24*, 2130. (d) Kouijzer, S.; Esiner, S.; Frijters, C. H.; Turbiez, M.; Wienk, M. M.; Janssen, R. A. J. *Adv. Energy Mater.*, **2012**, *2*, 945.
- 6 (a) Huang, F.; Wu, H.; Cao, Y. *Chem. Soc. Rev.*, **2010**, *39*, 2500; (b) Seo, J. H.; Gutacker, A.; Sun, Y.; Wu, H.; Huang, F.; Cao, Y.; Scherf, U.; Heeger, A. J.;

Imidazolium-substituted PTs as efficient electronic transport layers

- Bazan, G. C. *J. Am. Chem. Soc.*, **2011**, *133*, 8416; (c) Choi, H.; Park, J. S.; Jeong, E.; Kim, G. -H.; Lee, B. R.; Kim, S. O.; Song, M. H.; Woo, H. Y.; Kim, J. Y. *Adv. Mater. (Deerfield Beach, Fla.)*, **2011**, *23*, 2759; (d) Ratcliff, E.; Zacher, B.; Armstrong, N. R. *J. Phys. Chem. Lett.*, **2011**, *2*, 1337; (e) Yip, H. -L.; Jen, A. K. -Y. *Energy Environ. Sci.*, **2012**, *5*, 5994; (f) Chen, Y.; Jiang, Z.; Gao, M.; Watkins, S. E.; Lu, P.; Wang, H.; Chen, X. *Appl. Phys. Lett.*, **2012**, *100*, 203304; (g) Yang, T.; Wang, M.; Duan, C.; Hu, X.; Huang, L.; Peng, J.; Huang, F.; Gong, X. *Energy Environ. Sci.*, **2012**, *5*, 8208; (h) Duan, C.; Zhong, C.; Liu, C.; Huang, F.; Cao, Y. *Chem. Mater.*, **2012**, *24*, 1682; (i) Ying, L.; Zalar, P.; Collins, S. D.; Chen, Z.; Mikhailovsky, A. A.; Nguyen, T.-Q.; Bazan, G. C. *Adv. Mater. (Deerfield Beach, Fla.)*, **2012**, *24*, 6496.
- 7 (a) Duarte, A.; Pu, K. -Y.; Liu, B.; Bazan, G. C. *Chem. Mater.*, **2011**, *23*, 501; (b) Fang, J.; Wallikewitz, B. H.; Gao, F.; Tu, G.; Müller, C.; Pace, G.; Friend, R. H.; Huck, W. T. S. *J. Am. Chem. Soc.*, **2011**, *133*, 683; (c) Zhou, Y.; Fuentes-Hernandez, C.; Shim, J.; Meyer, J.; Giordano, A. J.; Li, H.; Winget, P.; Papadopoulos, T.; Cheun, H.; Kim, J.; Fenoll, M.; Dindar, A.; Haske, W.; Najafabadi, E.; Khan, T. M.; Sojoudi, H.; Barlow, S.; Graham, S.; Brédas, J. -L.; Marder, S. R.; Kahn, A.; Kippelen, B. *Science*, **2012**, *336*, 327.
- 8 Van Mierloo, S.; Hadipour, A.; Spijkman, M.; Van den Brande, N.; Ruttens, B.; Kesters, J.; D'Haen, J.; Van Assche, G.; de Leeuw, D. M.; Aernouts, T.; Manca, J.; Lutsen, L.; Vanderzande, D. J.; Maes, W. *Chem. Mater.* **2012**, *24*, 587.
- 9 He, Z.; Zhong, C.; Huang, X.; Wong, W. -Y.; Wu, H.; Chen, L.; Su, S.; Cao, Y. *Adv. Mater. (Deerfield Beach, Fla.)*, **2011**, *23*, 4636.
- 10 Wang, S.; Bazan, G. C. *Chem. Commun*, **2004**, 21, 2508.
- 11 Ghoos, T.; Malinkiewicz, O.; Lutsen, L.; Vanderzande, D.; Bolink, H. J.; Maes, W. work submitted.
- 12 (a) Bondarev, D.; Zedník, J. *J. Polym. Sci., Part A-1: Polym Chem.*, **2010**, *48*, 3073; (b) Knaapila, M.; Evans, R. C.; Gutacker, A.; Garamus, V. M.; Székely, N. K.; Scherf, U.; Burrows, H. D. *Soft Matter*, **2011**, *7*, 6863.
- 13 (a) Loewe, R. S.; Ewbank, P. C.; Liu, J.; Zhai, L.; McCullough, R. D. *Macromolecules*, **2001**, *34*, 4324; (b) Zhai, L.; Pilston, R. L.; Zaiger, K. L.;

Chapter 4

- Stokes, K. K.; McCullough, R. D. *Macromolecules*, **2003**, *36*, 61; (c) Iovu, M. C.; Sheina, E. E.; Gil, R. R.; McCullough, R. D. *Macromolecules*, **2005**, *38*, 8649.
- 14 (a) Blouin, N.; Michaud, A.; Leclerc, M. *Adv. Materials*, **2007**, *19*, 2295; (b) Blouin, N.; Michaud, A.; Gendron, D.; Wakim, S.; Blair, E.; Neagu-Plesu, R.; Belletête, M.; Durocher, G.; Tao, Y.; Leclerc, M. *J. Am. Chem. Soc.*, **2008**, *130*, 732; (c) Park, S. H.; Roy, A.; Beaupre, S.; Cho, S.; Coates, N.; Moon, J. S.; Moses, D.; Leclerc, M.; Lee, K.; Heeger, A. J. *Nat. Photonics*, **2009**, *3*, 297; (d) Peters, I. C. H.; Sachs-Quintana, T.; Kastrop, J. P.; Beaupré, S.; Leclerc, M.; McGehee, M. D. *Adv. Energy Mater.*, **2011**, *1*, 491.
- 15 Hadipour, A.; Cheyns, D.; Heremans, P.; Rand, B. P. *Adv. Energy Mater.* **2011**, *1*, 930.
- 16 Wang, Q.; Zhou, Y.; Zheng, H.; Shi, J.; Li, C.; Su, C. Q.; Wang, L.; Luo, C.; Hu, D.; Pei, J.; Wang, J.; Peng, J.; Cao, Y. *Org. Electron.*, **2011**, *12*, 1858.

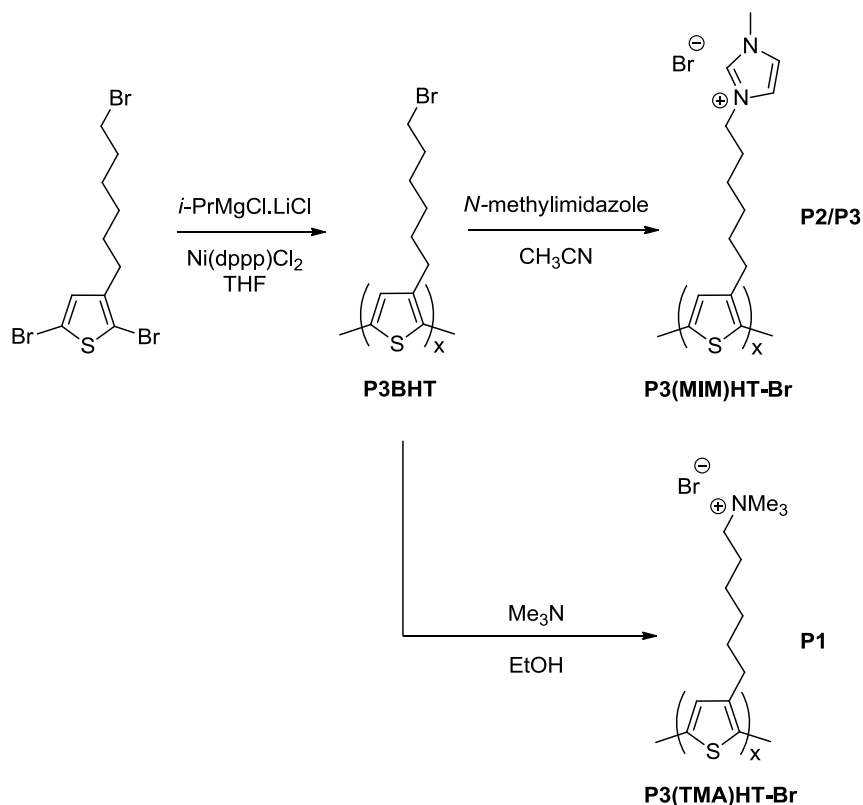
4.6 Supplementary Material

4.6.1 CPE synthesis and characterization

General experimental procedures

Unless stated otherwise, all reagents and chemicals were obtained from commercial sources and used without further purification. Tetrahydrofuran (THF) was dried using an MBraun MB-SPS 800 solvent purification system. NMR chemical shifts (δ , in ppm) were determined relative to the residual ^1H absorption of CHCl_3 (7.26 ppm) or the ^{13}C resonance shift of CDCl_3 (77.16 ppm). Analysis of the molecular weights and molecular weight distributions of the polymer samples was performed on a Tosoh EcoSEC System, comprising of an autosampler, a PSS guard column SDV (50 x 7.5 mm), followed by three PSS SDV analytical linear XL columns (5 μm , 300 x 7.5 mm), and a differential refractive index (Tosoh EcoSEC RI) and UV detector using THF as the eluent at 40 °C with a flow rate of 1.0 mL min $^{-1}$. The SEC system was calibrated using linear narrow polystyrene standards ranging from 474 to 7.5 x 10 6 g mol $^{-1}$ ($K = 14.1 \times 10^{-5}$ dL g $^{-1}$ and $\alpha = 0.70$). Microwave synthesis was performed on a CEM Discover SP synthesis platform. Optical absorption measurements were performed on a Cary500 UV-Vis-NIR instrument from Agilent. The optical bandgap was calculated from the intersection between the X-axis and the tangent line to the (film) absorption spectrum at the low energy side. Electrochemical measurements were performed with an Eco Chemie Autolab PGSTAT 30 potentiostat/galvanostat using a three-electrode microcell [Ag/AgNO $_3$ reference electrode (silver wire/0.01 M AgNO $_3$ /0.1 M NBu $_4$ PF $_6$ /MeCN); Pt counter electrode; Pt working electrode]. Freshly distilled anhydrous

MeCN containing 0.1 M NBu_4PF_6 was used as the electrolyte. To prevent air from entering the system, solutions were degassed with argon prior to each measurement and experiments were carried out under a curtain of argon. Films of the polymers on the working electrode were prepared by dipping the electrode in the polymer solution (solvent details can be found in **Table S4.1**) and waiting until the solvent had evaporated. All films were prepared in air. Cyclic voltammograms were recorded at a scan rate of 100 to 300 mV s^{-1} . The HOMO and LUMO energy levels were calculated from the onset oxidation and the onset reduction potential, respectively, and by assuming that the energy level of ferrocene/ferrocenium (Fc/Fc^+) has a value of -4.98 eV below the vacuum level.



Scheme S4.1: Synthesis of ionic polythiophenes **P1–P3**.

Poly[3-(6-bromohexyl)thiophene] (**P3BHT**) precursor polymers⁵

The monomer, 2,5-dibromo-3-(6-bromohexyl)thiophene^{5,6} (0.5 g, 1.2 mmol), was added to a flame-dried three-neck flask and dissolved in dry THF (15 mL). The reaction mixture was put under inert atmosphere and cooled to 0 °C. An $i\text{-PrMgCl}\cdot\text{LiCl}$ solution (1.3 M in THF, 0.923 mL, 1.2 mmol, 1 equiv) was added and the mixture was stirred for 30 min at 0 °C. To start the polymerization, 0.8 mol% of Ni(dppp)Cl_2 (5 mg, 0.01

⁵ Miyanishi, S.; Tajima, K.; Hashimoto, K. *Macromolecules*, **2009**, *42*, 1610–1618.

⁶ Bäuerle, P.; Würthner, F.; Heid, S. *Angew. Chem., Int. Ed. Engl.* **1990**, *29*, 419–420.

mmol) was added and the mixture was stirred for 2 h at 40 °C and 12 h at room temperature. The polymer was precipitated into an ice-cold HCl/MeOH (5%) mixture and the precipitated polymer was filtered off on a PTFE membrane (47 mm/0.45 μm). The polymer was purified using Soxhlet extraction for 24 h with methanol, *n*-hexane and chloroform, respectively. After evaporation of the solvent, the polymer was redissolved in chloroform and precipitated again from methanol, filtered, washed with methanol and dried, affording high- M_n polythiophene precursor **P3BHT-HMn** as a black powder (0.14 g, 48%). ^1H NMR (300 MHz, CDCl_3): δ = 6.96 (s, 1H), 3.41 (t, J = 6.7 Hz, 2H), 2.81 (t, J = 7.3 Hz, 2H), 1.88 (q, J = 6.8 Hz, 2H), 1.71 (br, 2H), 1.56–1.41 (m, 4H); UV-Vis (CHCl_3 , nm): λ_{max} = 447; SEC (THF, PS standards): M_n = 3.2×10^4 g mol $^{-1}$, M_w = 5.1×10^4 g mol $^{-1}$, D = 1.6.

When 1.6 mol% of Ni(dppp)Cl $_2$ catalyst (10 mg, 0.02 mmol) was added in the same polymerization procedure, a lower molecular weight precursor polymer **P3BHT-LMn** was obtained (0.10 g, 34%). ^1H NMR (300 MHz, CDCl_3): δ = 6.96 (s, 1H), 3.41 (t, J = 6.9 Hz, 2H), 2.80 (t, J = 8.2 Hz, 2H), 1.88 (br, 2H), 1.71 (br, 2H), 1.58–1.38 (m, 4H); UV-Vis (CHCl_3 , nm): λ_{max} = 447; SEC (THF, PS standards): M_n = 1.1×10^4 g mol $^{-1}$, M_w = 1.8×10^4 g mol $^{-1}$, D = 1.6.

Polymer functionalization with trimethylamine: poly[3-(6-trimethylammoniumhexyl)-thiophene] P3(TMA)HT-Br (P1)

P3BHT-HMn (0.040 g) was suspended in a solution of trimethylamine in EtOH (4.2 M, 2 mL) and added to a 10 mL microwave vial, which was then filled with Ar and closed. The reaction mixture was heated in

Imidazolium-substituted PTs as efficient electronic transport layers

the microwave at 100 °C for 3 h (with maximum power of 200 W and maximum pressure of 250 psi). After cooling down, the dark purple and viscous reaction mixture was added dropwise to Et₂O and a dark precipitate was obtained. The precipitated polymer was filtered off using a PTFE membrane (47 mm/0.45 μm) and dried carefully, affording **P3(TMA)HT-HMn** or **P1** as a purple-black powder (0.049 g, 99%). ¹H NMR (300 MHz, DMSO-*d*₆): δ = 7.25 (s, 1H), 3.09 (s, 9H), 2.81 (br, 2H), 1.70 (br, 4H), 1.55–1.21 (m, 4H) (2 protons are hidden under the H₂O signal); UV-Vis (MeOH, nm): λ_{max} = 443.

Polymer functionalization with *N*-methylimidazole: P3(MIM)HT-Br (P2/P3)

P3BHT-HMn (0.086 g) was suspended in acetonitrile (1 mL) in a 10 mL microwave vial and *N*-methylimidazole (1 mL) was added. The vial was filled with argon and closed. The reaction mixture was heated in the microwave at 100 °C for 3 h (maximum power 200 W, maximum pressure 250 psi). After cooling down, the reaction mixture was added dropwise to Et₂O and a dark precipitate was obtained. The precipitated polymer was filtered off using a PTFE membrane (47 mm/0.45 μm) and (freeze-)dried carefully, affording **P3(MIM)HT-HMn** or **P3** as a purple-black powder (0.109 g, 95%). ¹H NMR (300 MHz, DMSO-*d*₆): δ = 9.30 (s, 1H), 7.83 (s, 1H), 7.72 (s, 1H), 7.18 (s, 1H), 4.18 (br, 2H), 3.84 (s, 3H), 2.76 (br, 2H), 1.79 (br, 2H), 1.68–1.55 (m, 2H), 1.44–1.22 (m, 4H); UV-Vis (MeOH, nm): λ_{max} = 443.

P3BHT-LMn (0.090 g) was reacted in the same way, affording **P3(MIM)HT-LMn** or **P2** as a purple-black powder (0.108 g, 94%). ¹H NMR (300 MHz, DMSO-*d*₆): δ = 9.39 (s, 1H), 7.85 (s, 1H), 7.75 (s, 1H), 7.21 (s, 1H), 4.21 (br, 2H), 3.87 (s, 3H), 2.78 (br, 2H), 1.81 (br, 2H), 1.64 (br, 2H), 1.46–1.24 (m, 4H); UV-Vis (MeOH, nm): λ_{max} = 442.

Imidazolium-substituted PTs as efficient electronic transport layers

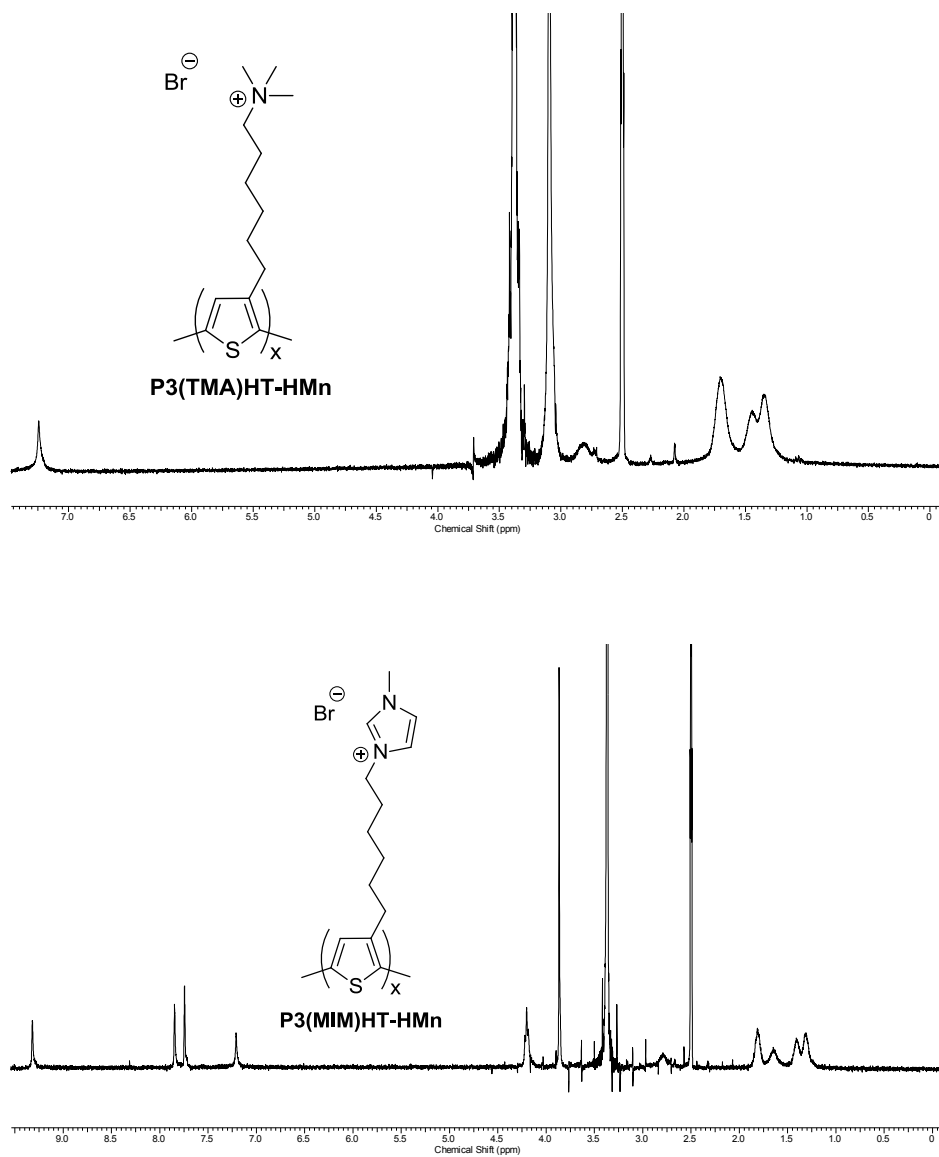


Figure S4.1: ¹H NMR spectra of ionic polythiophenes **P1** (top) and **P3** (bottom).

4.6.2 Optical and electrochemical characterization data

Table S4.1: Cyclic voltammetry and UV-Vis data (both in film) of the **P1–P3** ionic polythiophenes (and P3HT/PCDTBT under the same conditions).

Polymer	λ_{\max} (nm) ^{a)}	$E_{\text{onset}}^{\text{ox}}$ (V)	$E_{\text{onset}}^{\text{red}}$ (V)	HOMO (eV)	LUMO ^{b)} (eV)	E_g^{EC} (eV)	E_g^{OP} (eV) ^{a)}
P1	482	0.34	-1.98	-5.20	-2.88 (-3.19) ^{c)}	2.32	2.01
P2	504	0.33	-1.91	-5.19	-2.95 (-3.25) ^{c)}	2.24	1.94
P3	504	0.10	-1.93	-4.96	-2.93 (-3.00) ^{c)}	2.03	1.96
P3HT^{d)}	519	0.27	-2.24	-5.13	-2.62 (-3.23) ^{c)}	2.51	1.90
PCDTBT	579	0.47	-1.63	-5.43	-3.33 (-3.57) ^{c)}	2.10	1.86

^{a)} In film (**P1–P3** from tetrafluoropropanol, P3HT from chlorobenzene, PCDTBT from chlorobenzene/dichlorobenzene 70/30); ^{b)} Based on the onset of reduction; ^{c)} Values between brackets based on: LUMO = HOMO + E_g^{OP} ; ^{d)} $M_n = 2.5 \times 10^4$ g/mol, $D = 2.1$.

4.6.3 EQE and reflection measurements

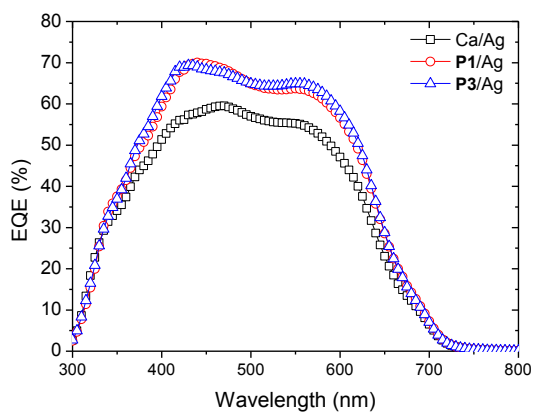


Figure S4.2: EQE spectra for devices containing the **P1** and **P3** CPEs (compared to a reference Ca/Ag device).⁷

⁷ Due to the different facilities that were used to produce these devices and the slightly different solar cell stack (Ag instead of Al), non-optimized results were obtained.

Imidazolium-substituted PTs as efficient electronic transport layers

Table S4.2: Photovoltaic performance of PCDTBT-based BHJ solar cell devices with and without the addition of CPE layers, as applied for the EQE measurements.^{7,8 a)}

Layer Sequence	V_{oc} (V)	J_{sc} (mA cm ⁻²) ^b	FF	Best η (%)	J_{EQE}
.../PCPDT- DTTzTz:PC ₇₁ BM/Ca/Ag	0.81	9.26	0.62	4.66	9.05
.../PCPDT- DTTzTz:PC ₇₁ BM/P2/Ag	0.87	10.2	0.65	5.79	10.6
.../PCPDT- DTTzTz:PC ₇₁ BM/P3/Ag	0.85	10.4	0.67	5.90	10.7

^{a)} Stack: glass/ITO/PEDOT-PSS/PCDTBT:PC₇₁BM/X/Ag with X = Ca or CPE. ^{b)} Uncorrected data.

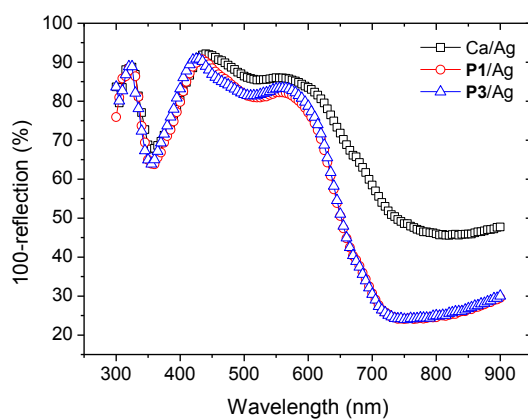


Figure S4.3: Reflectivity spectra for devices containing the **P1** and **P3** CPEs (compared to a reference Ca/Ag device).⁷

⁸ Global tilt ASTM G173-03 reference spectrum: <http://rredc.nrel.gov/solar/spectra/am1.5/>

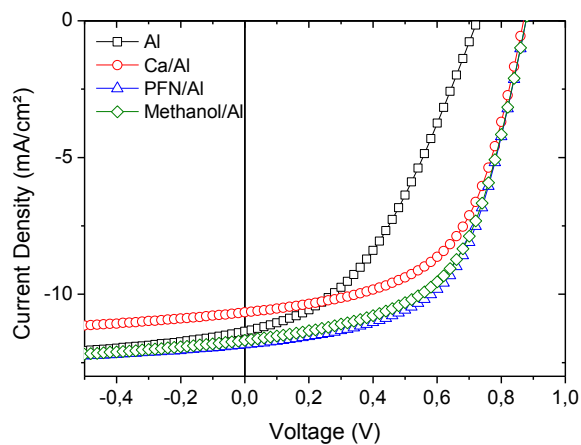
4.6.4 *J-V* Curves

Figure S4.4: *J-V* curves under illumination of PCDTBT:PC₇₁BM BHJ photovoltaic devices with and without additional CPE layers (averaged results).

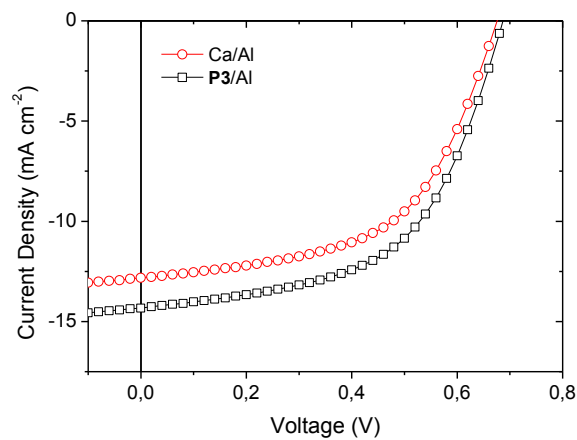


Figure S4.5: *J-V* curves under illumination of PCPDT-DTTzTz:PC₇₁BM BHJ photovoltaic devices with and without additional CPE layers (averaged results).

4.6.5 Atomic Force Microscopy

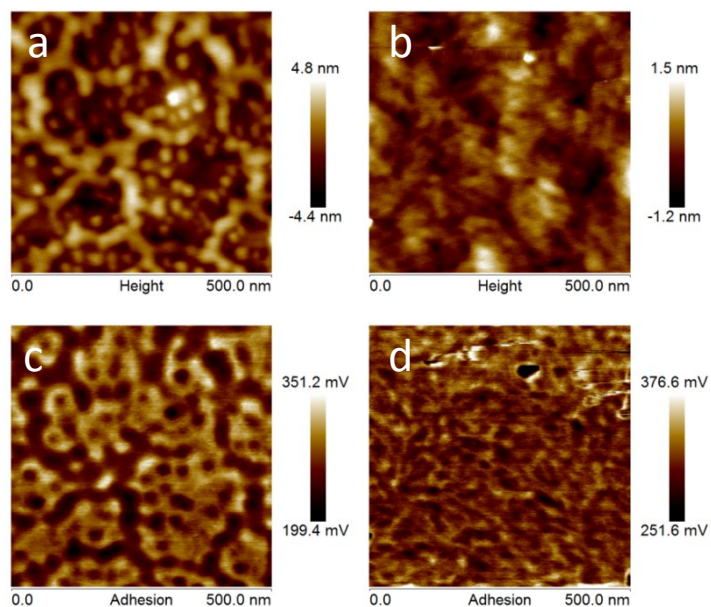


Figure S4.6: AFM (a,c: topography; b,d: adhesion) images ($500 \times 500 \text{ nm}^2$) of layer stacks with and without additional CPE layer: a,c) PCDTBT:PC₇₁BM/**P2**, b,d) PCDTBT:PC₇₁BM/MeOH.

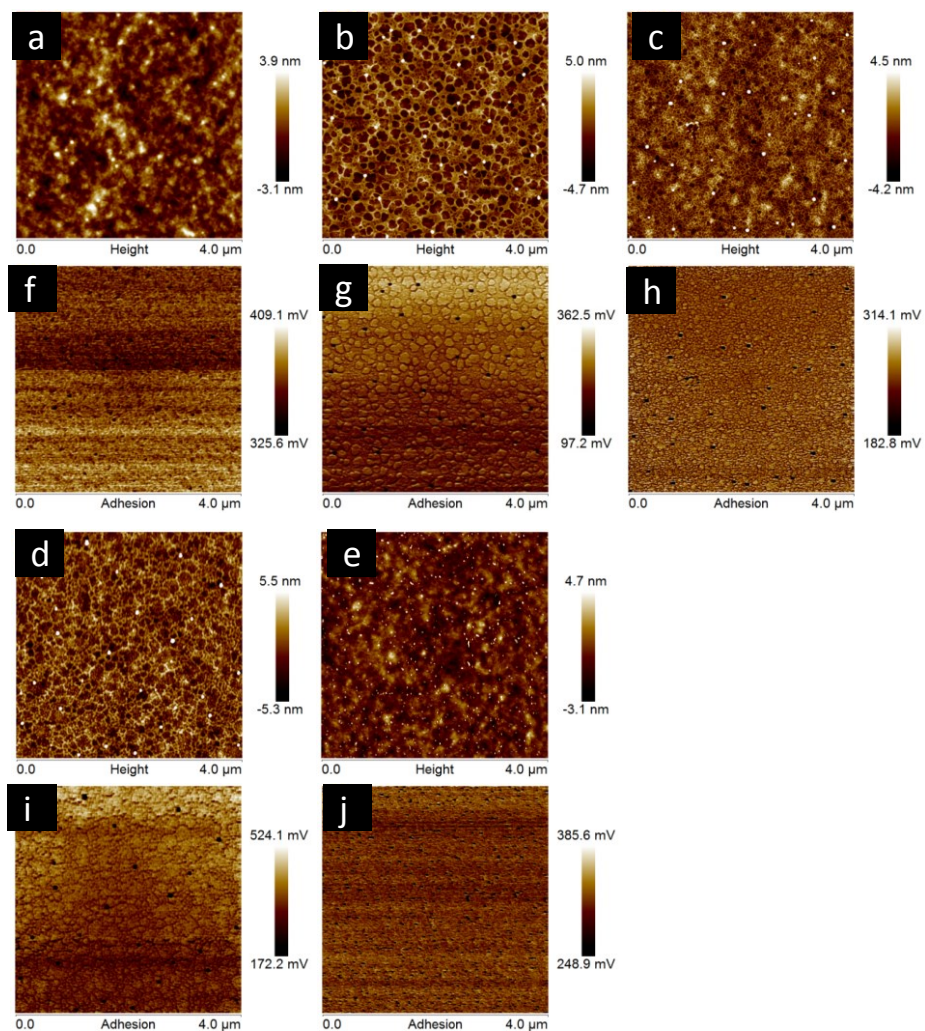


Figure S4.7: AFM (a-e: topography; f-j: adhesion) images ($4 \times 4 \mu\text{m}^2$) of layer stacks with and without additional CPE layers: a,f) PCDTBT:PC₇₁BM; b,g) PCDTBT:PC₇₁BM/P1; c,h) PCDTBT: PC₇₁BM/P2; d,i) PCDTBT:PC₇₁BM/P3; e,j) PDCTBT:PC₇₁BM/MeOH.

Chapter 5

Amphiphilic *N*-methylimidazole- functionalized diblock copolythiophenes for organic photovoltaics

Ghoos, T.; Van den Brande, N.; Defour, M.; Brassinne, J.; Fustin, C.-A.; Gohy, J.-F.;
Hoeppener, S.; Schubert, U. S.; Lutsen, L.; Vanderzande, D. J.; Van Mele B.; Maes W.
manuscript submitted to J. Polym. Sci. Part A: Polym. Chem.

5.1 Introduction

Poly(3-alkylthiophenes) (P3ATs) are widely studied in organic electronics due to their easy production and appealing optoelectronic and charge transport properties. In recent years, they have mostly been applied as light-harvesting electron donor materials in organic photovoltaics (OPV), the most prominent example being poly(3-hexylthiophene) (P3HT).^{1,2} Organic solar cells show a number of beneficial features compared to traditional crystalline Si-based devices, such as low cost large area fabrication by solution-processing techniques, reduced weight, flexibility, more appealing looks, and improved diffuse light operation, which render them a topic of high current interest.³ Main issues to be solved before successful market entry can be envisaged are OPV device efficiency and stability, and most current research efforts are hence directed toward these parameters. Another important aspect to be considered is the environmental impact of the OPV production process.⁴ At present, the active layer of the state of the art bulk heterojunction (BHJ) organic solar cells, an intimately mixed blend of a low bandgap donor polymer (or small molecule) and a fullerene acceptor, is generally deposited from solutions in high-boiling chlorinated solvents such as (di)chlorobenzene. To reduce the ecological footprint, solution processing from less harmful solvents is highly desirable. For that purpose, more polar polymers and fullerenes are pursued, allowing solubility in alcohols (and ultimately water). As an additional benefit, the increased polarity may also result in a higher dielectric constant, which has been considered as a potential pathway to a new efficiency regime for OPV.⁵

Amphiphilic *N*-methylimidazole-functionalized diblock copolythiophenes

We have recently prepared a series of imidazolium-substituted ionic polythiophenes, both in homopolymer and (statistical) copolymer configurations.⁶ The homopolymers were applied as active materials in efficient bi-layer solar cells^{6a} and as highly effective electron transport (ETL) materials improving photovoltaic performance,^{6b} outperforming the state of the art analogous ETLs such as PFN. In the latter study, a clear effect of molecular structure on ETL performance was observed, which seems to be related with the active layer coverage and molecular orientation within the interlayer.^{6c} Aiming at deeper fundamental understanding of the underlying structure-performance relationships, a series of ionic random copolymers was synthesized.^{6d} On the other hand, analogous block copolythiophenes are also of particular interest as the block structure may impose a well-defined nanoscale morphology. More in general, (all-)conjugated block copolymers may have several specific applications in OPV. They have already been used as active layer materials and compatibilizers in BHJ blends, increasing the efficiency and/or stabilizing the blend nanomorphology, and as self-organizing hole transport layers.⁷ Their exceptional solubility properties also enable these materials to be used as surfactants, for example for inorganic nanocrystals to be added to the active layer blend.⁸

When prepared through the Ni(dppp)Cl-initiated chain growth process,^{9,10} it is possible to control the polymerization process toward regioregular P3ATs. As such, the method is also suitable for the synthesis of all-conjugated block copolythiophenes by consecutive monomer addition.¹¹ This has been explored by a number of research groups focusing on the synthesis of different types of diblock

copolythiophenes. For example, the groups of Hayward and Park synthesized a series of amphiphilic diblock copolythiophenes containing a hydrophobic 3-alkylthiophene block and a hydrophilic poly(ethylene glycol-thiophene) block.^{11e,g} In chloroform/methanol or THF/methanol solvent mixtures, they observed the formation of superstructures with a hydrophobic core and the hydrophilic part exposed toward the polar environment. Ionic polythiophene derivatives were initially made by oxidative polymerization of charged thiophene monomers,¹² resulting in regiorandom materials. Later on, they were also produced by the introduction of charged moieties on the side chains of regioregular P3ATs by post-polymerization procedures (or by end-capping).¹³ Until very recently, mostly homopolymers and statistical copolymers were synthesized, and only a few reports focus on conjugated ionic block copolymers.^{13e-f}

In this work, we report on the synthesis of amphiphilic *N*-methylimidazole-functionalized diblock copolythiophenes toward applications in organic photovoltaics. The influence of the structural composition - random *vs* block - on the solution behavior and thermal properties of both the precursor and ionic block copolythiophenes is investigated.

5.2 Results and discussion

5.2.1 Block copolymer synthesis

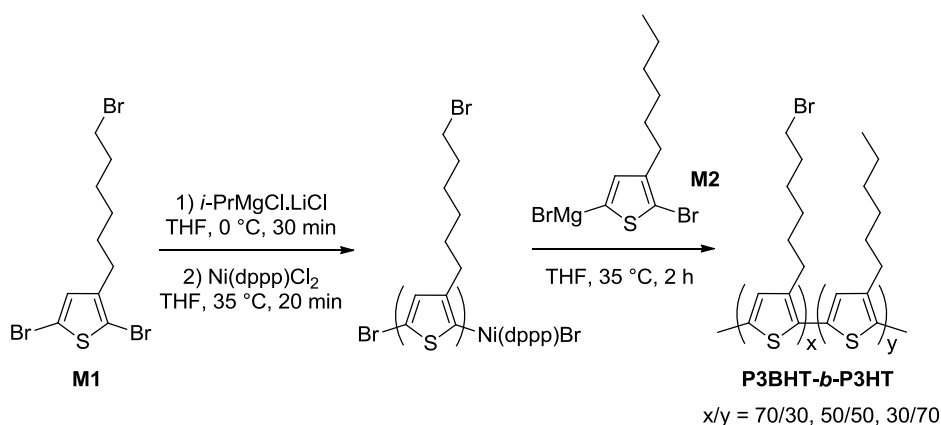
The ionic diblock copolythiophenes were synthesized by a two-step procedure, similar to the analogous random copolymers.^{6d} First of all, precursor block copolymers containing a particular ratio of bromohexyl

Amphiphilic *N*-methylimidazole-functionalized diblock copolythiophenes

side chains were synthesized via the quasi-living Grignard metathesis (GRIM) polymerization method.¹⁴ In a second step, these precursors were then converted to the desired *N*-methylimidazole-functionalized copolythiophene materials. The non-ionic poly[3-(6-bromohexyl)thiophene-*block*-3-hexylthiophene] or **P3BHT-*b*-P3HT** precursor copolymers were prepared in three different block ratios – **50/50**, **70/30** and **30/70** – by a slightly adapted GRIM polymerization procedure (**Scheme 5.1**). The first block was prepared by activating the functional 2,5-dibromo-3-(6-bromohexyl)thiophene monomer **M1** with an *i*-PrMgCl.LiCl solution at 0 °C for 30 minutes, and subsequently starting the polymerization by the addition of the Ni(dppp)Cl₂ catalyst and running the reaction for 20 minutes at 35 °C (the literature standard before addition of the second block). At that time, the activated 2,5-dibromo-3-hexylthiophene monomer **M2** was added to the first polymer block and the resulting mixture was reacted further for 2 hours at 35 °C (as previously indicated to be optimal for block copolymerization^{11b}). For the **30/70** block copolymer, the 3-hexylthiophene block was prepared first and then the activated monomer **M1** was added. Size exclusion chromatography (SEC) analysis during the reactions confirmed that all polythiophene chains continued growing, in a gradual fashion, after addition of the second monomer, indicating the ‘living’ character and the formation of real diblock copolymers (*vide infra*). The polymerization was quenched by addition of an HCl solution (3M) to promote the protonation of the chain ends and to avoid disproportionation.¹⁵ The precursor polymers were purified by

Chapter 5

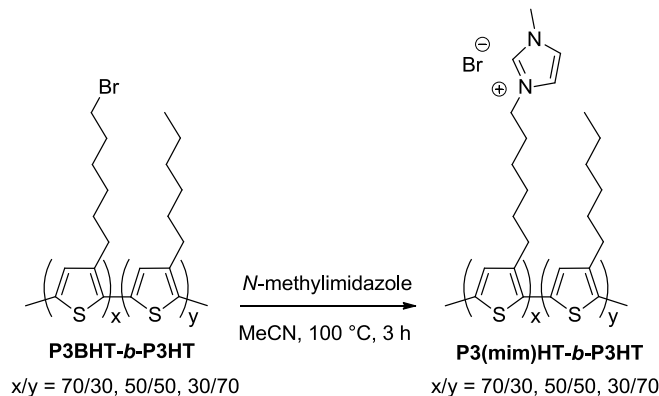
consecutive Soxhlet extractions with methanol, *n*-hexane and chloroform.



Scheme 5.1: Synthetic route applied toward the **P3BHT-*b*-P3HT** precursor block copolymers (reverse order of addition for the **30/70** derivative).

The amphiphilic **P3(MIM)HT-*b*-P3HT** diblock copolymers were then obtained via a simple substitution reaction on the bromide end groups with *N*-methylimidazole (**Scheme 5.2**). This reaction was performed under microwave irradiation, allowing to speed up the substitution reaction from 3 days to 3 hours.^{6d} The resulting ionic polymers were precipitated in the non-solvent diethyl ether, washed several times, dried under vacuum and used further on without any other purification.

Amphiphilic *N*-methylimidazole-functionalized diblock copolythiophenes



Scheme 5.2: Functionalization of the precursor polymers toward the amphiphilic **P3(mim)HT-*b*-P3HT** diblock copolythiophenes.

During the synthesis of the block copolymers, an aliquot was taken just before addition of the second monomer. This sample was added to a 3M solution of HCl in methanol and the resulting precipitate was filtered off and analyzed by SEC. When the SEC profile of this **P3BHT** sample was compared with the profile of the final **P3BHT-*b*-P3HT** precursor polymers, it was clear that the chains had grown further toward a diblock copolymer, as seen from the complete shift of the distribution (**Figure 5.1**). Contamination of the **P3BHT-*b*-P3HT** diblocks by **P3BHT** ‘dead’ homopolymers would result in a shoulder at low elution volume, which is not the case (see **Figure 5.1**, **S5.1**). Furthermore, the increase in molecular weight for the **P3BHT-*b*-P3HT** diblocks was qualitatively in good agreement with the feeding ratio (**Table S5.2**). From the SEC analyses, the block copolymer synthesis hence seemed successful. Reasonable number-average molecular weights (M_n), all in the same range of $8.1\text{--}9.4 \times 10^3$, were obtained, with rather narrow polydispersities (~ 1.3) (**Table 5.1**).

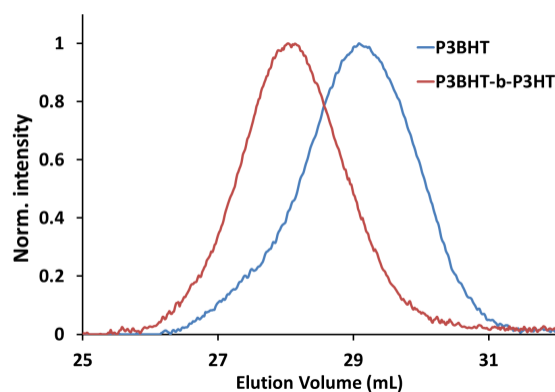


Figure 5.1: SEC profiles obtained during the synthesis of the **P3BHT-*b*-P3HT 50/50** block copolymer.

Table 5.1: SEC, NMR and UV-Vis characterization data for the precursor block copolymers **P3BHT-*b*-P3HT**.

Polymer	M_n (kDa)	M_w (kDa)	D	Ratio (NMR)	λ_{max}^a
P3BHT-<i>b</i>-P3HT 30/70	8.4	10.3	1.23	17:83	446 nm
P3BHT-<i>b</i>-P3HT 50/50	8.1	11.0	1.36	47:53	442 nm
P3BHT-<i>b</i>-P3HT 70/30	9.4	12.0	1.28	69/31	445 nm

^a in CHCl₃.

Further analysis was performed by ¹H NMR spectroscopy. It was confirmed that the ratio of the two building blocks in the block copolymer is in agreement with the feeding ratio (see SI and **Table 5.1**). NMR spectroscopy was also used to monitor the efficiency of the functionalization reaction, by following the shift of the protons on the side-chain carbon atoms next to the end groups, going from ~3.4 ppm for the precursor polymers to ~4.2 ppm for the ionic **P3(MIM)HT-*b*-**

P3HT copolymers. In the ionic block copolymers the ratio of the two blocks could be confirmed once again (see SI).

5.2.2 Solution behavior

As expected, the precursor polymers showed a similar solution behavior and absorption maxima (in chloroform) as normal **P3HT** (**Table 5.1**). After functionalization with the imidazolium moieties, the solution behavior changed quite drastically (**Figure 5.2**). The ionic block copolymers are soluble in more polar solvents. The **P3(MIM)HT-*b*-P3HT 50/50** and **70/30** copolymers, carrying most pendant ionic groups, are completely soluble in MeOH, DMSO, and even water. A red color is observed when these materials are dissolved in water. When the UV-Vis absorption spectra are compared, one can notice that the **70/30** copolymer is molecularly dissolved in MeOH and DMSO, whereas the **50/50** block copolymer is slightly aggregating, as seen by the small band broadening and the shoulder at ~605 nm.

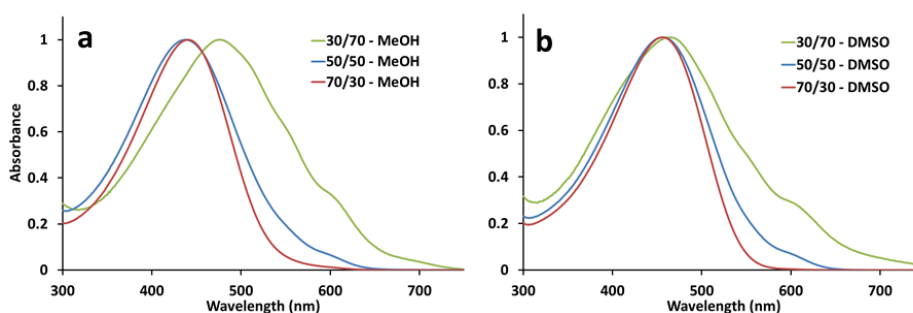


Figure 5.2: UV-Vis absorption spectra of the different **P3(mim)HT-*b*-P3HT** diblock copolymers in a) MeOH and b) DMSO.

In water, both diblock copolymers have almost similar absorption characteristics, with a definite band broadening and red-shift (to $\lambda_{\max} = \sim 485$ nm) compared to the solutions in MeOH (**Figure 5.3**). When these ionic block copolymers are compared with the random copolymer equivalents,^{6d} their solution behavior is comparable but not identical. The largest difference is observed for the **50/50** copolymers. The random copolymer is not soluble in water. It can, however, be dissolved in a 9/1 mixture water/THF. A ‘bordeaux’-red solution is obtained, with an even more pronounced red-shift ($\lambda_{\max} = 515$ nm) and distinct shoulders (at $\lambda_{\max} = 558$ and 604 nm).

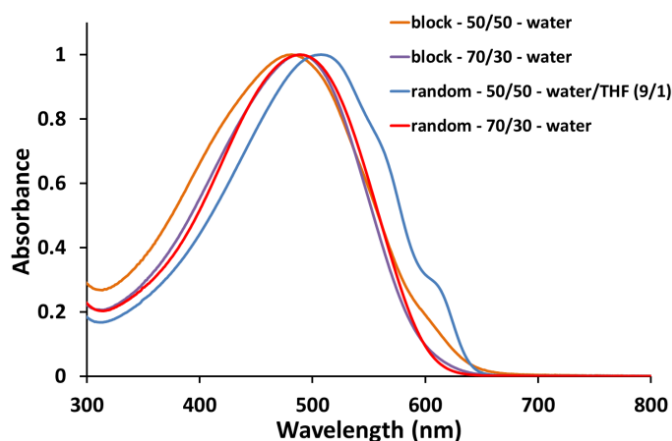


Figure 5.3: UV-Vis absorption spectra of the **50/50** and **70/30** random and block copolythiophenes in water (The **50/50** random copolymer was dissolved in 90/10 water/THF).

On the other hand, the **P3(MIM)HT-*b*-P3HT 30/70** material, containing a majority of hydrophobic hexyl side chains, is not completely soluble in any of these solvents. In MeOH and DMSO, only a part of the polymer is soluble and a very fine insoluble residue remains, even after heating the sample to 50 °C. The polymer is not soluble at all in water.

5.2.3 Characterization of the micellar structures

To get more insight on the possible formation of aggregates and/or ordered structures in solution (in particular in water), of importance for future OPV applications, dynamic light scattering (DLS) experiments and cryo-transmission electron microscopy (cryo-TEM) experiments were performed. The **P3(MIM)HT-*b*-P3HT 50/50** and **70/30** amphiphilic block copolymers could directly be dissolved in water, and a 0.1 g/mL solution was prepared for both. For the **70/30** copolymer, the DLS analysis revealed a bimodal size distribution (**Figure 5.4a**) with a first population around 8 nm and a second around 40 nm. The cryo-TEM picture of this sample (**Figure 5.4b**) revealed the presence of spherical micelles with an average radius of 6 ± 2 nm, in agreement with the first population observed by DLS. The second population in the DLS histogram could be attributed to the presence of some aggregated micelles (that are however not visualized by cryo-TEM) and/or to the so-called slow mode originating from the polyelectrolyte effect (the P3(MIM)HT are indeed typical polyelectrolyte blocks) which induces the appearance of a peak at high hydrodynamic radius in the size distribution.

The size distribution obtained for the **50/50** copolymer exhibited three populations with apparent hydrodynamic radii located around 7, 60 and 280 nm (**Figure 5.5a**). The size associated to the first population could again be attributed to the micelles. This is further confirmed by cryo-TEM analysis (**Figure 5.5b**) that essentially revealed small spherical micelles with an average radius of $5,5\pm 2$ nm, again in perfect agreement with the DLS results. Rod-like micelles that could originate from the

merging of the primary spherical micelles are also scarcely observed in the cryo-TEM pictures (**Figure 5.5b**). Compared to the previously investigated **P3(MIM)HT-*b*-P3HT 70/30** sample, the formation of rod-like micelles is likely in the **P3(MIM)HT-*b*-P3HT 50/50** one, according to the composition of the copolymer. Indeed, the latter contains a larger hydrophobic part thus promoting the formation of a rod-like morphology. Since the majority of the sample is observed as spherical micelles, one could conclude that the **P3(MIM)HT-*b*-P3HT 50/50** sample lies at the boundary between spherical and cylindrical micelles. Two other larger size populations are observed in the size distribution histogram (**Figure 5.5a**) and are more difficult to explain. There could be again contributions in the DLS signal from either clusters of micelles or the polyelectrolyte effect. The rod-like micelles observed in the cryo-TEM picture could also contribute to the DLS signal.

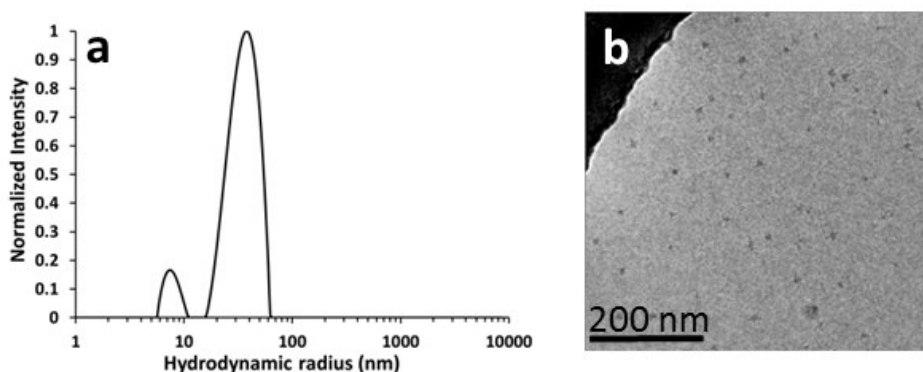


Figure 5.4: Size distribution histogram (a) and cryo-TEM picture (b) for the **P3(MIM)HT-*b*-P3HT 70/30** block copolymer in water.

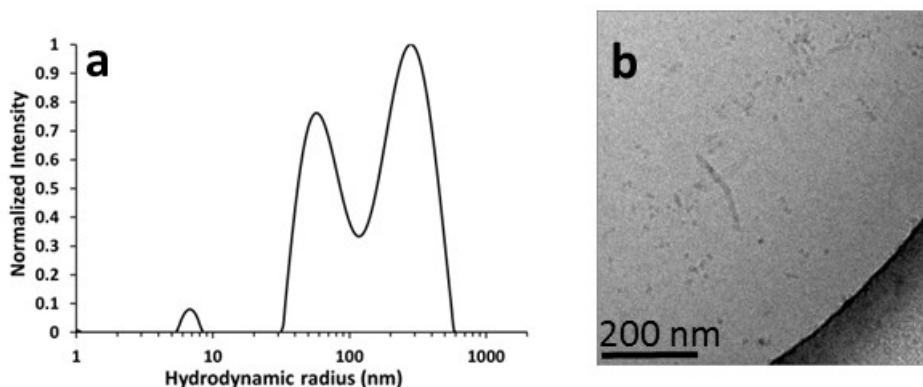


Figure 5.5: Size distribution histogram (a) and cry-TEM picture (b) for the **P3(MIM)HT-*b*-P3HT 50/50** block copolymer in water.

As the **P3(MIM)HT-*b*-P3HT 30/70** derivative is not directly soluble in water, another approach was required. The block copolymer was first dissolved in THF, and water was added drop-wise under stirring to reach a 8/2 water/THF composition. The same volume of water was then added in one shot to ‘freeze’ the formed (nano)structures in solution, yielding a 9/1 water/THF solvent mixture. Finally, the resulting solution was diluted 10 times with the same solvent mixture to reach a concentration of 0.1 g/L. The size distribution showed two populations around 120 and 1200 nm, (**Figure 5.6**) probably associated to clusters of micelles and/or polyelectrolyte effect, as explained above. The solution was diluted further (down to 0.005 g/L) without significant changes in the size distribution. Obviously, ‘frozen’ micellar nanostructures have been prepared from this copolymer, whose characteristic features are not dependent on concentration. This can be explained by the composition of this copolymer, which is mainly hydrophobic and has only a short hydrophilic block. Hence the co-solvent method had to be used for the

preparation of the micellar solutions, likely resulting in the formation of poorly stabilized nanoaggregates rather than true micelles. Cryo-TEM imaging was not successful on this sample.

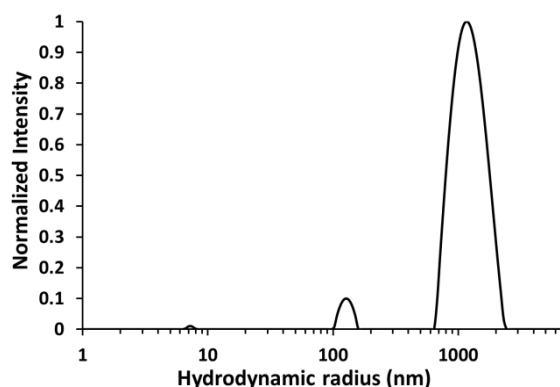


Figure 5.6: Size distribution histogram of the **P3(MIM)HT-*b*-P3HT 30/70** block copolymer in a 9/1 water/THF solution .

5.2.4 Thermal analysis

Information regarding the crystallinity of semiconducting materials is of high relevance when aiming at their application in organic electronics. Basic thermal analysis is also a prerequisite to construct phase diagrams of the donor-acceptor OPV active layer blends, from which fundamental understanding of the formation and evolution of the BHJ blend morphology can be deduced.¹⁶ Moreover, thermal analysis may provide additional experimental proof for the block architecture. The **P3BHT-*b*-P3HT** precursor materials show clear semi-crystalline behavior, with a glass transition (T_g) around 15–18 °C (**Figure 5.7**). A trend is visible in the crystallinity; a larger P3HT block length leads to higher-melting crystals and a higher degree of crystallinity, based on the measured

Amphiphilic *N*-methylimidazole-functionalized diblock copolythiophenes

enthalpy of melting ΔH_m (see **Table 5.2**). The same trend can be seen in the crystallization kinetics; the **P3BHT-*b*-P3HT 30/70** copolymer crystallizes during the previous cooling, whereas an increasing cold crystallization peak is seen for the **50/50** and **70/30** materials. The presence of a single melting peak in the second heating curves seems surprising for these block copolymers. However, a second, lower melting peak was seen when the material was stored at room temperature for several days (**Figure 5.8**). This indicates that the **P3BHT** blocks can also crystallize, but at a much slower rate than the **P3HT** blocks. Overall, when comparing with the random copolymer precursors prepared before, the melting and crystallization temperatures are all lower.^{6d} This can, however, also be explained by the lower molecular weights achieved for the block copolymers (**Table 5.1**).

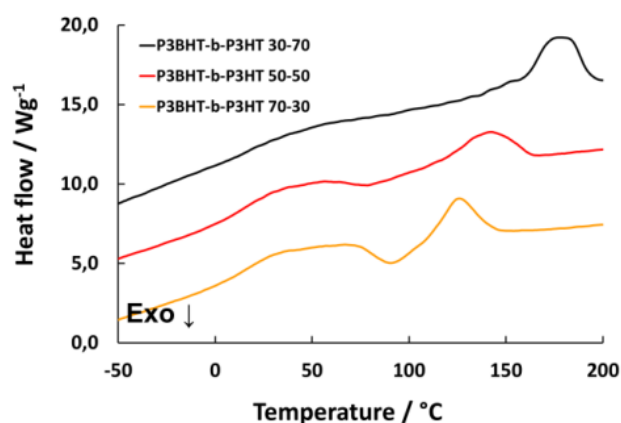


Figure 5.7: RHC thermograms depicting the second heating of the **P3BHT-*b*-P3HT** copolymer samples at 500 K min⁻¹. The curves were shifted vertically for clarity.

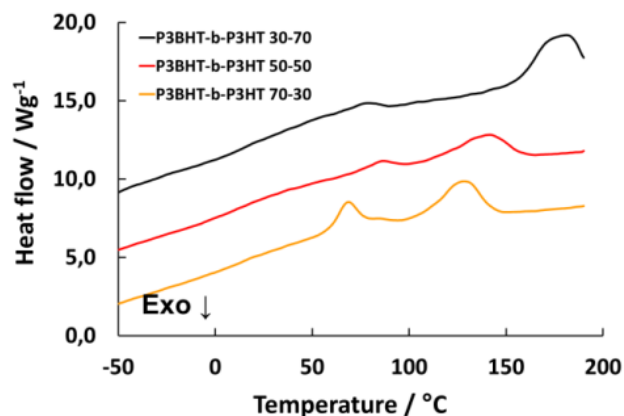


Figure 5.8: RHC thermograms depicting the first heating of the **P3BHT-*b*-P3HT** copolymer samples at 500 K min^{-1} , after being stored at room temperature for several days. Note the appearance of a second, lower melting peak. The curves were shifted vertically for clarity.

Table 5.2: Overview of the thermal transitions for all diblock copolymers.

Polymer	T_g (°C)	T_m (°C)	ΔH_m (J g ⁻¹)
P3BHT-<i>b</i>-P3HT 30/70	15	176	11.3
P3BHT-<i>b</i>-P3HT 50/50^a	16	141	7.3
P3BHT-<i>b</i>-P3HT 70/30^a	18	126	5.7
P3(MIM)HT-<i>b</i>-P3HT 30/70	63	181	10.7
P3(MIM)HT-<i>b</i>-P3HT 50/50	77	-	-
P3(MIM)HT-<i>b</i>-P3HT 70/30	81	-	-

^a Cold crystallization heating

For the ionic **P3(MIM)HT-*b*-P3HT** block copolymers a clear T_g can be seen for the three compositions, which seems to increase with the **P3(MIM)HT** block length (**Figure 5.9**, **Table 5.2**). The T_g values for

Amphiphilic *N*-methylimidazole-functionalized diblock copolythiophenes

both the **50/50** and **70/30** compositions seem to be relatively high compared to a T_g of 72 °C found for pure **P3(MIM)HT**.^{6d} This can be explained by the difference in scan rates between Rapid Heat-Cool Calorimetry (RHC), used here, and DSC used in the previous study. The **30/70 P3(MIM)HT-*b*-P3HT** block copolymer, however, exhibits a significantly lower T_g of about 63 °C. Taking into account the M_n of the block copolymer (**Table 5.1**), this is most likely the effect of a short **P3(MIM)HT** block. During the first heating a large endotherm is observed after the T_g , corresponding to the evaporation of water. It confirms the hygroscopic properties of the **P3(MIM)HT** block, related to the bromine counter ions, as already noticed for the random copolymers.^{6d} A melting peak can be seen for the **P3(MIM)HT-*b*-P3HT 30/70** block copolymer at a temperature of 181 °C, which is similar to the melting temperature of the precursor block copolymer. It indicates that this transition corresponds to the **P3HT** block. For the **50/50** and **70/30** compositions, no melting transition is observed, indicating that the crystallinity is strongly reduced by functionalization of the **P3BHT** blocks.

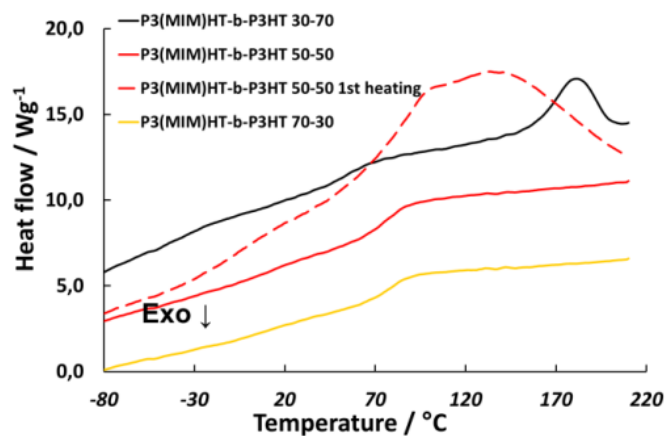


Figure 5.9: RHC thermograms depicting the second heating of the **P3(MIM)HT-*b*-P3HT** copolymer samples at 500 K min⁻¹. The first heating of the **50-50** composition is also shown. The curves were shifted vertically for clarity.

5.3 Conclusions

In summary, ionic block copolythiophenes were synthesized in an efficient way, in three different block ratios, and their solution properties and thermal characteristics were analyzed. Clear differences compared to the analogous statistical copolymers were observed. The novel materials show high potential toward integration in organic photovoltaics, notably as interlayer materials boosting the efficiency of BHJ polymer solar cells.

5.4 Experimental section

5.4.1 General experimental methods

Unless stated otherwise, all reagents and chemicals were obtained from commercial sources and used without further purification. Diethyl ether and THF were dried using a MBraun MB-SPS 800 solvent purification system, operating under N₂ according to the principles described by Pangborn *et al.*¹⁷ Microwave synthesis was performed on a CEM Discover SP synthesis platform. NMR chemical shifts (δ , in ppm) were determined relative to the residual ¹H absorption of CHCl₃ (7.26 ppm) or the ¹³C resonance shift of CDCl₃ (77.16 ppm). UV-Vis measurements of the polymers in solution were performed with a scan rate of 600 nm/min in a continuous run from 200 to 800 nm. Molecular weights and molecular weight distributions were determined relative to polystyrene standards (Polymer Labs) by SEC. Analysis of the molecular weights and molecular weight distributions of the polymer samples was performed on a Tosoh EcoSEC System, comprising of an autosampler, a PSS guard column SDV (50 x 7.5 mm), followed by three PSS SDV analytical linear XL columns (5 μ m, 300 x 7.5 mm), and a differential refractive index detector (Tosoh EcoSEC RI) and a UV-detector using THF as the eluent at 40 °C with a flow rate of 1.0 mL/min. The SEC system was calibrated using linear narrow polystyrene standards ranging from 474 to 7.5 x 10⁶ g/mol ($K = 14.1 \times 10^{-5}$ dL/g and $\alpha = 0.70$). Polymer concentrations were in the range of 3–5 mg/mL. Dynamic light scattering (DLS) experiments were performed on a Malvern CGS-3 apparatus equipped with a He–Ne laser with a wavelength of 632.8 nm and a thermostat. The measurements were performed at 20 °C and at an

Amphiphilic *N*-methylimidazole-functionalized diblock copolythiophenes

angle of 90°. In practice, the size distribution histograms were obtained from the auto-correlation curve by the Contin algorithm, a method based on the inverse-Laplace transformation of the DLS data. Rapid Heat-Cool Calorimetry (RHC) experiments were performed on a prototype RHC of TA Instruments, equipped with liquid nitrogen cooling and specifically designed for operation at high scanning rates.^{18,19} RHC measurements were performed at 250 or 500 K min⁻¹ in aluminum crucibles, using neon (6 mL min⁻¹) as a purge gas.

5.4.2 Polymer synthesis

2,5-Dibromo-3-(6-bromohexyl)thiophene (**M1**) was prepared using a modified procedure starting from the procedures of Bäuerle and Miyanishi,^{20,21} as outlined before.^{6d}

General precursor block copolymer synthesis: P3BHT-*b*-P3HT 50/50 (Scheme 5.1)

2,5-Dibromo-3-(6-bromohexyl)thiophene (**M1**) (0.429 g, 1.06 mmol) was dissolved in anhydrous THF (15 mL) and poured into a flame dried three-neck round bottom flask. 2,5-Dibromo-3-hexylthiophene (**M2**) (0.345 g, 1.06 mmol) was likewise dissolved in dry THF (15 mL) and poured into a flame dried three-neck round bottom flask. An *i*-PrMgCl.LiCl solution in THF (1.3M, 1 equiv, 1.06 mmol) was added to the two flasks at 0 °C. After stirring for 30 min at 0 °C under an inert atmosphere, the Ni(dppp)Cl₂ catalyst (3 mol%, 16 mg) was then added to the solution of **M1**. The resulting reaction mixture was stirred for 20 min at 35 °C, before the solution of the activated monomer **M2** was

added. The resulting reaction mixture was stirred further for 2 h at 35 °C. The reaction was quenched with a HCl/MeOH solution (3M, 3 mL) and then poured into ice cold MeOH, upon which precipitation occurred (of a dark red to black polymer material). The precipitated material was filtered off using a PTFE membrane (47 mm/0.45 μm). The polymer was purified using Soxhlet extraction for 24 h with methanol, *n*-hexane and chloroform, respectively. After evaporation of the solvent, the polymer was redissolved in chloroform and precipitated again from methanol, filtered, washed and dried, affording the **P3BHT-*b*-P3HT 50/50** block copolythiophene as a black powder (0.125 g, 31%). ¹H NMR (300 MHz, CDCl₃): δ = 6.96 (s, 1H), 3.45-3.33 (m, 1H), 2.88-2.72 (br, 2H), 1.94-1.78 (m, 1H), 1.76-1.61 (m, 1H), 1.59–1.20 (m, 4H), 0.94-0.77 (m, 1.5H); NMR ratio: 47/53; UV-Vis (CHCl₃, nm): λ_{max} = 442; SEC (THF, PS standards): $M_n = 8.1 \times 10^3$ g/mol, $M_w = 1.1 \times 10^4$ g/mol, PDI = 1.36.

P3BHT-*b*-P3HT 70/30

The same method was applied for the **70/30** block copolymer, using following amounts: **M1** (0.575 g, 1.42 mmol), **M2** (0.199 g, 0.61 mmol); 1 equiv of an *i*-PrMgCl.LiCl solution in THF (1.3M) for both monomers; 3 mol% of Ni(dppp)Cl₂ catalyst. The **P3BHT-*b*-P3HT 70/30** block copolythiophene was obtained as a black powder (0.187 g, 42%). ¹H NMR (400 MHz, CDCl₃): δ = 6.96 (s), 3.41 (t, *J* = 6.8 Hz), 2.85-2.74 (br), 1.88 (q, *J* = 6.6 Hz), 1.76-1.63 (m), 1.58–1.37 (m), 1.36–1.22 (m) 0.92-0.83 (m); NMR ratio: 69:31; UV-Vis (CHCl₃, nm): λ_{max} = 445; SEC (THF, PS standards): $M_n = 9.4 \times 10^3$ g/mol, $M_w = 1.2 \times 10^4$ g/mol, PDI = 1.28.

P3BHT-*b*-P3HT 30/70

The same method was again applied for the **30/70** block copolythiophene, but an opposite monomer order was used (first the P3HT block was made): **M1** (0.223 g, 0.551 mmol), **M2** (0.408 g, 1.25 mmol); 1 equiv of an *i*-PrMgCl.LiCl solution in THF (1.3M) for both monomers; 3 mol% of Ni(dppp)Cl₂ catalyst. The **P3BHT-*b*-P3HT 30/70** block copolythiophene was obtained as a black powder (0.106 g, 31%). ¹H NMR (400 MHz, CDCl₃): δ = 6.96 (s), 3.44–3.33 (m), 2.85–2.64 (br), 1.92–1.78 (m), 1.77–1.52 (m), 1.49–1.15 (m), 0.95–0.77 (m); NMR ratio: 17:83; UV-Vis (CHCl₃, nm): λ_{max} = 446; SEC (THF, PS standards): M_n = 8.4 x 10³ g/mol, M_w = 1.0 x 10⁴ g/mol, PDI = 1.23.

5.4.3 Ionic block copolymer synthesis

General procedure for the functionalization with *N*-methylimidazole (Scheme 5.2)

P3BHT-*b*-P3HT 50/50 (60 mg, M_n = 8.1 x 10³ g/mol, PDI = 1.4) was suspended in MeCN (2 mL) and *N*-methylimidazole (3 mL) was added. This suspension was stirred under microwave activation for 4 h at 100 °C (maximum power 200 W, maximum pressure 250 psi). Afterwards, the reaction mixture was added drop-wise to Et₂O and a dark red precipitate was formed. The precipitated material was filtered off using a PTFE membrane (47 mm/0.45 μm), affording the **P3(MIM)HT-*b*-P3HT 50/50** block copolymer as a black powder (25 mg, 42%). ¹H NMR (300 MHz, DMSO-*d*₆): δ = 9.28 (br, 1H), 7.83 (br, 1H), 7.74 (br, 1H), 7.21 (br, 1H), 4.18 (br, 2H), 3.86 (s, 3H), 2.79 (br, 2H), 1.81 (br,

2H), 1.64 (br, 2H), 1.48–1.09 (m, 4H), 0.87 (br, 3H); UV-Vis (MeOH, nm): $\lambda_{\max} = 437$.

P3(mim)HT-*b*-P3HT 70/30 (50 mg, $M_n = 9.4 \times 10^3$ g/mol, PDI = 1.3): black powder (59 mg, 93%); ^1H NMR (300 MHz, DMSO- d_6): $\delta = 9.32$ (s), 7.85 (s), 7.75 (s), 7.20 (s), 4.20 (br), 3.86 (s), 2.86–2.69 (br), 1.89–1.73 (br), 1.72–1.53 (m), 1.49–1.18 (m), 0.87 (br); UV-Vis (MeOH, nm): $\lambda_{\max} = 441$.

P3(mim)HT-*b*-P3HT 30/70 (50 mg, $M_n = 8.4 \times 10^3$ g/mol, PDI = 1.2); black powder (21 mg, 39%); ^1H NMR (400 MHz, CDCl_3): $\delta = 6.96$ (s), 4.48–4.20 (m), 4.19–3.91 (m), 2.88–2.43 (m), 2.06–1.75 (m), 1.74–1.50 (m), 1.48–1.11 (m), 0.97–0.72 (m); UV-Vis (CHCl_3 , nm): $\lambda_{\max} = 436$.

5.5 References

- (a) Dang, M. T.; Hirsch, L.; Wantz, G. *Adv. Mater.* **2011**, *23*, 3597–3602; (b) Marrocchi, A.; Lanari, D.; Facchetti, A.; Vaccaro, L. *Energy Environ. Sci.* **2012**, *5*, 8457–8474; (c) Dang, M. T.; Hirsch, L.; Wantz, G.; Wuest, J. D. *Chem. Rev.* **2013**, *113*, 3734–3765.
- Seo, J. H.; Gutacker, A.; Sun, Y.; Wu, H.; Huang, F.; Cao, Y.; Scherf, U.; Heeger, A. J.; Bazan, G. C. *J. Am. Chem. Soc.* **2011**, *133*, 8416–8419.
- (a) Brabec, C. J.; Gowrisanker, S.; Halls, J. J. M.; Laird, D.; Jia, S.; Williams, S. P. *Adv. Mater.* **2010**, *22*, 3839–3856; (b) Nelson, J. *Mater. Today* **2011**, *14*, 462–470; (c) Kumar, P.; Chand, S. *Prog. Photovoltaics* **2012**, *20*, 377–415; (d) Li, G.; Zhu, R.; Yang, Y. *Nat. Photonics* **2012**, *6*, 153–161; (e) Jørgensen, M.; Norrman, K.; Gevorgyan, S.; Tromholt, T.; Andreasen, B.; Krebs, F. C. *Adv. Mater.* **2012**, *24*, 580–612; (f) He, Z.; Zhong, C.; Su, S.; Xu, M.; Wu, H.; Cao, Y. *Nat. Photonics* **2012**, *6*, 591–595.
- Ancil, A.; Babbitt, C. W.; Raffaele, R. P.; Landi, B. J. *Prog. Photovolt.: Res. Appl.* **2012**, DOI: 10.1002/pip.2226.
- (a) Koster, L. J. A.; Shaheen, S. E.; Hummelen, J. C. *Adv. Energy Mater.* **2012**, *2*, 1246–1253; (b) Chiechi, R. C.; Hummelen, J. C. *ACS Macro Lett.* **2012**, *1*, 1180–1183.
- (a) Ghoo, T.; Malinkiewicz, O.; Lutsen, L.; Vanderzande, D. J.; Bolink, H. J.; Maes, W. *RSC Adv.*, manuscript under revision; (b) Kesters, J.; Ghoo, T.; Penxten, H.; Drijkoningen, J.; Vangerven, T.; Lyons, D. M.; Lutsen, L.; Vanderzande, D.; Manca, J.; Maes, W. *Adv. Energy Mater.* **2013**, DOI: 10.1002/aenm.201300049; (c) Drijkoningen, J.; Kesters, J.; Vangerven, T.; Lutsen, L.; Vanderzande, D.; Maes, W.; D’Haen, J.; Manca, J. *Sol. Energy Mater. Sol. Cells*, manuscript submitted.; (d) Ghoo, T.; Brassine, J.; Fustin, C.-A.; Gohy, J.-F.; Defour, M.; Van Den Brande, N.; Van Mele, B.; Lutsen, L.; Vanderzande, D.; Maes, W. manuscript submitted.
- (a) Ren, G.; Wu, P.-T.; Jenekhe, S. A. *Chem. Mater.* **2010**, *22*, 2020–2026; (b) Yun, H. M.; Kim, J.; Yang, C.; Kim, J. Y. *Sol. Energy Mater. Sol. Cells* **2012**,

- 104, 7–12; (c) Chen, H.; Chen, J.; Yin, W.; Yu, X.; Shao, M.; Xiao, K.; Hong, K.; Pickel, D. L.; Kochemba, W. M.; Kilbey II, S. M.; Dadmun, M. *J. Mater. Chem. A* **2013**, *1*, 5309–5319; (d) Ouhib, F.; Tomassetti, M.; Manca, J.; Piersimoni, F.; Spoltore, D.; Bertho, S.; Moons, H.; Lazzaroni, R.; Desbief, S.; Jerome, C.; Detrembleur, C. *Macromolecules* **2013**, *46*, 785–795; (e) Yao, K.; Chen, L.; Chen, X.; Chen, Y. *Chem. Mater.* **2013**, *25*, 897–904.
- 8 (a) Park Y.; Advincula, R. C. *Chem. Mater.* **2011**, *23*, 4273–4294; (b) Zhao L.; Lin, Z. *Adv. Mater.* **2012**, *24*, 4353–4368.
- 9 (a) Sheina, E. E.; Liu, J.; Iovu, M. C.; Laird, D. W.; McCullough, R. D. *Macromolecules* **2004**, *37*, 3526–3528; (b) Iovu, M. C.; Sheina, E. E.; Gil, R. R.; McCullough, R. D. *Macromolecules* **2005**, *38*, 8649–8656.
- 10 (a) Yokoyama, A.; Miyakoshi, R.; Yokozawa, T. *Macromolecules* **2004**, *37*, 1169–1171; (b) Miyakoshi, R.; Yokoyama, A.; Yokozawa, T. *J. Am. Chem. Soc.* **2005**, *127*, 17542–17547.
- 11 (a) Zhang, Y.; Tajima, K.; Hirota, K.; Hashimoto, K. *J. Am. Chem. Soc.* **2008**, *130*, 7812–7813; (b) Zhang, Y.; Tajima, K.; Hashimoto, K. *Macromolecules* **2009**, *42*, 7008–7015; (c) Ge, J.; He, M.; Qiu, F.; Yang, Y. *Macromolecules* **2010**, *43*, 6422–6428; (d) Hammer, B. A. G.; Bokel, F. A.; Hayward, R. C.; Emrick, T. *Chem. Mater.* **2011**, *23*, 4250–4256; (e) Kim, J.; Song, I. Y.; Park, T. *Chem. Commun.* **2011**, 4697–4699; (f) Verswyvel, M.; Monnaie, F.; Koeckelberghs, G. *Macromolecules* **2011**, *44*, 9489–9498; (g) Lee, E.; Hammer, B.; Kim, J. K.; Page, Z.; Emrick, T.; Hayward, R. C. *J. Am. Chem. Soc.* **2011**, *133*, 10390–10393; (h) Higashihara, T.; Ohshimizu, K.; Ryo, Y.; Sakurai, T.; Takahashi, A.; Nojima, S.; Ree, M.; Ueda, M. *Polymer* **2011**, *52*, 3687–3695; (i) Smeets, A.; Willot, P.; De Winter, J.; Gerbaux, P.; Verbiest, T.; Koeckelberghs, G. *Macromolecules* **2011**, *40*, 6017–6025; (j) Song, I. Y.; Kim, J.; Im, M. J.; Moon, B. J.; Park, T. *Macromolecules* **2012**, *45*, 5058–5068.
- 12 (a) Chayer, M.; Faïd, K.; Leclerc, M. *Chem. Mater.* **1997**, *9*, 2902–2905; (b) Ho, H. A.; Leclerc, M. *J. Am. Chem. Soc.* **2003**, *125*, 4412–4413; (c) Viinikanoja, A.; Areva, S.; Kocharova, N.; Aaritalo, T.; Vuorinen, M.; Savunen, A.; Kankare, J.; Lukkari, J.; *Langmuir* **2006**, *22*, 6078–6086; (d) Burns, C. T.; Lee, S.; Seifert, S.;

Amphiphilic N-methylimidazole-functionalized diblock copolythiophenes

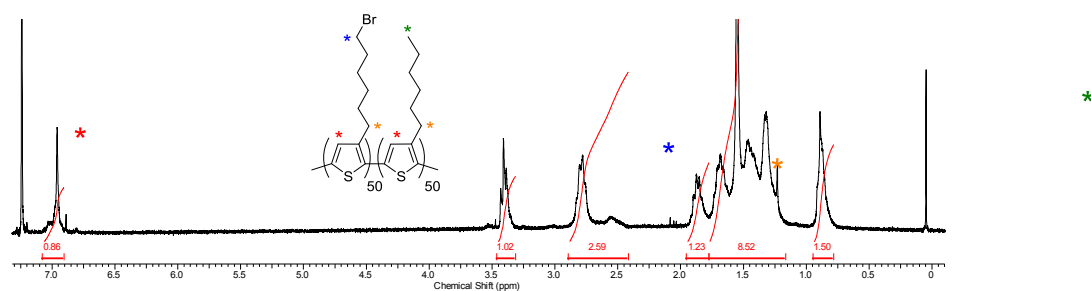
- Firestone, M. A. *Polym. Adv. Technol.* **2008**, *19*, 1369–1382; (e) Page, Z. A.; Duzko, V. V.; Emrick, T. *Macromolecules* **2013**, *46*, 344–351.
- 13 (a) Elbing, M.; Garcia, A.; Urban, S.; Nguyen, T.-Q.; Bazan, G. C. *Macromolecules* **2008**, *41*, 9146–9155; (b) Bondarev, D.; Zednik, J.; Sloufova, I.; Sharf, A.; Prochazka, M.; Pflieger, J.; Vohlidal, J. *J. Polym. Sci., Part A: Polym. Chem.* **2010**, *48*, 3073–3081; (c) Kazim, S.; Pflieger, J.; Prochazka, M.; Bondarev, D.; Vohlidal, J. *J. Colloid Interface Sci.* **2011**, *354*, 611–619; (d) Knaapila, M.; Evans, R. C.; Gutacker, A.; Garamus, V. M.; Székely, N. K.; Scherf, U.; Burrows, H. D. *Soft Matter* **2011**, *7*, 6863–6872; (e) Ying, L.; Zalar, P.; Collins, S. D.; Chen, Z.; Mikhailovsky, A. A.; Nguyen, T.-Q.; Bazan, G. C. *Adv. Mater.* **2012**, *24*, 6496–6501; (f) Suspène, C.; Miozzo, L.; Choi, J.; Gironda, R.; Geffroy, B.; Tondelier, D.; Bonnassieux, Y.; Horowitz, G.; Yassar, A. *J. Mater. Chem.* **2012**, *22*, 4511–4518; (g) Richter, T. V.; Bühler, C.; Ludwigs, S. *J. Am. Chem. Soc.* **2012**, *134*, 43–46.
- 14 (a) Loewe, R. S.; Ewbank, P. C.; Liu, J.; Zhai, L.; McCullough, R. D. *Macromolecules* **2001**, *34*, 4324–4333; (b) Zhai, L.; Pilston, R. L.; Zaiger, K. L.; Stokes, K. K.; McCullough, R. D. *Macromolecules* **2003**, *36*, 61–64.
- 15 Miyakoshi, R.; Yokoyama, A.; Yokozawa, T. *Macromol. Rapid Commun.* **2004**, *25*, 1663–1666.
- 16 Zhao, J.; Swinnen, A.; Van Assche, G.; Manca, J.; Vanderzande, D.; Van Mele, B. *J. Phys. Chem. B* **2009**, *113*, 1587–1591.
- 17 Pangborn, A. B.; Giardello, M. A.; Grubbs, R. H.; Rosen, R. K.; Timmers, F. J. *Organometallics* **1996**, *15*, 1518–1520.
- 18 Danley, R. L.; Caulfield, P. A.; Aubuchon, S. R. *Am. Lab.* **2008**, *40*, 9–11.
- 19 Wouters, S.; Demir, F.; Beenaerts, L.; Van Assche, G. *Thermochim. Acta* **2012**, *530*, 64–72.
- 20 Bäuerle, P.; Wurthner, F.; Heid, S. *Angew. Chem., Int. Ed. Engl.* **1990**, *29*, 419–420.
- 21 Miyanishi, S.; Tajima, K.; Hashimoto, K. *Macromolecules* **2009**, *42*, 1610–1618.

Chapter 5

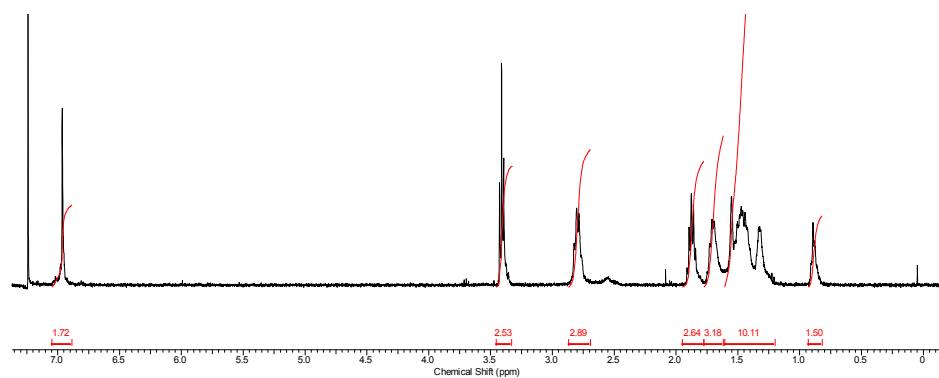
5.6 Supporting information

5.6.1 ^1H NMR spectra of the P3BHT-*b*-P3HT precursors and the P3(MIM)HT-*b*-P3HT ionic block copolythiophenes

P3BHT-*b*-P3HT 50/50

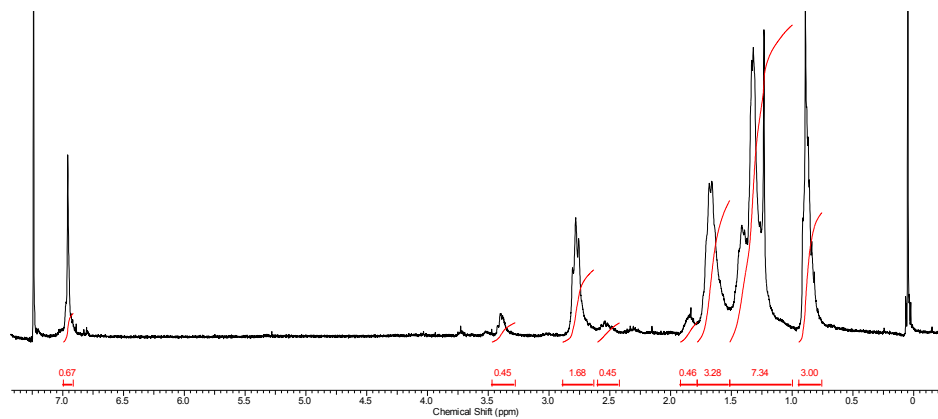


P3BHT-*b*-P3HT 70/30

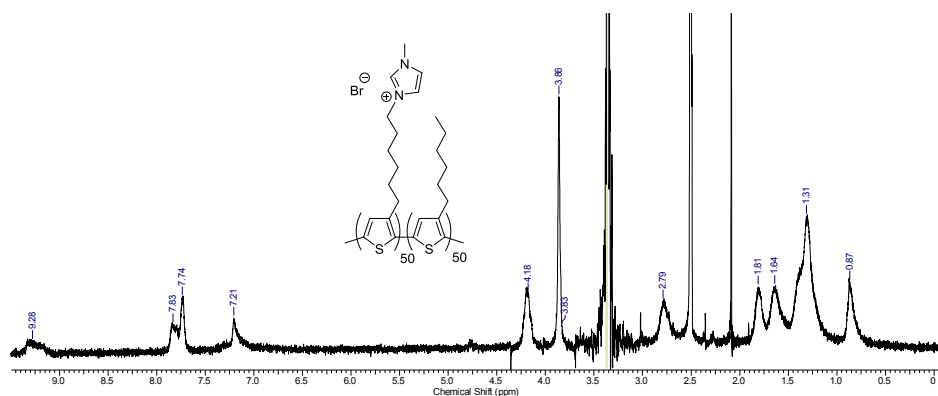


Amphiphilic *N*-methylimidazole-functionalized diblock copolythiophenes

P3BHT-*b*-P3HT 30/70

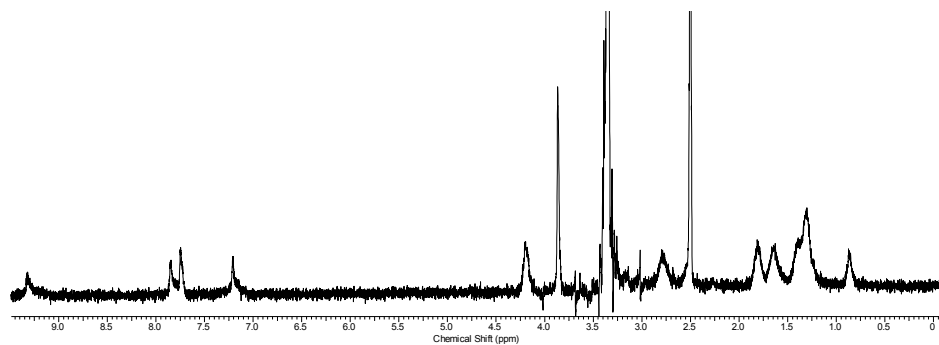


P3(MIM)HT-*b*-P3HT 50/50

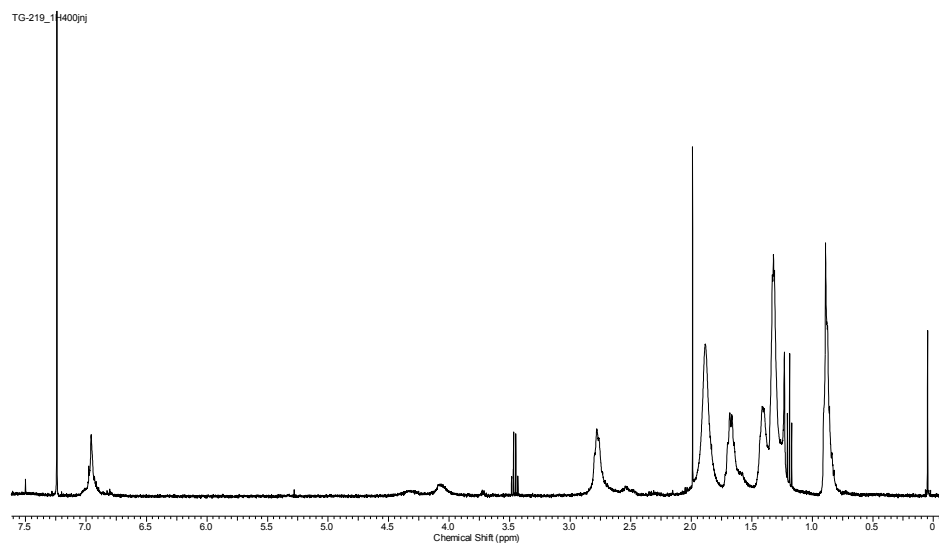


Chapter 5

P3(MIM)HT-*b*-P3HT 70/30



P3(MIM)HT-*b*-P3HT 30/70



5.6.2 Additional SEC profiles and molecular weight (distribution) data

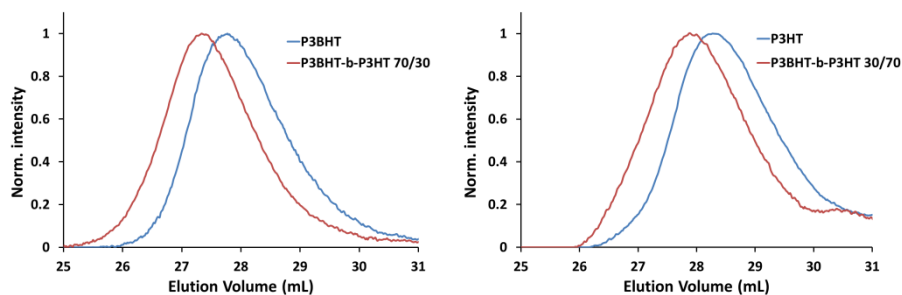


Figure S5.1: SEC profiles obtained during block copolymer synthesis of the **P3BHT-*b*-P3HT 30/70** and **70/30** derivatives.

Table S5.1: Molecular weights of the intermediate (first block) and final precursor diblock copolymers.

Polymer	M_n 1 st block (kDa) ^a	PDI 1 st block	M_n total (kDa) ^b	PDI total
P3BHT-<i>b</i>-P3HT 30/70	4.3	1.4	5.3	1.4
P3BHT-<i>b</i>-P3HT 50/50	3.6	1.3	6.5	1.3
P3BHT-<i>b</i>-P3HT 70/30	6.4	1.4	8.9	1.4

^a Without soxhlet purification; ^b Before soxhlet purification.

Chapter 6

General conclusions

This manuscript is a compilation of the research work conducted over 3 years, mainly focusing on the GRIM polymerization procedure to synthesize bromine-functionalized polythiophene homopolymers, statistical copolymers and block co-polythiophenes, and their applications in organic photovoltaics. The standard poly (3-alkylthiophenes) synthesized in literature are generally soluble in rather apolar organic solvents. Via functionalization of the synthesized (co)polymers with ionic moieties, the materials become (more) soluble in environmentally acceptable solvents. With these ionic groups in place, the polymers also exhibit some special properties which effect the performance of organic solar cells.

In a first instance it was demonstrated that the GRIM polymerization procedure is a versatile method to synthesize a broad range of bromine-functionalized random copolythiophenes. Post-polymerization modification of these polymers with *N*-methylimidazole via microwave activation resulted in a smooth and efficient conversion to the ionic copolymers. These ionic polymers are in general (more) soluble in polar solvents and some of them even in water. Later on, when the polymerization method was optimized, also ionic block co-polythiophenes could be synthesized.

UV-Vis measurements of the ionic (co)polythiophenes revealed an unusual solution behavior. The idea of aggregate formation was posed and dynamic light scattering (DLS) was used to get more insight in the size of the formed aggregates in solution. In good agreement with the UV-Vis studies, DLS confirmed that the **P3HT-P3(MIM)HT-Br 50/50** statistical copolymer forms aggregates in water-rich solvent mixtures.

The ionic block copolymers exhibit a similar solution behavior. The **P3(MIM)HT-*b*-P3HT 50/50** and **70/30** block copolymers are soluble in water and have the tendency to form micelle-like structures in solution. Although it is quite clear that structures are formed in solution, the solubility characteristics were too complicated for DLS to give a clear view on the formed aggregates in solution. Cryo-TEM was hence executed to freeze the aggregate solution. In this way the aggregates could be visualized, but even then no clear conclusions could be drawn.

From thermal analysis it could be concluded that all the synthesized precursor polymers are semi-crystalline. For all of these materials, a larger amount of bromine-functionalized repeating units lead to melting at lower temperatures. The semi-crystalline behavior changes to fully amorphous for the ionic **P3(MIM)HT-Br** polymers, where only a glass transition is seen. This lack of order was in agreement with the UV-Vis results on thin films. In both DSC and TGA it could be seen that the latter materials are hygroscopic. A striking change in the thermal behavior of the imidazolium-substituted polythiophenes was seen when the bromine counter ion was replaced by either **TFSI** or **PF₆**. In the former case, a strong plasticizing effect was observed, while in the latter case the polymer could easily get semi-crystalline (after a cold-crystallization thermal annealing step).

The **P3BHT-*b*-P3HT** precursor copolymers also showed clear semi-crystalline behaviour and a trend was visible in the crystallinity; a larger **P3HT** block length leads to higher-melting crystals and a higher degree of crystallinity. It was also shown that the **P3BHT** blocks can crystallize as well, but at a much slower rate than the **P3HT** blocks. After

functionalization one can see a clear T_g for the three ionic **P3(MIM)HT-*b*-P3HT** block copolymers, which seems to increase with the **P3(MIM)HT** block length. A melting peak is only observed for the **P3(MIM)HT-*b*-P3HT 30/70** block copolymer at a temperature of 181 °C, which is similar to the melting temperature of the precursor block copolymer. It indicates that this transition corresponds to the **P3HT** block.

Some of the novel materials were already applied in OPV. The main difference between a non-ionic and an ionic polythiophene is the fact that the latter one is not soluble in chlorobenzene, thus enabling processing of bi-layer configurations from solution. We have shown that our modified **P3(MIM)HT-TFSI** polymer shows the same or even slightly superior performance as compared to standard P3HT in a bi-layer configuration. We underline that the novel ionic P3HT derivative synthesized in this work shows excellent film-forming properties and devices were highly reproducible. Using it in combination with PC₇₁BM as the acceptor, power conversion efficiencies of 1.6% were achieved for these simple solution-processed bi-layer solar cells.

On the other hand, we have also shown that the device performance of polymer solar cells can be remarkably improved by incorporation of a thin electron transport layer (ETL) based on an imidazolium-substituted ionic polythiophene (**P3(MIM)HT-Br**; 20% increase in PCE up to an average value of 6.2% for PCDTBT:PC₇₁BM). The beneficial effect is notably higher than for previously reported materials such as an analogous trimethylamine-functionalized ionic polythiophene or PFN. Best results were obtained for the highest molecular weight ETL

General Conclusions.

material, pointing to an important influence of polymer chain length on ETL performance. Remaining questions on the exact influence of polymer molecular weight (and its relation to active layer coverage) and the polythiophene backbone need to be addressed in future work.

List of Publications

- *Imidazolium-substituted polythiophenes as efficient electron transport materials improving photovoltaic performance*

Kesters, J.; Ghooos, T.; Penxten, H.; Drijkoningen, J.; Vangerven, T.; Lyons, D. M.; Verreet, B.; Aernouts, T.; Lutsen, L.; Vanderzande, D. J.; Manca J.; Maes, W. *Adv. Energy. Mater.*,
DOI: 10.1002/aenm.201300049

- *Imidazolium-substituted ionic (co)polythiophenes: compositional influence on solution behavior and thermal properties*

Ghooos, T.; Brassinne, J.; Fustin, C.-A.; Gohy, J.-F.; Defour, M.; Van den Brande, N.; Van Mele, B.; Lutsen, L.; Vanderzande, D. J.; Maes, W. manuscript submitted to *Polymer*

- *Solution-processed bi-layer polythiophene-fullerene organic solar cells*

Ghooos, T.; Malinkiewicz, O.; Lutsen, L.; Vanderzande, D. J.; Bolink, H. J.; Maes, W. manuscript submitted to *RSC Advances*.

- *Amphiphilic N-methylimidazole-functionalized diblock copolythiophenes for organic photovoltaics*

Ghooos, T.; Van den Brande, N.; Defour, M.; Brassinne, J.; Fustin, C.-A.; Gohy, J.-F.; Hoepfener, S.; Schubert, U. S.; Lutsen, L.; Vanderzande, D. J.; Van Mele B.; Maes W. manuscript submitted to *J. Polym. Sci. Part A: Polym. Chem.*

